Pressurized Solid Oxide Fuel Cell/ Gas Turbine Power System

Final Report

Contract Start Date: 29 May 1998
Contract End Date: 30 November 1999

Principal Authors:

W. L. Lundberg **R. A. Holmes** **J. E. King**
G. A. Israelson **P. R. Zafred** **R. E. Kothmann (Consultant)**
R. R. Moritz (Rolls-Royce Allison)
S. E. Veyo, Project Manager

February 2000

Contract No. DE-AC26-98FT40355

by

Siemens Westinghouse Power Corporation
SOFC Power Generation
1310 Beulah Road
Pittsburgh, PA 15235-5098

and under subcontract

Rolls-Royce Allison
2001 South Tibbs Avenue
Indianapolis, IN 46241

for

U. S. Department of Energy
Federal Energy Technology Center
P.O. Box 10940, MS 921-143
Pittsburgh, PA 15236-0944

PD-99-091A

“This report was prepared as an account of work sponsored by an agency of the United States Government. Neither the United States Government nor any agency thereof, nor any of their employees, makes any warranty, express or implied, or assumes any legal liability or responsibility, for the accuracy, completeness, or usefulness of any information, apparatus, product, or process disclosed, or represents that its use would not infringe privately owned rights. Reference herein to any specific commercial product, process, or service by trade name, trademark, manufacturer, or otherwise does not necessarily constitute or imply its endorsement, recommendation, or favoring by the United States Government or any agency thereof. The views and opinions of authors expressed herein do not necessarily state or reflect those of the United States Government of any agency thereof.”

ABSTRACT

Power systems based on the simplest direct integration of a pressurized solid oxide fuel cell (SOFC) generator and a gas turbine (GT) are capable of converting natural gas fuel energy to electric power with efficiencies of approximately 60% (net AC/LHV), and more complex SOFC and gas turbine arrangements can be devised for achieving even higher efficiencies. The results of a project are discussed that focused on the development of a conceptual design for a pressurized SOFC/GT power system that was intended to generate 20 MWe with at least 70% efficiency. The power system operates baseloaded in a distributed-generation application. To achieve high efficiency, the system integrates an intercooled, recuperated, reheated gas turbine with two SOFC generator stages – one operating at high pressure, and generating power, as well as providing all heat needed by the high-pressure turbine, while the second SOFC generator operates at a lower pressure, generates power, and provides all heat for the low-pressure reheat turbine. The system cycle is described, major system components are sized, the system installed-cost is estimated, and the physical arrangement of system components is discussed. Estimates of system power output, efficiency, and emissions at the design point are also presented, and the system cost of electricity estimate is developed.

TABLE OF CONTENTS

LIST OF FIGURES

LIST OF TABLES

1. EXECUTIVE SUMMARY

1.1 Power System Design Description

Operating at atmospheric pressure, the efficiency horizon for an SOFC power system is 45% (net AC/LHV), while a gas turbine will typically convert to electric power 30% of the fuel energy supplied to the gas turbine (Brayton) cycle. When the SOFC generator and the gas turbine are integrated, as depicted in the hybrid cycle of Figure 1.1, system efficiency near 60% can be achieved. This is due to the enhanced performance of the SOFC generator at elevated pressure, and to the processing to power of SOFC exhaust heat by the gas turbine. Maximum system efficiencies are achieved when no fuel is fired at the GT combustor, which is possible since gas turbines can operate with turbine inlet temperatures in the 850°C to 870°C range, which are typical SOFC exhaust temperatures. With no combustor firing, all fuel enters the system via the SOFC generator, and the fuel energy will have two opportunities for conversion to power — first, by the SOFC electrochemical process, and second, by the Brayton-cycle conversion of SOFC exhaust heat.

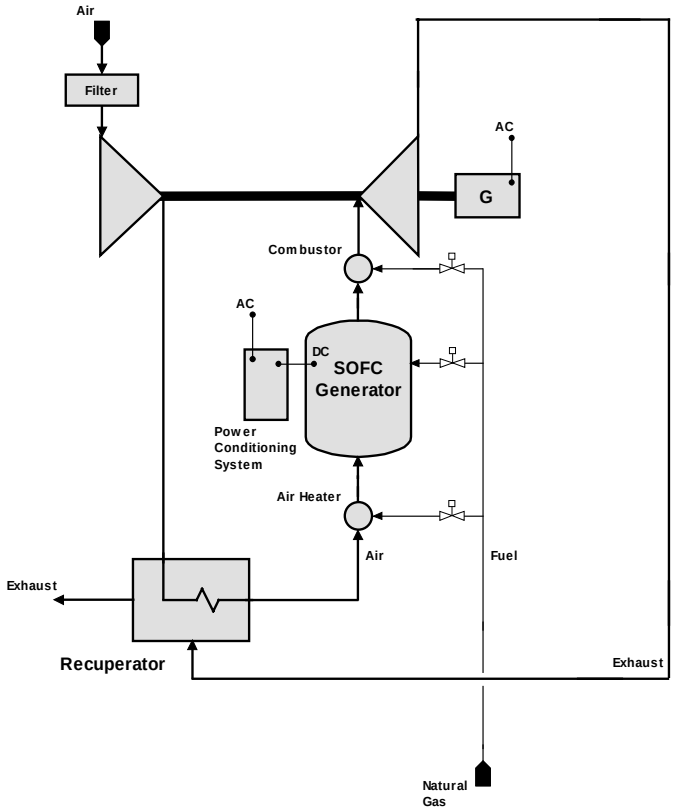

Figure 1.1 — Simplified PSOFC/GT hybrid power system cycle.

The High Efficiency Fossil Power Plant (HEFPP) system concept developed by Siemens Westinghouse uses this cycle as its basis, but it incorporates additional features and components that boost the system efficiency to levels nearer the target 70%. The reference HEFPP system concept is depicted in Figure 1.2. Components from the basic hybrid cycle (Figure 1.1) are visible, as well as those added for increased system efficiency. They are the intercooler, the low-pressure (LP) reheat turbine section, and the LP SOFC generator. The intercooler reduces the compressor work input requirement, and reheating increases the turbine shaft power output. Both effects also act to increase the cycle efficiency, provided the cycle is recuperated. The LP generator provides another instance for the serial processing of power system fuel because, in addition to generating power, it provides the heat for the LP turbine, supplanting the reheat combustor. In addition, because of the reheat feature, and relative to the optimum pressure ratio for the basic PSOFC/GT hybrid cycle, the HEFPP system cycle optimizes at a higher compressor pressure ratio. As a result there is a stronger positive effect of elevated pressure on cell voltage at the HP SOFC generator. Figure 1.2 provides detail on the low-maintenance fuel desulfurization system, which is based on the processing of sulfur-bearing compounds to hydrogen sulfide in a cobalt-molybdenum catalyst bed, and the adsorption of the resulting H_2S on heated zinc oxide.

A pictorial view of the power system is presented in Figure 1.3. The dimensions of the rectangular plot plan depicted in the figure are 61 m x 41 m (200 ft x 135 ft), corresponding to a site footprint of approximately 0.6-acre. Visible in the figure are the SOFC generators at the HP and LP locations. Each generator consists of several SOFC modules that are arranged in flow parallel between process air and exhaust manifolds, and each module is a horizontal cylindrical pressure vessel, flanged at the middle, that houses an assembly of 11,520 SOFCs. (An individual fuel cell is tubular, having an active length of 1500 mm and a diameter of 22 mm.) The overall length of a module is approximately 11 m (36 ft), and its diameter is 3.5 m (11.5 ft). The HP SOFC generator consists of four modules, and the LP SOFC generator, five modules — a combination that was selected for maximum system efficiency. It is to be noted that while the power system design was developed for high system efficiency, the reference fuel cost of $3.00/MMBtu does not permit the maximum efficiency and the minimum cost-of-electricity (COE) to occur at the same design point. This will happen most probably only if the power system is deployed in a region with a higher fuel cost. The reheat gas

turbine, with intercooler and recuperator, is installed between the HP and LP SOFC generators. Rolls Royce Allison specified the turbine and associated equipment.

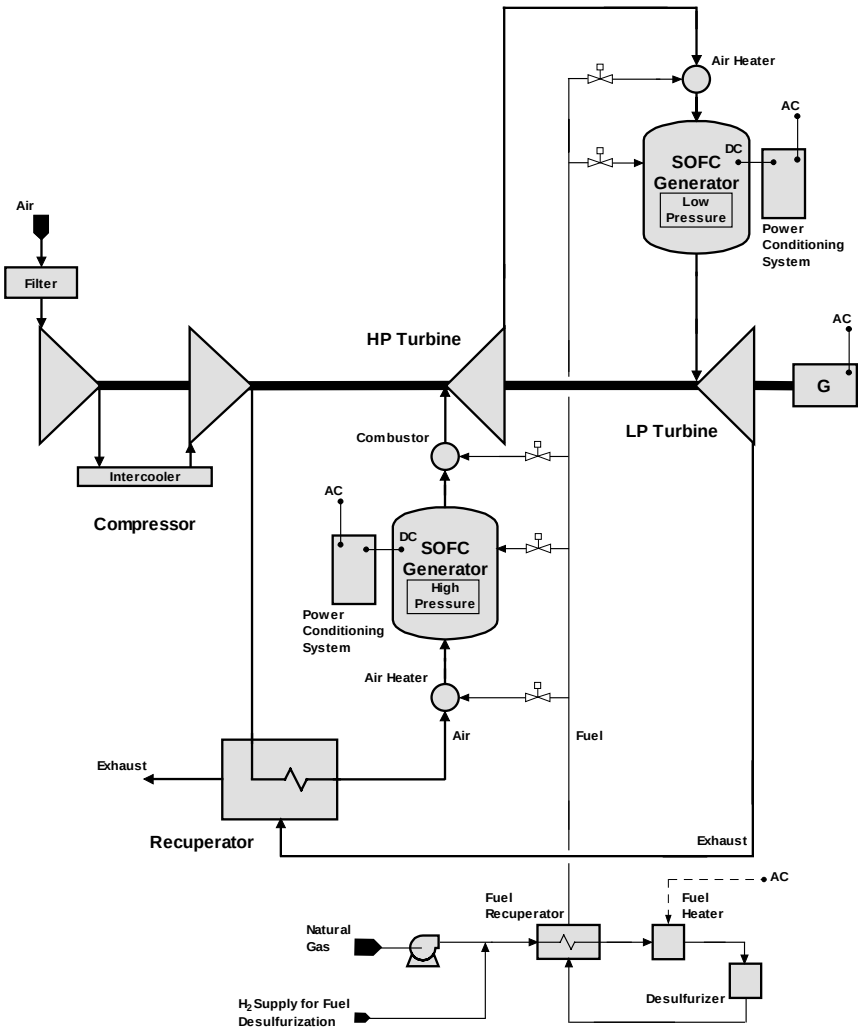

Figure 1.2 — HEFPP system cycle.

In the SOFC generator design, the flows of air and reformed-fuel on the cathode and anode of each fuel cell occur cocurrently and parallel to the cell axis. This is the conventional configuration that has been used by Siemens Westinghouse in all demonstration SOFC generators designed and operated to date. It was selected for the application in the HEFPP system concept after consideration of the staged-cell SOFC generator concept. The staged-cell design, which retained the conventional air delivery design on the cell cathode side, but employed crossflow on the fuel (anode) side, was originally believed to enable the SOFC generator to operate at very high fuel utilizations, thereby contributing to the achievement of higher generator and system efficiencies.

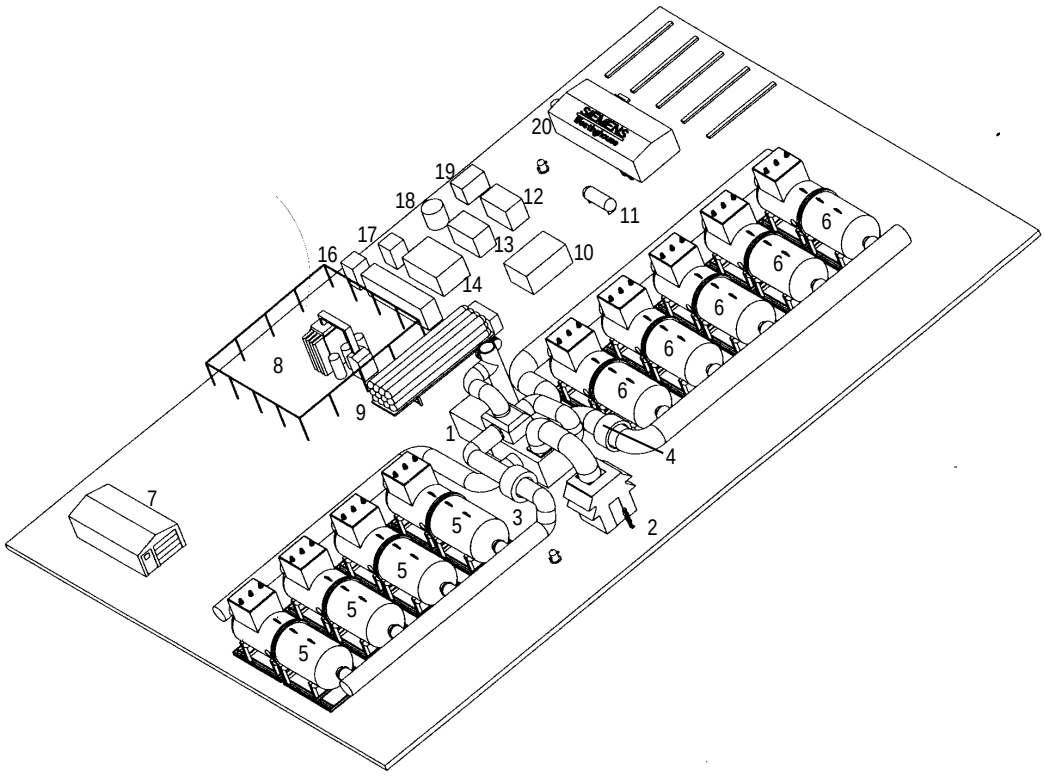

Key:
1. GT Skid
2. Filter House
3. HP Air Heater
4. LP Air Heater
5. HP SOFC Vessel
6. LP SOFC Vessel
7. Storage Shed
8. 20 MW Substation
9. N_2 Tube Trailer
10. N_2 Generator/Compressor
11. Propane Tank
12. Auxiliary Air Compressor
13. Nat. Gas Compressor
14. Desulfurizer
15. Elec. Cabinets
16. UPS Shed
17. H_2 Generator/Compressor and Gas Mixer
18. Water Storage Tank
19. Startup Boiler
20. Control/Meeting Room

Figure 1.3 — Power system site arrangement.

Based upon analysis, the potential benefits of staging proved elusive for two major reasons. First, since the first cell stage is fed relatively cold fuel, the first few cell stages operate at substantially less than optimum temperature for yttria stabilized zirconia electrolyte cells.

Second, the last cell stage can not be operated at fuel utilization greater than that for the co-current flow stack because the approximately parabolic axial temperature distribution and concomitant non-uniform current density distribution place the cell hot spot

at hazard for anode oxidation at roughly the same average fuel utilization achievable in a non-staged stack.

1.2 Performance Estimates

The power system is designed for baseload operation at the peak-efficiency system design point. At that point, the estimated system net AC power output is 19.0 MWe, and its efficiency is 67.3% (net AC/LHV). Approximately 15 MWe are derived from the SOFC generator modules, and the remainder from the gas turbine. The estimated rates of CO_2 and NOx emission at the system design point are 300 kg/MWh (5.7 vol %) and 0.006 kg/MWh (1 ppm_v), respectively; the exhaust flow rate and temperature are 19 kg/s (41 lb/s) and 225°C (437°F).

The PSOFC/GT power system conceptual design reported herein misses the target efficiency of 70% by 2.7 points. The desulfurization scheme used is a contributing factor to this efficiency shortfall because it employs an electrolyzer to provide the small stream of H_2 gas needed. If an ambient-temperature sorbent (as assumed in past studies) were practical, the resultant system efficiency would be 68% at a system net power output of 19.2 MWe. In addition, the SOFC power conditioning system (PCS) efficiency was set at 94% for the conceptual design. This value is two percentage points less than the more optimistic value applied in past HEFPP studies. Improvements in PCS performance, which may be possible, and should be evaluated, would translate directly to a higher HEFPP system efficiency. For example, at the current HEFPP system design point, a boost in PCS efficiency to 97% would result in an increase in system power output to 19.5 MWe and in efficiency to 69%. Finally, the two to five point efficiency gain believed possible for the proposed electrochemical staging of the tubular SOFC was determined to be unobtainable in practice for fuel cells operating at economically meaningful current density. When the projected effects of the passive ambient-temperature desulfurizer sorbent and the improved PCS performance are combined, the estimated system power output and efficiency are 19.7 MWe and 69.6%, and the addition of a small low-pressure steam turbine cycle would result in system net AC output of 20 MWe, at an efficiency of 71%. Thus, it appears that the target efficiency of 70% may be achievable through improvements in PCS efficiency and the desulfurization technique, and through the addition of the steam turbine generator, without electrochemical SOFC staging.

1.3 System Cost and Economics

The system installed-cost estimate is $1431/kWe. It includes costs related to site preparation, equipment procurement, shipping, and installation, as well as allowances for G&A, sales and marketing, and profit. Mature technologies and products were assumed. The distribution of the power system installed cost is provided in Table 1.1.

Table 1.1 — HEFPP System Installed Cost Summary

	Cost, $/kWe
SOFC Generator Equipment	471
SOFC Power Conditioning Equipment	107
Gas Turbine Equipment	211
Balance of Plant Equipment	259
Subtotal	1048
Site Preparation	22
Project Management and Engineering	48
Overhead and Profit	291
Total Plant Cost	1409
Spare Parts, Startup, and Land Allowance	22
Total Capital Requirement	1431

COE estimates have been developed for the HEFPP system, operating at its design point, and also for a competing technology, which was assumed to be a 20 MWe-class gas turbine combined cycle power system. Table 1.2 summarizes input used in the analysis, and also the results.

The projected COE is approximately 3% higher than conventional-technology COE. The conventional-technology power system will emit more NOx and SOx (see emission estimate summary in Table 1.2), and the cost of equipment to reduce those emissions to HEFPP levels would improve the relative COE performance of HEFPP system. Comparing the systems in a higher fuel cost environment would also improve the COE attractiveness of the HEFPP system. For example, with $6 fuel, the HEFPP system COE estimate is 7% less than the conventional-system COE (66 mills/kWh, vs. 71 mills/kWh), and with $9 fuel it is 13% less (83 mills/kWh, vs. 95 mills/kWh).

Table 1.2 — Economic Analysis Summary of Results

	HEFPP system (PSOFC/GT)	**Conventional-Technology Power System (Gas Turbine/Steam Turbine Combined Cycle)**
No. of round-the-clock operators	1	1
No. systems in operation	5	5
Labor cost components	System operation & house-keeping maintenance	System operation & house-keeping maintenance
Gas turbine/steam turbine system maintenance	$0.01/GT kWe	$0.007/system kWe
Power system capacity factor	0.92	0.92
Capital charge rate	15%	15%
Fuel cost	$3/MMBtu	$3/MMBtu
Power system capital cost	$27.3M	$14.9M
Power output	19.0 MWe	17.9 MWe
Emissions estimates CO_2 NOx SOx	 **300 kg/MWh** **0.006 kg/MWh** (1 ppm_v) **Virtually zero**	 420 kg/MWh 0.380 kg/MWh (25 ppm_v) 2.5 g/MWh (4 ppm_v S in fuel)
Power system efficiency (net AC/LHV), %	**67.3**	47.9
Cost of electricity, mills/kWh	49.1	47.6

* Source: Gas Turbine World 1997 Handbook, turnkey power generation projects, p. 24.

1.4 Conclusions and Recommendations

Study conclusions can be summarized as follows:

- A PSOFC/GT system concept of near 20 MW capacity has been devised that is conservatively capable of 67% efficiency, a value ten points greater than that achievable with the best available large-plant conventional power generation technology, and twenty points above the efficiency achieved by a conventional 20 MW-class gas turbine combined cycle power system.
- The specific power system concept developed during this study, integrating HP and LP SOFC generators with an intercooled, SOFC-reheated gas turbine, achieves an estimated power output of 19 MWe at an efficiency of 67.3% (net AC/LHV). Improvements in the performance of major system components, particularly in the SOFC PCS, for which there was no study design task, and employment of an ambient-temperature passive sorbent technology for fuel desulfurization would cause the system efficiency estimate to approach very closely the 70% efficiency target. The addition of the steam turbine cycle, which could have a marginal practicality due to its small output and the increased power system complexity and maintenance, could boost the power system efficiency to slightly above 70%.

- The staged-cell SOFC stack design does not offer the large SOFC efficiency gain (over the standard cocurrent axial flow stack design) that was projected originally. Cell cooling in the fuel-entry cell rows reduces the average cell voltage while there is little increase in average fuel utilization at the last cell row at meaningful current densities because of the hazard of anode oxidation.
- For the reference fuel cost of $3.00/MMBtu, the estimated COE for the HEFPP system is 3% higher than the COE estimate for a conventional 20 MW-class gas turbine/steam turbine power system. Leveraged by its significantly higher efficiency, the HEFPP system would have a COE advantage in a higher fuel cost environment. For example, with $6 fuel, the HEFPP COE would be 7% less than the conventional-system COE.

Recommendations:

- Desulfurization technologies not requiring a source of hydrogen, and capable of operation at ambient-temperature levels, should be developed.
- Power conditioning topologies with greater than 95% efficiency should be developed.
- For deployment in SOFC/GT hybrid cycle power systems, small, efficient, highly-reliable, recuperated gas turbines with turbine inlet temperature commensurate with SOFC exhaust gas exit temperatures (870°C) should be developed.
- A PSOFC/GT power system of 70% efficiency potential should be developed and demonstrated at the smallest capacity class practical for proof-of-concept.
- SOFC development should be pursued to improve intrinsic power density and to ensure operational feasibility at elevated pressures beyond 3 atmospheres.

2. INTRODUCTION

A simplified cycle diagram for a simple-cycle, atmospheric pressure SOFC power system is provided in Figure 2.1. Fuel cell process air is supplied by the air blower, and the air is preheated as needed for SOFC thermal management using heat recovered at the recuperator from the SOFC exhaust gas. The SOFC generator operating pressure is near atmospheric, typically being in the 30 to 50 mbarg (10 to 20 in. H_2O) range. SOFC power systems based upon this cycle are capable of electric generating efficiencies in the 45% to 50% (net AC/LHV) range. The 100 kWe SOFC combined heat and power (CHP) demonstration power system operating in the Netherlands is based on this cycle. That system, designed and fabricated by Siemens Westinghouse and EDB/ELSAM, a team of Dutch and Danish generating and distribution companies, and sponsored by EDB/ELSAM, is installed at a utility site near Arnhem. To date, the unit has logged over 10,000 operating hours, it is generating approximately 110 kWe net AC power at 46% efficiency (net AC/LHV) for the utility grid, and it also produces hot water for the local district heating system. The demonstrated system energy efficiency is nearly 75%.

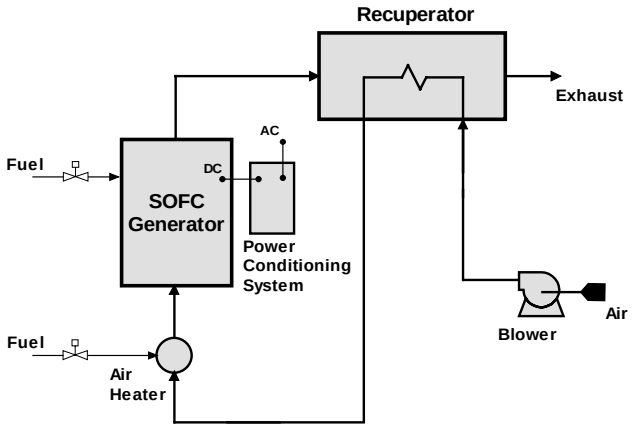

Figure 2.1 — Atmospheric pressure SOFC power system cycle.

Power system efficiency can be increased by integrating the SOFC generator with a gas turbine in the cycle depicted in Figure 2.2. The SOFC generator in this cycle is pressurized (PSOFC), operating on air coming directly from the compressor discharge, via the turbine exhaust recuperator. The system based upon this cycle achieves high efficiencies due to the utilization by the gas turbine generator of thermal energy in the pressurized SOFC exhaust stream. Power system performance is also enhanced by

SOFC generator operation at elevated pressure. For a given cell operating current, cell voltage, and hence cell power output and efficiency, increase with pressure. Assuming PSOFC operation at 50% efficiency and the conversion of SOFC exhaust heat to power by the gas turbine at 30% efficiency, it is clear that the cycle efficiency can be made to approach 60%. This is predicated on the restriction that the gas turbine combustor is not fired during normal, high-efficiency power operation. It could, however, be fired for peak-power purposes. While combustor firing would indeed result in more power from the system, it would not increase the system efficiency because the incremental fuel is converted to power at the relatively low gas turbine efficiency level. The SOFC generator is ideally suited for deployment in a power system of this type since the SOFC exhaust gas has a temperature of about 870°C. Gas turbines can operate with turbine inlet temperatures of 870°C, and therefore the two technologies are directly integrable, with the SOFC generator effectively supplanting the turbine combustor.

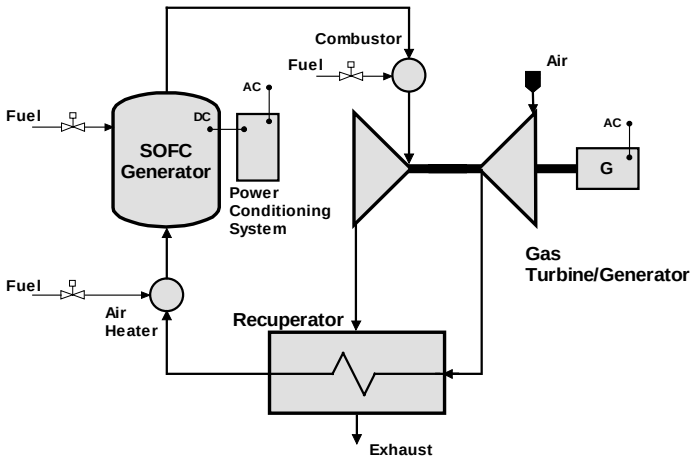

Figure 2.2 — Simplified PSOFC/GT hybrid power system cycle.

The purpose of the present project, undertaken by Siemens Westinghouse Power Corporation, in conjunction with Rolls Royce Allison, was to develop a conceptual design and feasibility study for a power system that utilizes the PSOFC/GT cycle to achieve a system electric generation efficiency of 70%. An adjunct objective is that the system yield a reduced cost-of-electricity (COE) relative to the COE for a conventional power system, which, for this study, was assumed to be a gas turbine combined cycle. The power system capacity was to be 20 MWe. The reference power system in the Siemens Westinghouse/Rolls Royce Allison study is based upon a recuperated reheat

gas turbine cycle. In the reheat turbine cycle, the gas turbine has two expander stages, each stage is equipped with a combustor, and after the hot gas produced at the HP combustor expands partially across the HP turbine, it is reheated at the LP combustor before the expansion process is completed across the LP turbine stage. The recuperated reheat turbine cycle will have a higher efficiency than the recuperated single-stage cycle because reheating increases the cycle's average heat reception temperature, without affecting the temperature at which heat is rejected. Then, applying that cycle, and supplanting both combustors with SOFC generators, efficiencies well above the 60% level forecast for the simpler PSOFC/GT cycle of Figure 2.2 should be achieved. The efficiency improvement is due to the implementation of the more efficient gas turbine cycle (intercooled, reheated) and to the cycle's optimization at higher compressor pressure ratios. As the result of the higher pressure ratio, there is a stronger positive effect of elevated pressure on cell voltage at the HP SOFC generator.

The conceptual design of a high-efficiency power system based upon the reheat turbine cycle is developed and discussed in this report. Tradeoff studies are discussed, the features of the main components in the reference power system design are described, and power system performance and COE estimates are presented.

3. RESULTS AND DISCUSSION

3.1 Power Plant Conceptual Design

3.1.1 Design Requirements and Objectives

3.1.1.1 Introduction

This document establishes requirements and specifications for use by the Siemens Westinghouse Power Corporation in developing the conceptual design for a high-efficiency fossil-fueled power plant. The plant concept to be developed by Siemens Westinghouse is based on the integration of solid oxide fuel cell (SOFC) and gas turbine technologies.

3.1.1.2 Design Basis

Power Plant Application	Commercial distributed-power generation
Output Power Specification	60 Hz AC, at utility-grid voltage
Utility AC Grid Connection	The power plant will be connected to the utility grid, and all net plant power will be exported to the grid.
Dispatch Mode	Base load
Power Plant Heat Recovery	Heat will be recovered for plant power generation support; no heat will be recovered for site thermal application.
Power Plant Startup	The utility AC grid will be available for plant startup operations.
Installation	Outdoors.
Conceptual Design Scope	Power plant equipment between the site fuel supply point and the AC grid interface will be included in the design. The equipment considered will be essential for plant startup, operation, control, shutdown, and maintenance.

3.1.1.3 Performance Requirements

Power Plant Design-Point Capacity	20 MW net AC, +/- 2 MW
Design-Point Efficiency	70% (net AC/LHV)
Power Plant Normal-Operation Turndown Requirement	None
Power Plant Overpower Requirement	None
Output Power Conditions	60 Hz Utility-grid quality
Acoustic Noise Control	Consistent with typical gas turbine practice.

3.1.1.4 Fuel and Oxidant Specifications at the Power Plant Design Point

Power Plant Fuel	Natural gas
Fuel composition	(mol percentages)
Methane	96
Nitrogen	2
Carbon dioxide	2
Sulfur bearing compounds	Mercaptans
Sulfur concentration	4 ppmv
Fuel supply pressure	1.034 barg (15 psig)
Fuel supply temperature	15°C (59°F)
Oxidant	Air (ISO conditions)
Air composition	(mol percentages)
Oxygen	20.7
Nitrogen	78.0
Carbon dioxide	0.3
Water	1.0 (60% relative humidity)
Ambient air temperature	15°C (59°F)
Ambient air pressure	1.014 barg (14.7 psia)

3.1.1.5 Ambient Air Ranges

Pressure	Sea level to 1500 m (5000 ft)
Temperature	-29°C to 49°C (-20°F to 120°F)
Relative Humidity	0 to 100%

3.1.1.6 Power Plant Physical Design Objectives

Major Subsystem Fabrication	Maximum practicable skid mounting at the factory.
Transportation Options	Truck, sea, air, rail
Site Installation Operations	Minimum component/skid assembly at installation site. Interconnect factory-assembled skids at the site. Interface the power plant with the site.
Plant Design Lifetime	Conventional power plant equipment - 25 years.

3.1.1.7 Power Plant Operation

Normal Power Operation Mode	Automatic, unattended, remotely monitored
Power Plant Startup	Attended
Annual Operating Time	Fifty weeks
Annual Planned Shutdown	Two weeks

3.1.1.8 System/Site Interface Requirements

Appropriate interface points will be available at the installation site for:

- Fuel supply
- Obtaining utility AC power during plant startup operations.
- Connecting the plant power output with the utility grid.

3.1.1.9 Economic Evaluation Parameters

Power System Cost Estimation Basis	Costs will be based on the projected needs of mature SOFC/gas turbine technologies and commercial power plant operation, not first-of-a-kind.
Cost Basis	Mid-1998 US dollars

3.1.1.10 Economic Evaluation Parameters (continued)

Fuel Cost	$3.00/MMBtu (HHV)

Capital Charge Rate	15%
Availability	92%
COE Evaluation Method	Constant dollars
Power Plant Optimization Basis	Consistent with >70% (LHV) efficiency, achieve a design-point COE that is 10-20% below the COE of today's conventional plants.
Transportation Cost Basis	800 km (500 miles) - factory to installation site.
Conventional Power Plant COE Basis	Gas turbine combined cycle

3.1.2 Cycle and Power System Description

The direct integration of a pressurized SOFC generator and a gas turbine in the basic PSOFC/GT hybrid cycle, Figure 2.2, enables the generation of electric power at high efficiencies - typically in the 55% to 60% (net AC/LHV) range. As explained above, this is due to the extended processing by the gas turbine of system fuel energy that is not converted electrochemically to power by the fuel cell, and to the operation of the SOFC generator at elevated pressure. With a peak cycle temperature of 870°C (the SOFC generator exhaust temperature), the optimum compressor pressure ratio is 2.5:1 to 3.0:1, and the SOFC generator therefore operates at a pressure in the 2.5 bar(abs) to 3.0 bar(abs) range. The optimum pressure ratio is determined from peak-efficiency considerations, and is found by trading the positive effect of increasing pressure on SOFC efficiency against the negative effect of operating the SOFC generator at higher, less efficient, cell currents. As the design pressure ratio is increased, while the turbine inlet temperature is fixed at 870°C, the turbine exit temperature drops, cooling the re-cuperator and requiring the SOFC generator to operate at the high currents.

The advanced power system cycle upon which the 20 MWe PSOFC/GT power plant design is based is depicted in Figure 3.1. It builds on the basic PSOFC/GT hybrid cycle, but it provides for further increases in the system efficiency by three mechanisms – higher SOFC operating pressure [>3 bar(abs)], compressor intercooling, and turbine reheat. Since the peak cycle temperature, occurring at the two turbine inlets, is 870°C, the optimum expansion across each turbine will again be in the 2.5:1 to 3.0:1 range. Thus, the LP SOFC generator will operate, as does the generator in the basic

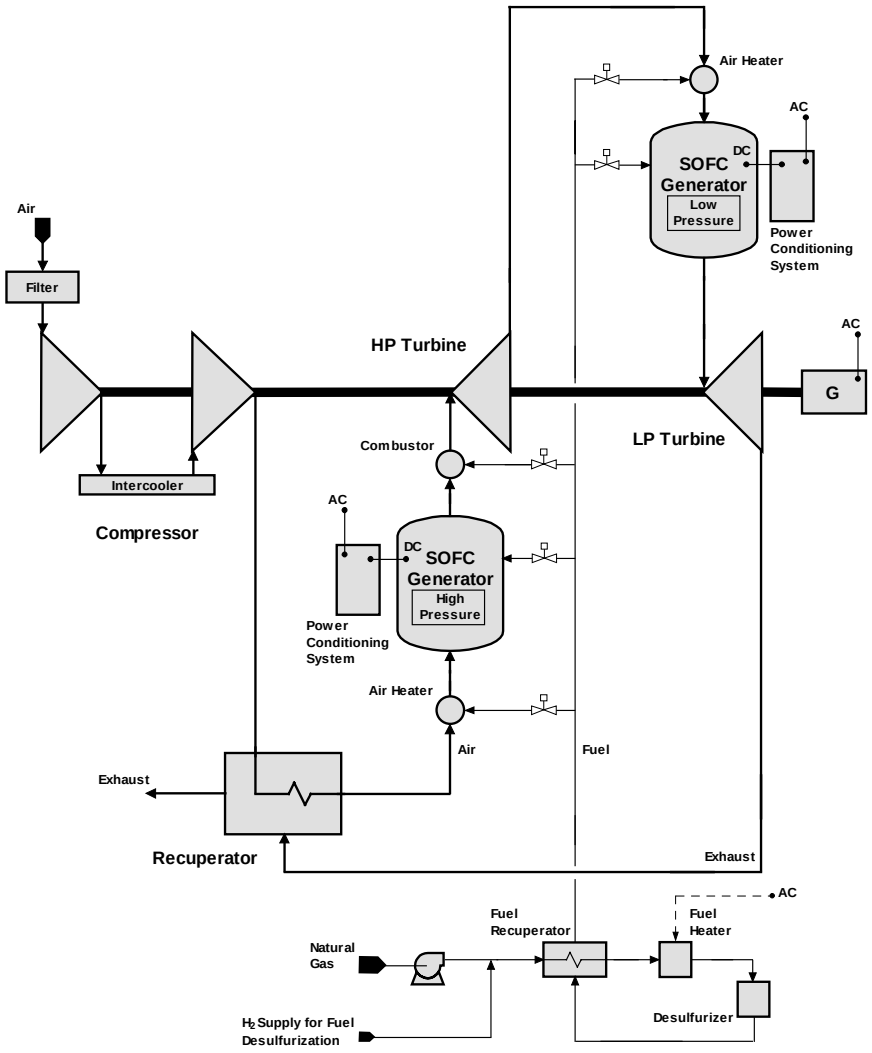

Figure 3.1 — Simplified PSOFC/GT power system cycle diagram.

PSOFC/GT cycle, at pressures in the 2.5 bar(abs) to 3.0 bar(abs) range, but the pressure level at the HP SOFC generator will now be in the 6.0 bar(abs) to 9.0 bar(abs) range. Consequently, there will be a larger positive effect of elevated pressure on cell voltage at the HP generator than there is in the basic PSOFC/GT cycle, and a larger impact on plant efficiency. Intercooling reduces compressor work, at the expense of an intercooler heat rejection parasitic power requirement, causing a net increase in the gas turbine net AC power output; intercooling also contributes to an increased cycle efficiency, provided the cycle is recuperated. The intercooler in the power plant design is assumed to be water-cooled, and heat is rejected to the ambient air via a forced-air water-

to-air heat exchanger. Reheating, again in combination with recuperation, increases the average Brayton cycle heat reception temperature, without changing the average heat rejection temperature, and this also translates directly to a higher Brayton cycle efficiency. The system components are flow matched, the fuel cell operating points are chosen such that the SOFC generator exhaust temperatures are approximately 870°C, and there is no firing of fuel at the gas turbine combustor and air heaters. The combustor and heaters will typically function only during system startup operations, although it is conceivable that the combustor could be fired to achieve peak power output.

The system fuel is pipeline natural gas, assumed in this study to consist of 96 vol % methane, 2% nitrogen, and 2% carbon dioxide. The gas also contains sulfur-bearing compounds, occurring naturally, or added to enable leak detection. The sulfur concentration in the raw fuel, per the design requirements, is 4 ppmV, and it must be reduced to the 0.1 ppmV level prior to SOFC generator entry to preclude the adsorption (reversible) of sulfur on SOFC nickel components. After the fuel has been hydrogenated, the desulfurizer in this power system concept processes the sulfur to hydrogen sulfide in a cobalt-molybdenum catalyst bed, and the H_2S is adsorbed on a bed of hot zinc oxide that operates optimally at 350°C to 400°C (660°F to 750°F). This temperature level is achieved recuperatively and by electric heat addition. The power required for fuel heating is small, and the system is simple and requires low maintenance. Alternatively, the heat for this process could be derived from the turbine exhaust, at the expense of complicating the turbine exhaust design. Hydrogen for the fuel desulfurization process is generated on site.

The SOFC generators produce DC power, which is prepared for export to the utility AC grid by the power conditioning systems. AC power is also produced for export by the gas turbine.

The gas turbine compressor is composed of two radial stages separated by the intercooler. The compressor air intake rate is approximately 18 kg/s (40 lb/s), and the design compressor pressure ratio is 7:1. The stage pressure ratio, allowing for intercooler pressure drop, is 2.73:1. The HP and LP turbine sections each consist of a single axial wheel.

As Figure 3.1 indicates, the rotating gas turbine components are installed on a single shaft, and it is noted that the electric load on the gas turbine generator will be modu-

lated to maintain set-point shaft speed. This feature will assure a steady flow of air to the HP SOFC generator, an important function of the gas turbine, and a necessity to provide for SOFC thermal management.

If the LP turbine were a free power turbine, the expansion ratio across the HP turbine would be set by work-balancing the HP turbine with the compressor. Given a compressor pressure ratio, this would determine the gas temperatures at the HP and LP SOFC inlets, the cell current levels, and the cell operating efficiencies. However, with the single-shaft arrangement, the HP turbine expansion ratio can be an independent variable, and since it does influence the performance of both the HP and LP SOFC generators, an optimum value for the ratio can be determined for maximum system efficiency. It is found that the optimum HP turbine expansion ratio is a function of the compressor ratio, ranging between 0.55 for a pressure ratio of 5:1, and 0.35 at 12:1; for the design pressure ratio of 7:1, the optimum expansion ratio is 0.5. Additional discussion of the optimum expansion ratio, and of the optimum compressor pressure ratio for the high-efficiency power system, is presented in Section 3.4.1. A discussion of compressor intercooling is provided in Section 3.4.2. As noted there, intercooling does increase system efficiency and power output, but due to increased capital cost and the added maintenance requirements, a reduced COE does not necessarily follow. The intercooling feature was selected for the HEFPP cycle due to the project's high-efficiency focus.

A pictorial view of the power system is presented in Figure 3.2. Visible are the SOFC generators at the HP and LP locations. Each generator consists of several SOFC modules that are arranged in flow parallel between process air and exhaust manifolds. Each module is a horizontal cylindrical pressure vessel, flanged at the middle, that houses a cell stack assembly. The basic stack building block is the 576-cell substack pictured in Figure 3.3. The individual cells are tubular, with active lengths of 1500 mm and diameters of 22 mm. They are arranged in the substack in the vertical orientation, with closed ends at the bottom. Shown at the top of the substack are air distribution plena through which process air is admitted to the cell air injection tube inlets, and on the side of the substack, shown are the depleted-fuel recirculation plenum, the ejector that drives the depleted-fuel recirculation, the fuel prereformer, and the ducting for distributing the fresh-fuel/recirculated-fuel mixture to the underside of the substack. Within the substack, methane reformation occurs in the in-stack reformers located between

the cell bundles, and the reformed fuel mixture is then distributed to the individual cells. At the cells, the fuel mixture and air flow cocurrently from the cell closed ends, and a fraction of the CO and H_2, typically 85% to 90%, is processed electrochemically. For the high-efficiency power system, twenty 576-cell substacks compose the cell stack assembly in a single generator module. The HP SOFC generator consists of four modules, manifolded as indicated in Figure 3.2, and the LP SOFC generator is composed of five modules. It is to be noted that this power system design has been developed for maximum system efficiency, realizing that the main objective of the project was the development of a power system concept that could reach the 70% efficiency (net AC/LHV) level.

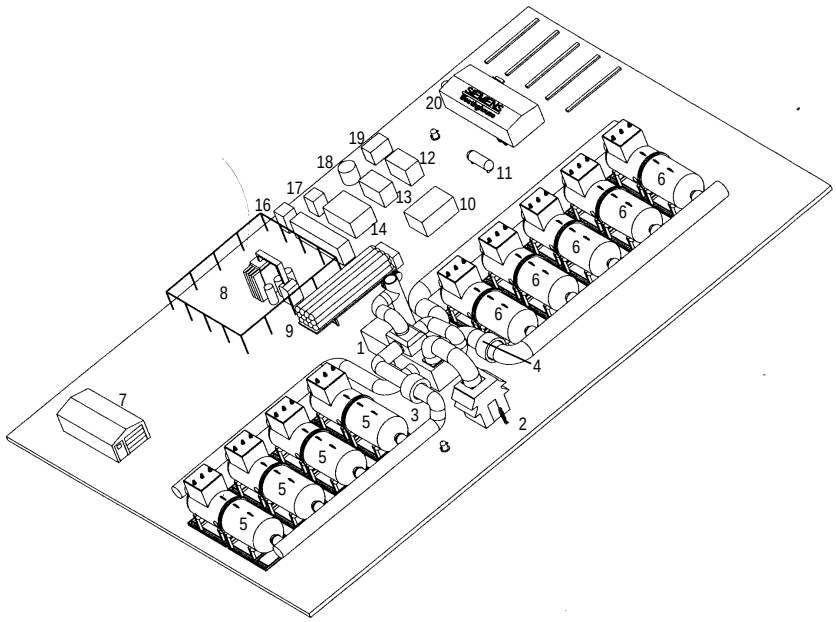

Key:
1. GT Skid
2. Filter House
3. HP Air Heater
4. LP Air Heater
5. HP SOFC Vessel
6. LP SOFC Vessel
7. Storage Shed
8. 20 MW Substation
9. N_2 Tube Trailer
10. N_2 Generator/Compressor
11. Propane Tank
12. Auxiliary Air Compressor
13. Nat. Gas Compressor
14. Desulfurizer
15. Elec. Cabinets
16. UPS Shed
17. H_2 Generator/Compressor and Gas Mixer
18. Water Storage Tank
19. Startup Boiler
20. Control/Meeting Room

Figure 3.2 — Power system site arrangement.

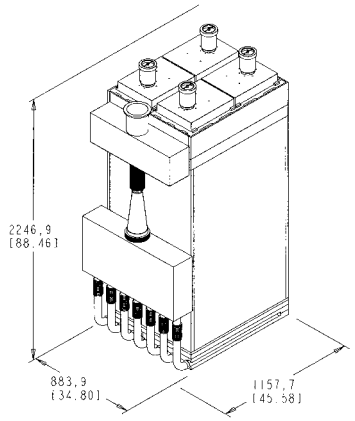

mm (in.)

Figure 3.3 — Basic stack building block is the 576-cell substack.

3.1.3 Power System Performance Analysis

3.1.3.1 Analysis Basis

Basic input for the analysis such as fuel composition, fuel supply conditions, and ambient-air conditions were taken from the design requirements, Section 3.1. Additional information on key input is provided in the following:

- Cell V-I characteristic – the V-I characteristic is graphed in Figure 3.4. It is a projected characteristic for the mature SOFC product that will be available in 2005 to 2010. The V-I characteristic applies to operation at 1 atm (abs), 85% fuel utilization, and to a peak cell temperature of 1020°C (1870°F).

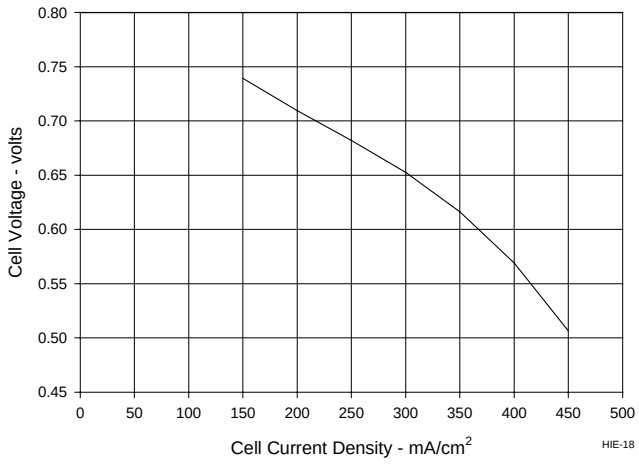

Figure 3.4 — Cell V-I characteristic.

- Cell voltage correction for SOFC generator operation at elevated pressure – A cell voltage adjustment for operation at pressures above 1 atm (abs) is presented in Figure 3.5. Given an operating pressure, the corresponding voltage adjustment is added to the base cell voltage from Figure 3.4. Data for Figure 3.5 were obtained from cell testing (Test No. 503) performed at Ontario Hydro Technologies (OHT) in Toronto, Ontario, Canada by OHT personnel. The test article was designed and supplied by Siemens Westinghouse. The tests covered the pressure range from 1 atm (abs) to 15 atm (abs). Over the cell current density range of interest in this conceptual design study, the adjustment for pressure is essentially independent of current density.

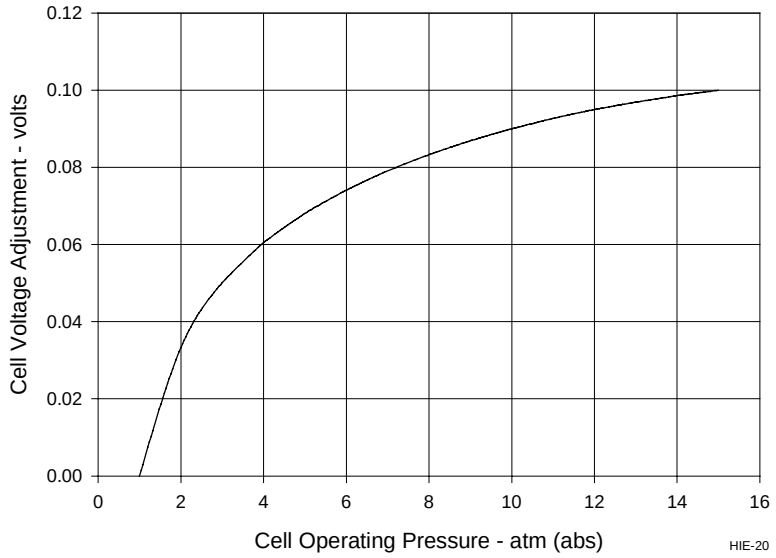

Figure 3.5 — Cell voltage adjustment for pressure.

- Stoichs profile – air flow to the HP SOFC generator is determined by the stoichs profile that is graphed in Figure 3.6. Its application results in cell operation with a peak cell temperature of 1020°C (1870°F) and a generator combustion zone exhaust temperature of approximately 870°C (1600°F). One stoich provides the normal-air flow needed to supply oxygen for the cell electrochemical process. A generator air flow based upon multiple stoichs provides the required amount of oxygen for that process, and it flattens the cell axial temperature distribution, thereby raising the cell average temperature. From energy balance considerations, and given a set combustion zone exhaust temperature, the generator air inlet temperature increases with decreasing cell current.
- Electrochemical fuel utilization – generator fuel consumption was set at 90%, meaning 90% of the fuel admitted to the SOFC generator was consumed electrochemically on the cell active surface and by the ionic and molecular leakage of oxygen from the cathode side of the cell to the anode. Approximately 89% of the generator fuel is consumed electrochemically.

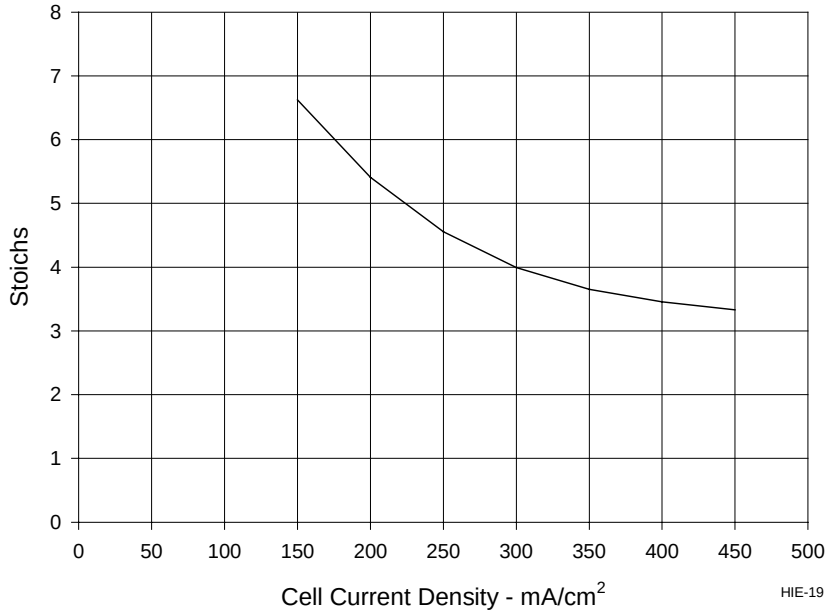

Figure 3.6 — Stoichs profile.

- SOFC power conditioning system efficiency – the development of a power-conditioning concept was not a task in this project. For the performance estimates, the power conditioning efficiency was assumed to be 94%. This value covers system losses from the SOFC DC terminals to the utility AC grid.
- Gas turbine generator efficiency – 96%.
- Gas turbine compressor isentropic efficiency – 86.4%.
- HP turbine isentropic efficiency – 90.7%.
- LP turbine is isentropic efficiency – 91.3%
- Auxiliary power losses – 125 kWe [I&C, cabinet ventilation, and intercooler heat rejection (water circulation and forced-air fan power)].

3.1.3.2 Power System Performance Estimates

Power system design-point performance has been analyzed; results are summarized in Table 3.1.

Table 3.1 — Power System Design-Point Performance Estimates

Compressor air intake rate	18.1 kg/s
Compressor pressure ratio	7:1
HP SOFC generator DC power	9.0 MWe
LP SOFC generator DC power	7.5 MWe
SOFC gross AC power	15.6 MWe
Compressor shaft power	4.1 MW
HP turbine shaft power	3.4 MW
LP turbine shaft power	4.9 MW
Gas turbine gross AC power	4.1 MWe
Power system net AC power	19.0 MWe
Fuel flow rate to power system	0.62 kg/s
Efficiency (net AC/LHV)	67.3%
Carbon dioxide emission	300 kg/MWh
Nitrogen oxide emission (based on 1.0 ppm_v)	0.006 kg/MWh
Exhaust flow rate	18.7 kg/s

Corresponding to the operating point represented in Table 3.1, and for the points identified in Figure 3.7, estimates of cycle statepoint parameters are provided in Table 3.2.

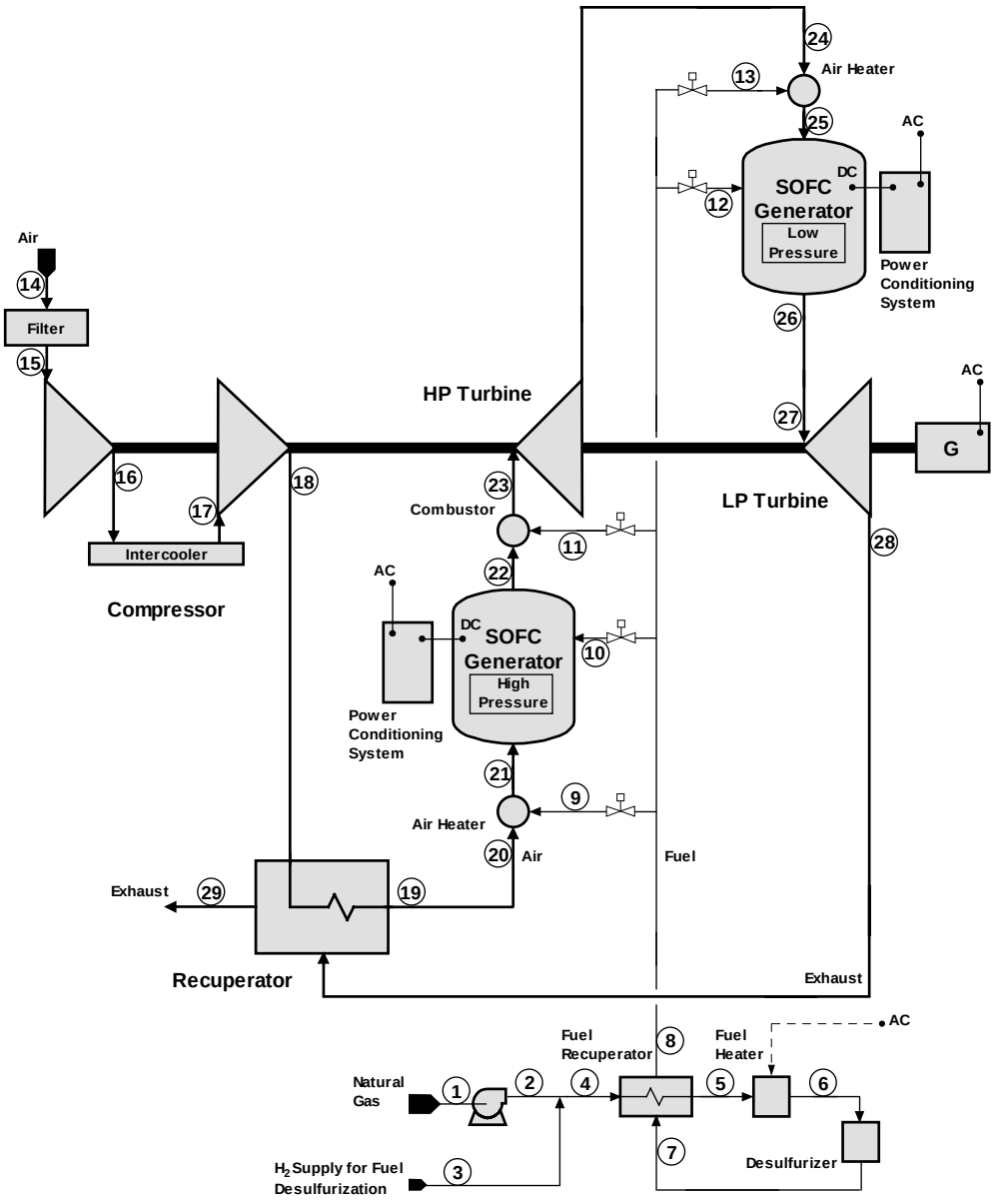

Figure 3.7 — Power system state point diagram.

Table 3.2 — Power System Statepoint Parameter Estimates

Statepoint ID	Mass Flow, kg/h	Temperature, °C	Pressure, bara	Molecular Weight	Enthalpy Flux, MW
1	2,224	15	2.05	16.8	-0.014
2	2,224	187	10.14	16.8	0.249
3	3	15	10.14	2.0	
4	2,226	187		16.7	0.249
5	2,226	378		16.7	0.609
6	2,226	399		16.7	0.653
7	2,226	399		16.7	0.653
8	2,226	208		16.7	-0.058
9	0				0.000
10	1,248	93		16.7	0.056
11	0				0.000
12	978	93		16.7	0.044
13	0				0.000
14	65,285	15	1.01	28.8	-0.182
15	65,285	15	1.01	28.8	-0.182
16	65,285	125	2.75	28.8	1.834
17	64,959	24	2.59	28.8	-0.021
18	64,959	137	7.06	28.8	2.048
19	63,980	608		28.8	11.056
20	63,980	603		28.8	10.956
21	63,980	603		28.8	10.956
22	65,228	876		28.4	17.578
23	65,228	871	6.34	28.4	17.466
24	65,718	703	3.17	28.4	13.862
25	65,718	703		28.4	13.862
26	66,695	875		28.1	18.465
27	66,695	870	2.82	28.1	18.347
28	67,185	647	1.07	28.1	13.281
29	67,185	225	1.01	28.1	4.029

3.1.3.3 Discussion

Power System Efficiency. The predicted power system efficiency (67.3%) is 2.7 points less than the 70% project target. However, it appears the target could be reached through improvements in the performance of the fuel desulfurization and SOFC power conditioning systems, combined with the generation of additional power by a small steam turbine generator; steam for the turbine would be produced via the recovery of heat at the recuperator exhaust. In the reference HEFPP power system design, the fuel desulfurization system uses hot catalysis and sorbent beds in which temperature is

maintained with the aid of a parasitic electric heat input, and for which a small hydrogen stream produced by the electrolysis of water (also needing power input) is required. Eliminating both parasitics through the application of an effective ambient-temperature fuel desulfurization process, and one needing no hydrogen input, would increase the system net AC power output by 200 kWe, and the system net AC efficiency by one-half of one percentage point.

Concerning the SOFC power conditioning system (PCS), and as noted in Section 3.1.3.1, the power system performance estimates assumed a PCS DC-to-AC-grid efficiency of 94%. A one-point increase in that efficiency, achieved through engineering development of the PCS technology, would increase the power system output by approximately 160 kWe, producing an increase in system efficiency of approximately six-tenths of one percentage point.

Relative to steam turbine power, the heat available for steam generation at the recuperator exhaust is of low grade, and the steam pressure that could be developed for effective use would be low, probably 5.5 barg to 7.0 barg. Nonetheless, if it were done, and assuming a 25% steam turbine cycle efficiency, it would be possible to generate 360 kWe of additional AC power output.

The individual and combined effects of these component improvements and cycle modifications (i.e., application of low-temperature, zero-H_2 desulfurization technology; use of a higher-efficiency PCS; and the generation of steam turbine power) are graphed in Figure 3.8. Combining them, it appears that the 70% efficiency goal is achievable. A complete evaluation of the effects must be done that considers cost and maintenance effects as well as the performance benefits. This has not been done in the present study for these particular system refinements, and it is an area for further work. It is noted in particular that the steam cycle would add complexity and maintenance needs to the power system, and these will have to be weighed carefully against the benefit gained. A distinct advantage of the reference system concept is that it is dry; as a result, it involves none of the maintenance demands related to water treatment, corrosion, etc, and it imposes no on-site operator requirements that are frequently associated with pressurized, steam-related systems.

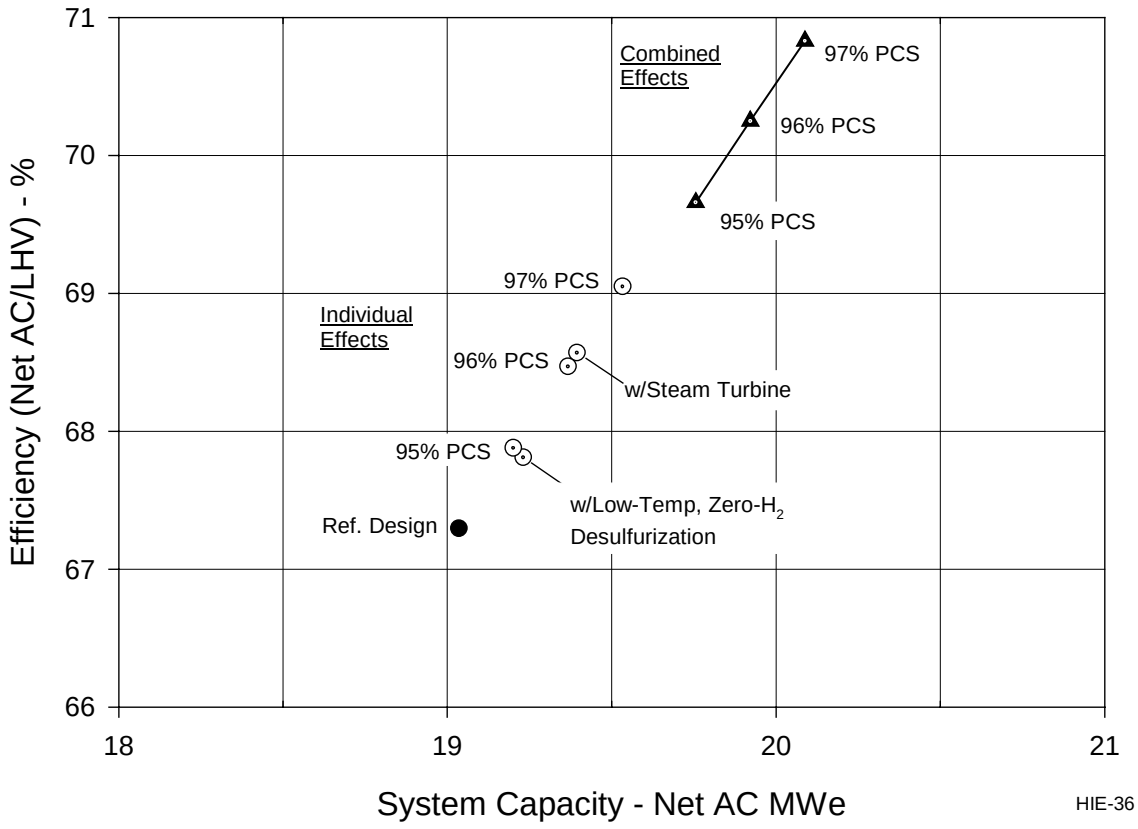

Figure 3.8 — Power system performance sensitivities.

Elevated SOFC Generator Operating Pressure. As indicated earlier, the HEFPP SOFC generator design utilizes the conventional generator configuration, and in addition, the design assumes the uniform distribution of air flow between cells, and the uniform distribution of reformed-fuel flow on the cell anode side. In the conventional generator configuration, fuel flows upwards along the cell exterior surfaces (anodes) in the system of communicating parallel flow channels that is defined by the anodes. That this configuration is suitable for atmospheric-pressure generators has been confirmed via current and past field unit demonstrations, and a pressurized bundle at three atmospheres pressure has also exhibited good, stable performance. However, it is not known with certainty that this parallel flow channel configuration is suitable for higher pressure SOFC generators. Flow channel pressure drop is determined by friction and buoyancy components. At low pressures, the friction component, varying inversely with gas density, and hence with pressure, is dominant, and the buoyancy effects of modest channel-to-channel temperature or composition variations are of little conse-

quence. However, at elevated operating pressures, the buoyancy effect, being proportional to density differences, has more influence, while the friction pressure drop component, with its inverse pressure relationship, is diminished. At higher pressure (P >3 atm) transverse channel-to-channel parameter variations could affect parallel-channel flow stability, and this is of special concern considering the density of the oxidation product stream that exits the channels at the top will be larger than the density of the reformed fuel stream that enters at the bottom. It is therefore clear that cell-stack thermal and hydraulic interactions need to be well understood, particularly relative to stack operation at elevated pressure levels. A very reasonable first step in developing this understanding would be to undertake a detailed analytical evaluation of the anode-side flow field and of the effect of operating pressure on that field.

3.1.4 Power Plant and Site Arrangement

Power system pictorial and plan views are presented in Figure 3.9 and Figure 3.10.

The arrangement includes a trailer mounted control/meeting room with sanitary facilities and four-space parking area, a storage shed, a 20 MW substation/switchyard, two fire hydrants, intake air filter house and the BOP equipment block. The BOP equipment block is shown between the control trailer and switchyard. The BOP equipment block is comprised of several equipment, component and electrical skids. Each skid is mounted to a dedicated concrete pad or foundation. The various skids are in weather-proof enclosures:

- Electrical cabinets
- Water storage tank/pump skid
- Packaged startup boiler
- Auxiliary air compressor with dual fuel engine
- Propane tank
- Natural gas compressor and accumulator

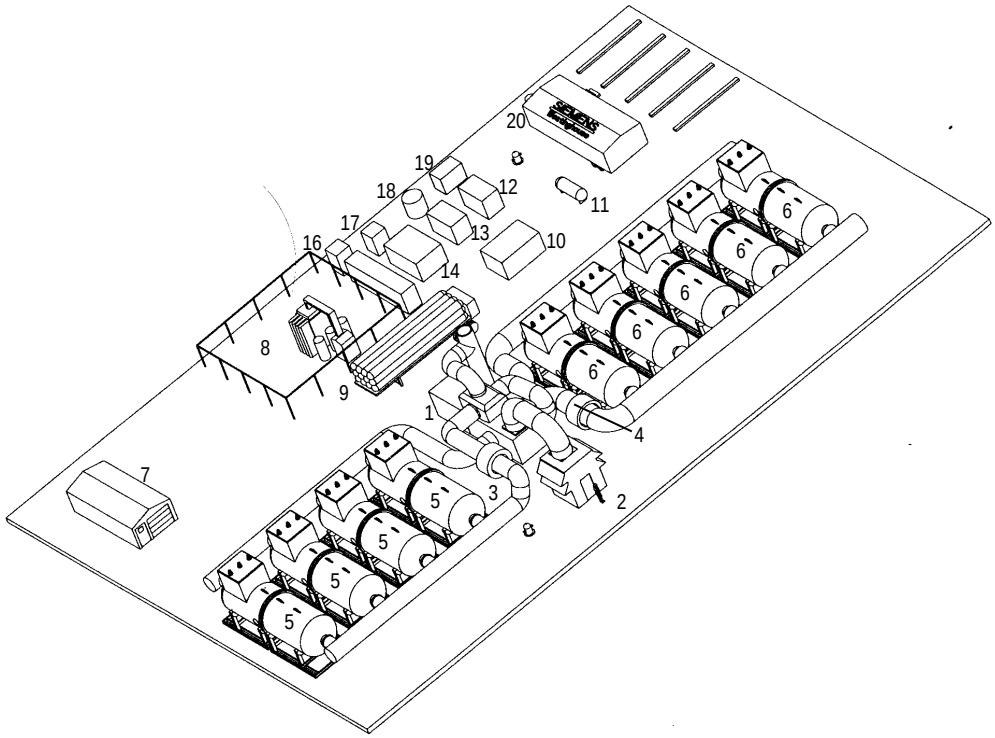

Key:
1. GT Skid
2. Filter House
3. HP Air Heater
4. LP Air Heater
5. HP SOFC Vessel
6. LP SOFC Vessel
7. Storage Shed
8. 20 MW Substation
9. N_2 Tube Trailer
10. N_2 Generator/Compressor
11. Propane Tank
12. Auxiliary Air Compressor
13. Nat. Gas Compressor
14. Desulfurizer
15. Elec. Cabinets
16. UPS Shed
17. H_2 Generator/Compressor and Gas Mixer
18. Water Storage Tank
19. Startup Boiler
20. Control/Meeting Room

Figure 3.9 — Power System Arrangement — Isometric View.

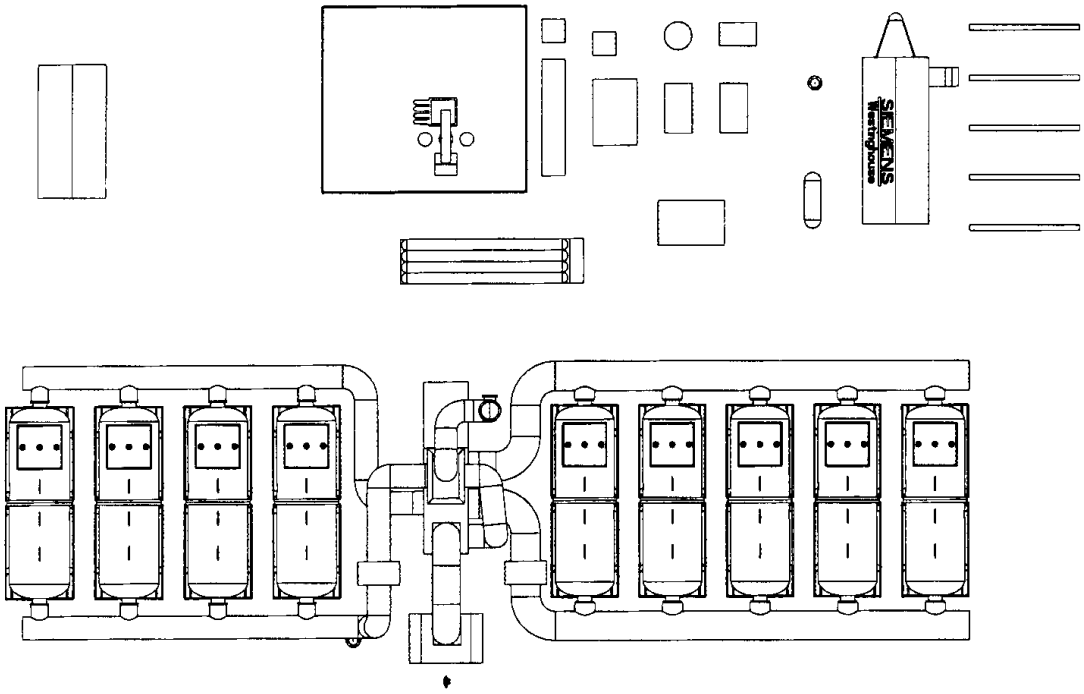

Figure 3.10 — Power System Arrangement — plan view.

- Natural gas desulfurizer
- Pressurized nitrogen storage cylinders
- Nitrogen generator and compressor
- Hydrogen generator, compressor and gas mixing equipment

Not shown are the security fence and its gates around the perimeter or any storm water drainage features. These features will generally be site specific. The overhead high voltage power lines and their poles from the SOFC vessels and GT skid are also not shown.

For this study it is presumed that direct access to the site is via paved roadway capable of bearing the loads from the heaviest items [GT skid weight is 29,000 Kg (64,000 lb), and the SOFC vessel half weight with internals is 25,400 Kg (56,000 lb)]. The site must also have direct connections to natural gas, city water, sanitary sewer, telephone and electric power. The sites, as shown, do not allow for sanitary sewer drain fields or wells for water.

To minimize field construction, each SOFC vessel half with SOFC stacks installed is factory fabricated on a transportable trailer/skid. This foundation trailer is field mated with the trailer bearing the other half of the SOFC vessel. After proper alignment of the vessel/trailer halves, the trailers are blocked and the wheels removed. In the event that a vessel half is to be returned to the factory for maintenance or repair, the wheels can be reinstalled on the foundation trailer, the blocks removed and the trailer towed away.

Access to the switchyard is available on three sides and the BOP equipment block also has fork truck clearance between skids. The process piping is factory-fabricated, internally-insulated, flanged sections. Where possible, externally-jacketed thermal insulation is applied at the factory to minimize field construction. These sections are relatively large and heavy, varying from about 1000 kg per meter (750 pounds per linear foot) to more than 2500 kg per meter (1700 pounds per foot). They are assembled on site by landing them on their pipe supports and bolting together the gasketed, flanged joints. Thermal expansion joints are provided between significant runs of piping as needed. The plant arrangement drawings do not show the detail of the flanged joints in the process piping or the pipe supports.

The arrangement uses SOFC pressure vessels with process air entry and exhaust exit at opposite ends. This vessel and internal SOFC stack is the easiest design. The pneumatic balancing for equal distribution of air to the cells is straightforward. The significant consequence of the vessel with nozzles on both ends is the need to use a relatively large quantity of large diameter, internally and externally insulated piping. This plant occupies the largest amount of ground of the three arrangements studied (see Section 3.4.3). The plot shown is 61 m (200 ft) by 41 m (134 ft), or 0.6 acres.

The SOFC generator modules are accessible from each end, and there is space for a vehicle access road at each end. Access for inspection, repair or maintenance is good. Routing of high voltage electric power lines from the SOFC vessels to the switchyard is efficient. The DC power generated in each vessel is routed through thermally and electrically insulated feedthroughs directly into a top-mounted package containing a DC to AC inverter with step-up transformer. The inverter/transformer package is mounted onto each pressure vessel at the site. Shipping restrictions prevent installation of this electrical equipment at the factory. The top of the inverter/transformer package terminates with three standard high voltage insulators. The three phase 13.8 kV high voltage lines rise from the inverter/transformer package and connect to their respective phase feeder lines. These feeder lines run overhead to the switchyard.

3.2 Systems and Components

A simplified process diagram that identifies systems and components is presented in Figure 3.11. In this process diagram only one vessel of four is shown on the HP side of the plant and one vessel of five is shown on the LP side. The distribution of air and fuel within the vessels has not been shown, but is alluded to by the flow arrows branching from lines inside the vessels.

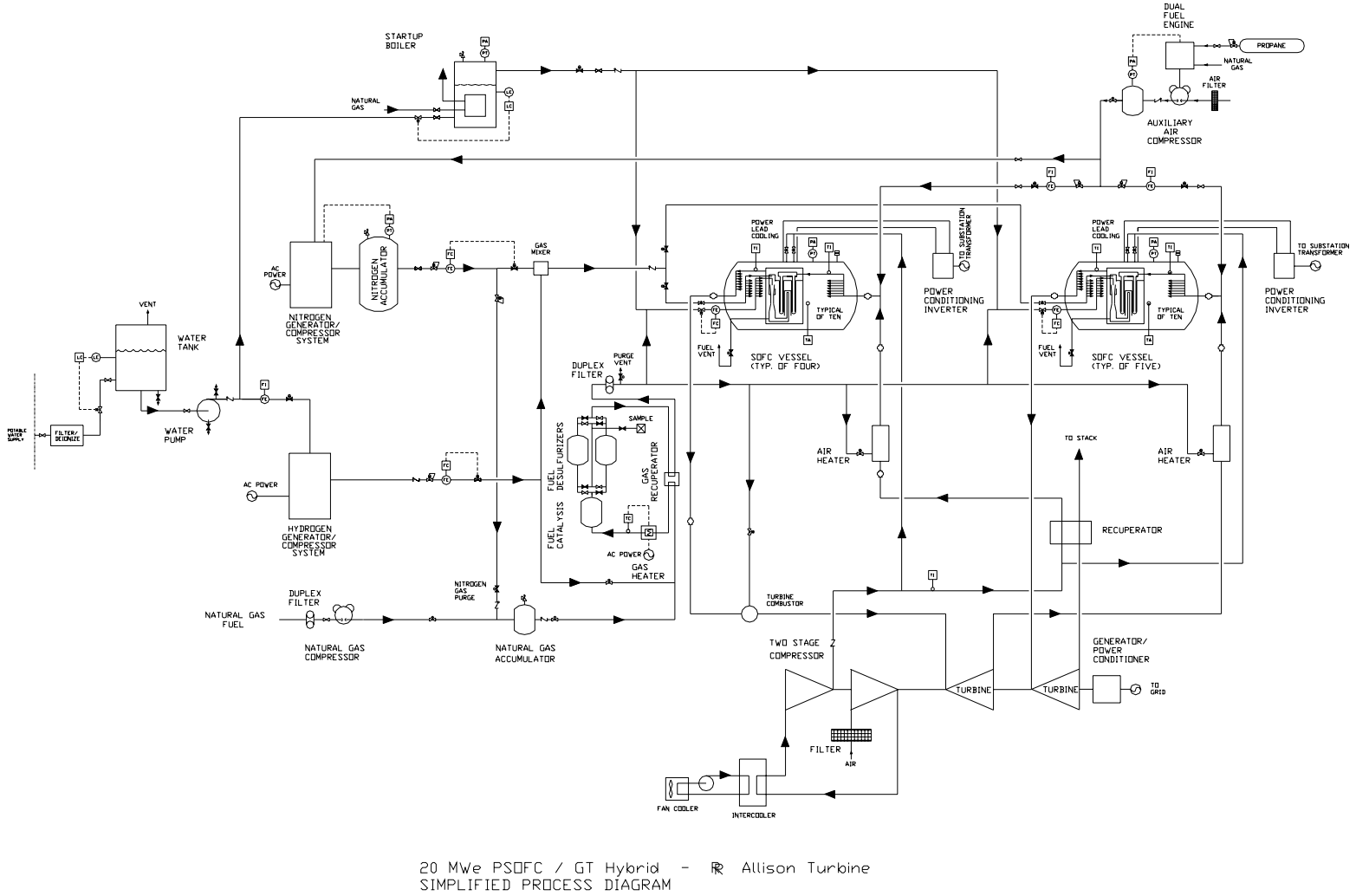

Figure 3.11 — 20 MW_e PSOFC/GT Hybrid Simplified Process Flow Diagram.

3.2.1 SOFC Generator

3.2.1.1 Staged-Cell Generator Concept Evaluation

Two separate analyses were made to evaluate the staged fuel cross-flow stack concept. The original analysis was the coupled thermal/electrochemical model and applied specifically to the tubular SOFC geometry. This analysis and its results are summarized below. The isothermal model was created to independently verify that the benefits of staging were much smaller than had been anticipated. The isothermal model is general and is not limited to a particular cell or stack geometry. The isothermal model is presented in the Appendix. The results of the two analyses are combined in the summary at the end of this section. The analytical models consider an SOFC bundle row consisting of four bundles, each bundle consists of a three-cell-in-parallel by eight-cells-in-series array. The bundle row is flanked by in-stack reformers.

3.2.1.1.1 Coupled Analysis of the Staged Fuel Cross-flow Stack

This section gives an overview of the coupled cell/stack analysis model used to evaluate the staged fuel cross-flow stack. The model was based on cross-flow of fuel through four bundles in series. Thus, fuel passes sequentially across a total of 32 cells. The cross flow stack analysis model was developed for a stack that would replace a conventional stack that has axial fuel flow. The staged-cell stack has recirculated fuel and is coupled to the in-stack reformer board (SRB) assembly positioned between each pair of bundle rows. Thus the cell configuration of the stack remains essentially unchanged, with the exception that fuel flows in at one side, through the stack, and exits on the other side. From there the fuel passes back through the recirculation zone to the inlet side of the stack where it is mixed with fuel feed and pre-reformed. The exhaust portion of the spent fuel exits to the combustion zone as it passes through the recirculation zone. A side view of the fuel flow through the stack and SRBs is shown in Figure 3.12.

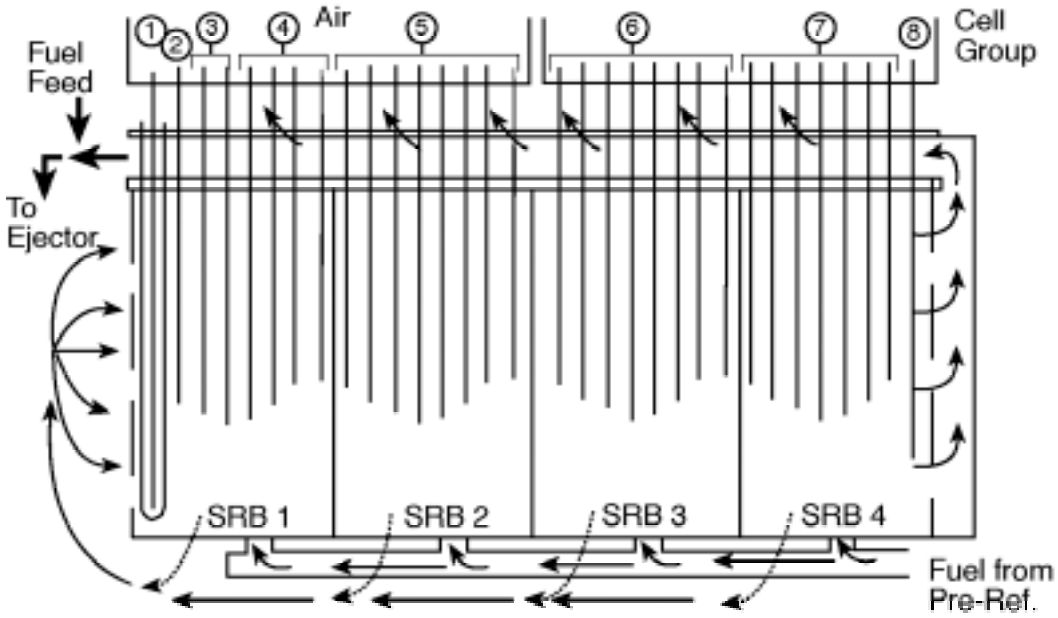

Figure 3.12 — Staged-Cell Generator Concept.

The model is a fully coupled heat transfer, mass transfer, and electrochemical analysis. Local temperatures are used to evaluate all local properties including thermal conductivity, mass diffusion coefficients, electrical resistivity, and gas transport properties. Local temperatures and concentrations are used to calculate the Nernst potential, cell resistance, polarization losses, and the local current density. Fuel and oxidant streams are depleted based on local current density. Local heat generation includes the excess heat of reaction, Joule and polarization losses, and heating due to O_2 ionic leakage through the cell. Heat transfer coefficients are also based on properties evaluated at local temperatures. Radiation heat transfer is calculated based on the fourth power law. For all models that include an SRB, the temperature and the heat flux from the cell are matched with the temperature and the heat flux to the SRB. The reformation model of the SRB satisfies heat transfer, mass diffusion, reaction rate and chemical equilibrium conditions.

The development of the analysis model for the cross flow stack is based on a similar model that has been used for the conventional stack. To include a number of stages, the number of axial segments per stage between the closed end of the cell and the fuel recirculation zone was reduced to 20. Further, it was decided to divide the 32 cell stages into groups of cells. The cells in each group would be represented by the condi-

tions at the center cell of the group. The group arrangement selected is shown in Figure 3.12. To provide detail at the inlet fuel side of the stack, the first two groups include only one cell each. The third group includes 2 cells, the fourth group includes 4 cells, and the fifth and the sixth groups include 8 cells each. The seventh and eighth groups include seven cells and one cell, respectively. Note that the bundle and SRB boundaries coincide with group boundaries. This was required to simplify the coupling of the SRBs and the cells.

The initial results from the staged configuration analysis were disappointing. The problems can be described as follows.

1. The first cell row (at the fuel inlet) was too cold and final cell rows were too hot. This is a consequence of the large flow of relatively cold fuel that impacts directly onto the first stage or the first cell row. The latter cell rows become hotter as the fuel temperature increases and cell losses increase as fuel is depleted.

2. The overall temperature uniformity was poor. This is a result of the combination of the superposition of the row to row temperature distribution on the axial temperature distribution. The overall non-uniformity is the sum of the two.

3. The fuel concentration becomes non-uniform in the latter cell rows. The fuel is consumed at a higher rate at the hotter portions of the cell due to the lower local cell resistance. After passing a number of cell rows, the fuel becomes depleted in the central region of the cells. To preclude anode oxidation, the average fuel utilization at bundle row exit must be comparable to that for an axial-flow cell stack — a higher fuel utilization is not feasible.

4. The average cell voltage was lower than for an axial flow stack due to the lower overall average temperature.

Several modifications were made to the model stack to address the issues of temperature uniformity.

1. The inserts normally used to enhance heat transfer within the combustion zone region were removed from the air feed tubes in the last three cell bundles (24 cell rows). Removal of the inserts results in reduced pressure drop which acts to increase the cooling flow of air to the last 24 cell rows relative to the cooling flow to the first 8 cell rows. Removal of inserts also reduces the pre-heating of cooling air to the last 24 cell rows, thereby lowering their temperature relative to the inlet cell rows.

2. The fuel flow to the SRB adjacent to the first cell bundle was restricted by an orifice. This reduces the cooling of the first 8 cell rows at the inlet side of the

stack. It also increases cooling of the last cell rows by shifting the reformation heat load toward the exit side of the stack.

3.2.1.1.2 Results of Coupled Analysis of Staged-Cell Stack

Analysis results for the staged-cell stack with the modifications listed above are shown in Figure 3.13, Figure 3.14, and Figure 3.15. The cell current was 253 A/cell corresponding to a current density of 304 mA/cm^2. Air inlet temperature was selected to give a maximum local cell temperature of 1020°C (1870°F). The temperature distributions of the cells at the center of each of the 8 cell groups are shown in Figure 3.13. Figure 3.14 displays the average cell temperature and the terminal voltage as a function of the cell row position. The fuel concentration profiles at the exit of the 8 cell groups are shown in Figure 3.15.

The stack model modifications made significant improvements in the stack temperature uniformity, but the predicted performance of the cross-flow stack was still lower than for a conventional stack with the same maximum temperature limit. This result was obtained although several idealistic assumptions were made for the analysis which enhance performance relative to what would actually be expected. These assumptions included

1. The lateral heat losses at fuel inlet and exit were neglected. This would further reduce temperature of the first cell rows.

2. It was assumed that the fuel mass flow rate was uniform per unit axial length of the cell and bypass of fuel at the inactive ends of the cells was neglected. Actual fuel flow through the central portions of the cells would be reduced due to the effect of higher temperature by the combined effects of low density and high viscosity. This is the same elevation where the current density — hence, fuel consumption, is higher than the average rate.

3. The influence of dimensional tolerances on fuel flow distributions was ignored. The actual fuel flow distribution would be sensitive to the lateral spacing between cells and to the cell-to-SRB gap.

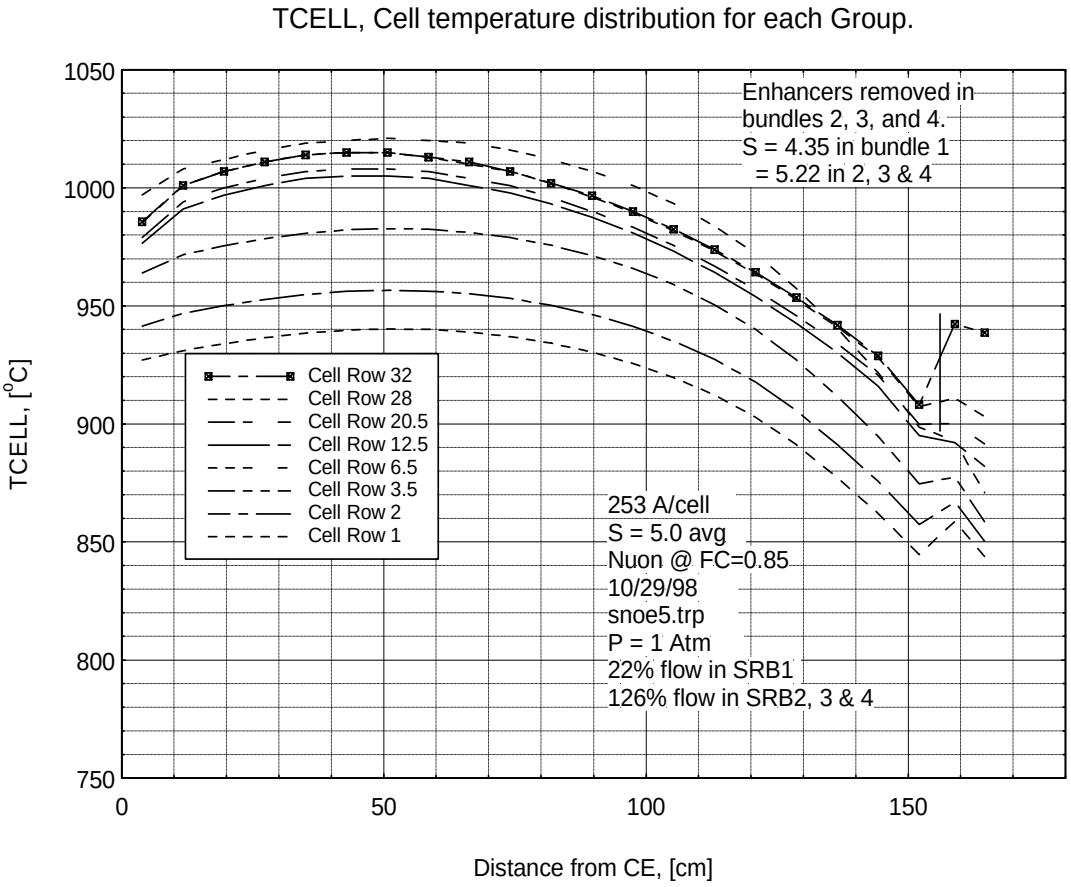

Figure 3.13 — Temperature Profiles in Staged-Cell Generator.

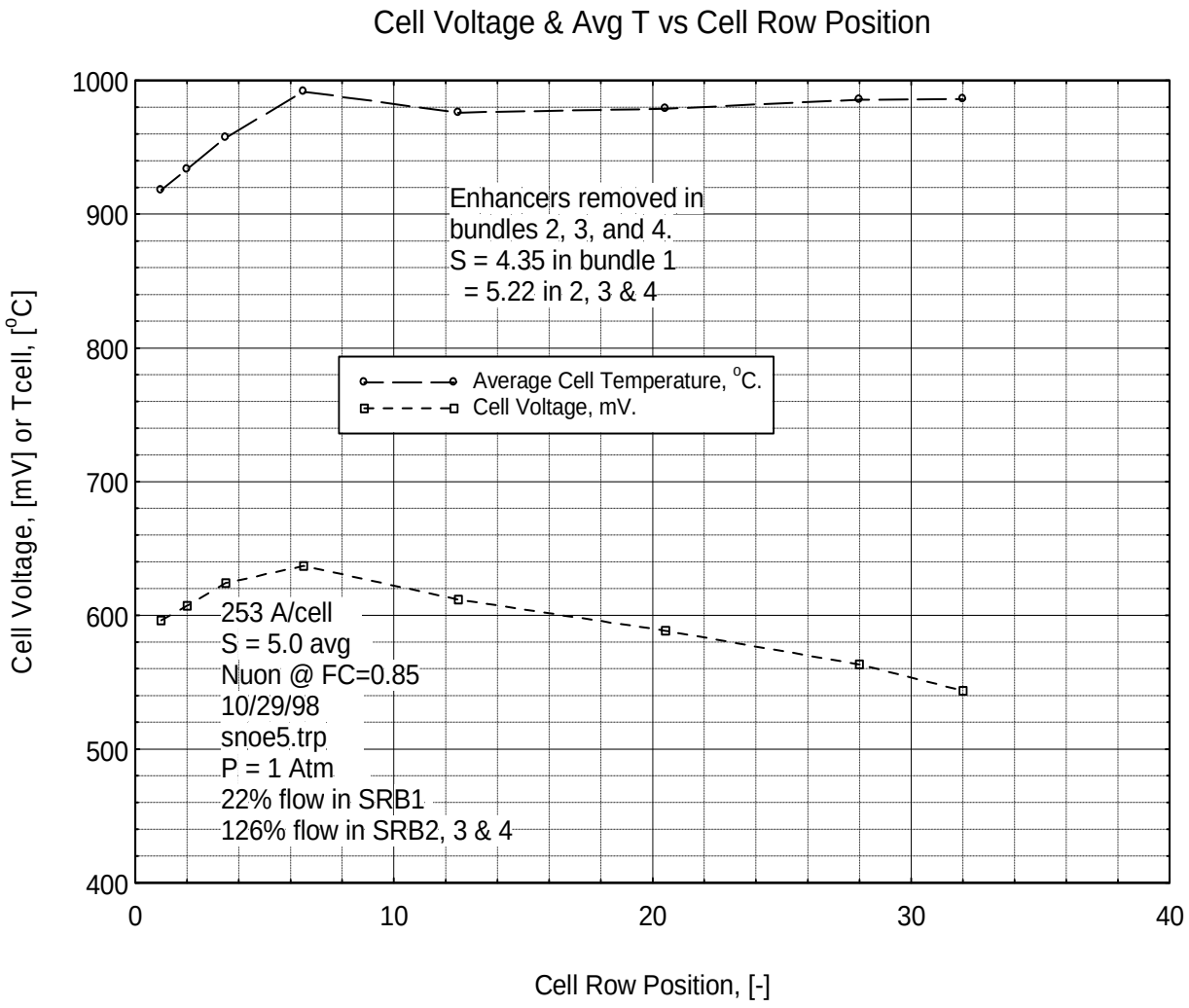

Figure 3.14 — Cell Voltage and Average Temperature in a Staged-Cell Generator.

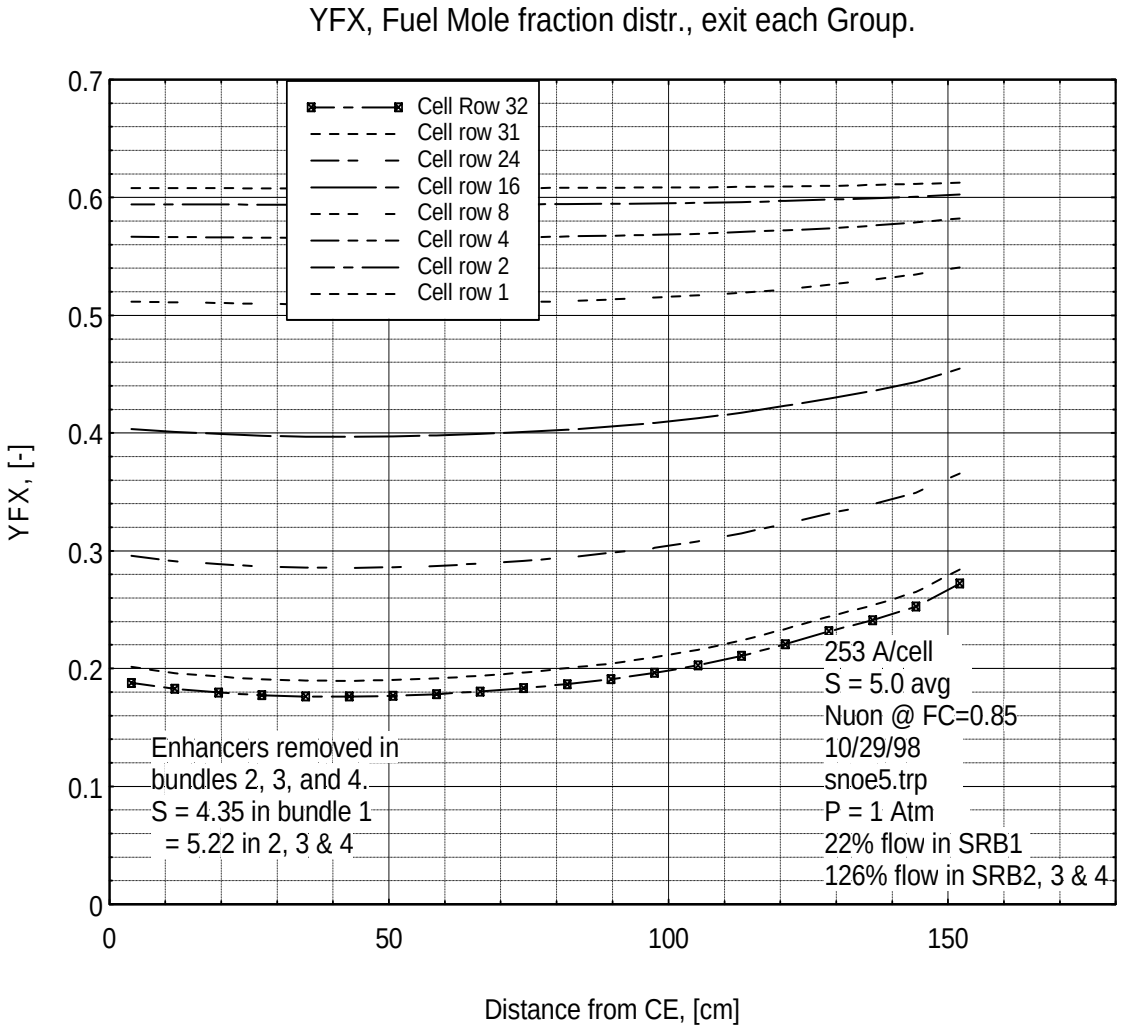

Figure 3.15 — Fuel Mole Fraction Distribution in a Staged-Cell Generator.

Even with these assumptions, the fuel utilization in the staged cell design is limited due to the non-uniform consumption of fuel as it passes each cell. The fuel concentration at the exits of each stage at 92% fuel utilization is shown in Figure 3.16. In Figure 3.17, the partial pressure of O_2 at the fuel electrode is compared to the equilibrium partial pressure of O_2 for the Ni/NiO/O_2 reaction. The comparison is made for the exit stage cell. Oxidation of the fuel electrode is likely whenever the O_2 pressure is within two orders of magnitude of the equilibrium pressure. It is seen that this limit is exceeded for much of the cell length (data points are equally spaced).

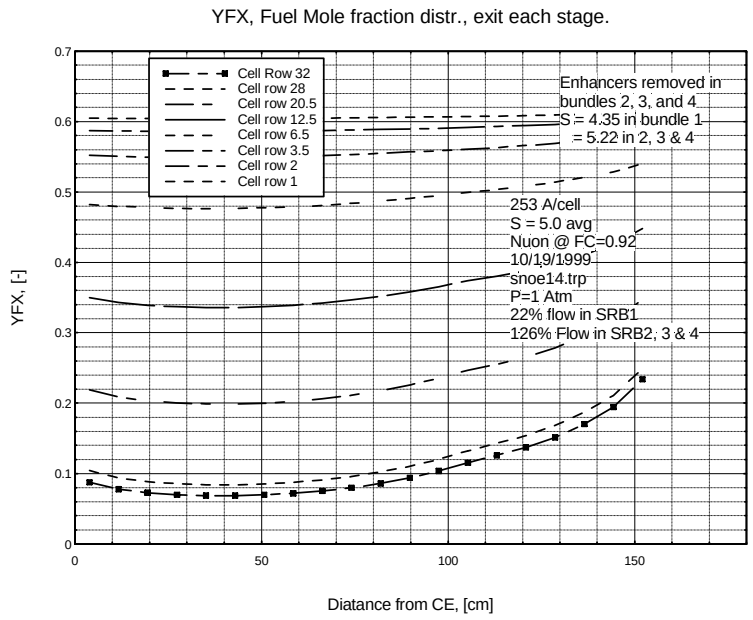

Figure 3.16 — Fuel Concentration at the exit of each group of cells.

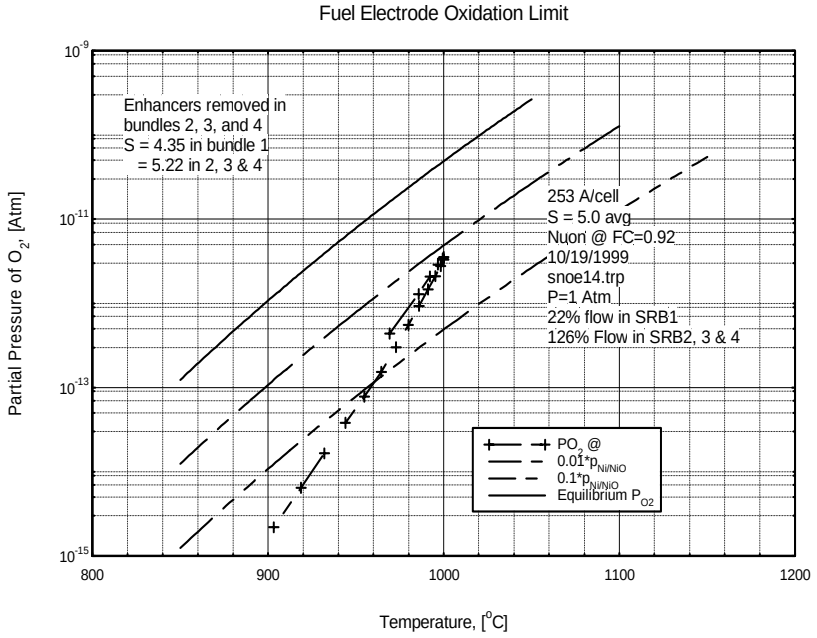

Figure 3.17 — Nickel Fuel Electrode Oxidation Limit – Cross Flow Stack at FU = 92%.

3.2.1.1.3 Summary of Staged-Cell Generator Concept Evaluation

The conclusion from the isothermal model analysis in the Appendix is that there is only a small improvement in stack efficiency available due to cell staging at current densities near the point of maximum power. At the maximum power point, the improvement in power output due to staging is less than 0.6% for 85% fuel utilization, and less than 1.2% for 95% fuel utilization.

In the coupled model analysis the small benefits of staging were eroded by the effects of fuel cross flow on the overall stack temperature distribution. The inlet fuel for 32 cells impinges on each of the cells in sequence. This high flow of relatively cold fuel removes several times more heat from the first cell row than is generated. Radiation from the neighboring rows provides a large amount of heat but it is insufficient to achieve satisfactory temperatures in the first rows. A way to improve the effects of cold fuel would be to heat the fuel exiting from the SRBs. We were unable to find a reasonable way to effect heat exchange between the inlet fuel and a hotter exhaust stream without incurring significant pressure drops and complicating the stack design.

The previously assumed benefit of higher fuel utilization with a staged-cell concept was not available due to uneven consumption of fuel in the direction perpendicular to the fuel flow. Fuel was locally depleted to the point of fuel electrode oxidation before the fuel utilization reached 95% even with the optimistic fuel flow distribution assumptions used in the model. Due to this effect and to the cool-cell effect in the fuel-entry rows, it was concluded that the SOFC generator module design should retain the conventional co-current fuel flow and air flow configuration.

3.2.1.2 SOFC Generator Design Description

Much of the HEFPP/SOFC Generator system design philosophy and implementation is influenced by technology derived from two sources: the conventional 100 kWe SOFC generator operating at atmospheric pressure and the pressurized SOFC generator in the 220 kWe hybrid cycle power system which is designed to operate at 3 atmospheres.

The generator submodule design philosophy is an extrapolation of the current 200 kW SOFC Generator configuration with the exception that the stacks are housed in a hori-

zontal pressure vessel. Each stack assembly is installed on a common removable support structure lined with high performance thermal insulation.

This configuration greatly simplifies assembly of internal components by utilizing common parts and a modular, reusable insulation system.

The design basis for the HEFPP SOFC Power Generation System is the air electrode supported (AES) fuel cell derived from the porous support tube (PST) cell. To date, PST test cells have achieved over 65,000 hours of operation. The AES fuel cell operating and durability history of over 32,000 hours reflects an improved design with significant advancements in material composition and processing.

Figure 3.18 shows a simplified array of closed tubular cells composed of concentric electrodes separated by a layer of solid electrolyte. Fuel for the electrochemical reaction flows upward between the tube exteriors, while process air flows upwards in the annular space between the air feed tube and the cell inner surface. Unreacted or spent fuel is burned above the bundles of tubes to preheat the incoming air. Nickel felt contacts provide flexible electrical connections between cells.

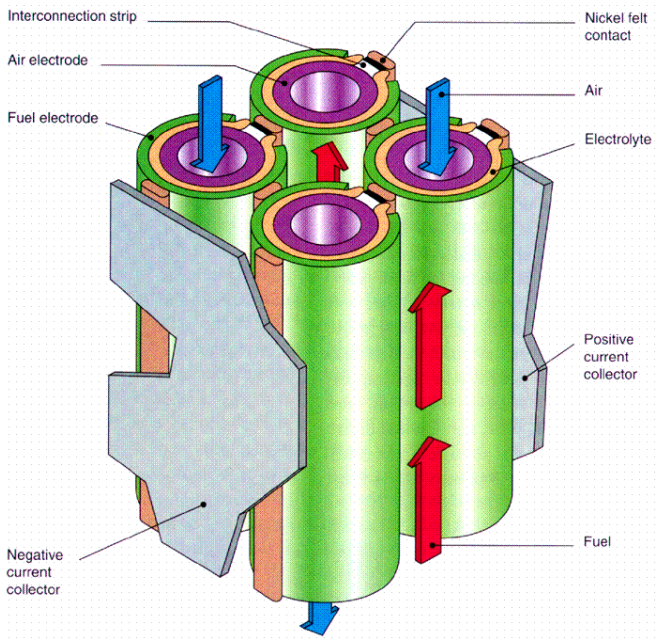

Figure 3.18 — Schematic fuel cell array.

Each substack contains 576, 22 mm OD, 1500 mm active length tubular fuel cells, each generating over 200 watts, arranged in 6 bundle rows. The cells are arranged in three parallel paths for improved reliability.

The submodule configuration is depicted in Figure 3.19. As shown, it includes ten fuel cell substacks, each fueled at the base by a fuel prereformer with integral fuel distribution manifolds and recirculation plenum, air manifold, DC power leads and stack internal insulation.

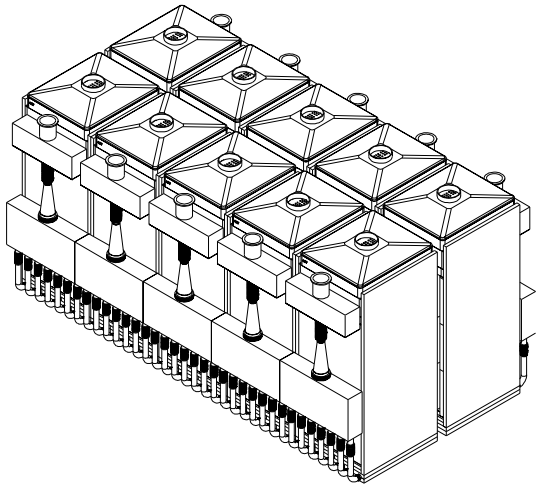

Figure 3.19 — Ten substacks isometric view.

Each substack is fed from a fuel supply system including a recirculation loop, ejectors, a prereformer and a fuel manifold with riser tubes. The recirculation plenum is used to mix the depleted fuel extracted from the stack with the fresh incoming fuel injected through an ejector nozzle. The mixture is then directed to a prereformer chamber where higher hydrocarbons are reformed to prevent carbon deposition in the stack reformers where full reformation of methane occurs. From the prereformer exit, the fuel mixture is distributed to each stack through a series of 7 bottom manifolds.

Process air is introduced into the submodule through one inlet nozzle connected to a centrally located air duct branching to individual smaller ducts feeding a large air plenum located on top of each stack. Each air plenum supplies air to 576 adjacent cells through ceramic air feed tubes. Air flows from the air plenum into the air feed tubes, which convey the oxidant to the lower, closed-end of each fuel cell.

Exhaust from the substack is collected from side manifolds and ducted through larger side ducts terminating in a common transition fitting connected to the pressure vessel exhaust nozzle.

Fuel Cell Substack. The tubular SOFC cell features a porous air electrode made of doped lanthanum manganite ceramic material. A gas-tight electrolyte layer of yttria-stabilized zirconia covers the air electrode, with the exception of an axial strip along the entire active length of the cell. This strip of bare air electrode material is covered by a thin, dense layer of doped lanthanum chromite. This layer, known as the cell interconnection, serves as the electric contact area to an adjacent cell or to a power contact. A top layer, the fuel electrode, is a nickel-zirconia cermet and covers the electrolyte surface except in the vicinity of the interconnection.

To construct an electric SOFC generator, individual cells are bundled into an array of electrically connected fuel cells, forming a monolithic structure that constitutes the basic generator stack.

The proposed fuel cell substack consists of a number of bundle arrays of 3x8 cells with an active (interconnection) length of 150 cm (59 in.). The cells are electrically interconnected in three parallel paths, each with 192 cells connected in series.

The three series-connected paths are intermittently connected by parallel shunts to improve reliability and gross electrical performance of the cell substack. An exploded view of the substack, as shown in Figure 3.20, is composed of 6 groups of cells, referred to as bundle rows, separated by electrically insulating in-stack reformers. Each bundle row includes 96 cells (three parallel paths of 32 series-connected cells).

These bundle rows are series-connected in a serpentine configuration and terminate at power take-offs that transfer current to the two opposite power leads. The metallic power leads may be air-cooled to withstand the high temperature environment surrounding the cell substack.

Each fuel cell substack is assembled externally on a common support structure prior to final installation into the pressure vessel.

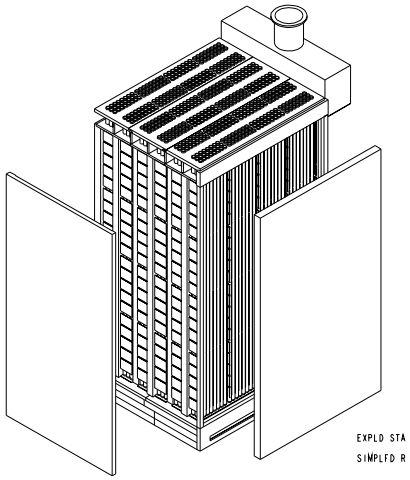

Figure 3.20 — Exploded view of SOFC substack basic building block.

Stack Liner. Each cell substack is enclosed with a liner assembly composed by vertical panels made of Haynes® 214 alloy foil, 0.25 mm (0.010 in.) thick, and each panel is joined full length by resistance or fusion welding process to form four individual subassemblies which are welded at the four corner seams.

The liner assembly incorporates a bottom metallic sealing with the lifting tray and the fuel manifold penetration sealing typical of the 220kW PSOFC design. This type of design minimizes fuel leakage and it provides an effective barrier between the cell substack and the outer insulation made of low purity material.

Each panel includes a layer of "puff" board tiles bonded to the surface facing the substack. "Puff" boards are manufactured from layers of Saffil blanket material saturated with an organic binder and compressed to a 3.2 mm (0.125 in.) thickness to obtain the required density. During generator start up, the organic binder burns off and the Saffil layer is free to expand and fill the volume between the cell stack outer wall and the liner, thus preventing fuel bypass which may occur as a result of foil warpage under high temperature conditions. Each panel includes a series of "puff" board tiles, 305 mm (12 in.) wide, 406 mm (16 in.) high and 3.2 mm (0.125 in.) thick, glued to the stack with an organic adhesive.

Each liner panel includes two edge flexural flanges that are formed to a special shape designed to absorb thermal differential expansion of the panel in the direction normal to the flange length. The contour of the flexural flange is designed so that it achieves

maximum displacement, minimum stress when the panels are welded side by side to form a complete subassembly; these multiple ribs produce a substantial stiffness and load capacity improvement in the direction of the ribs. The ribbed or corrugated sheet basically exhibits one way flexural behavior, since the perpendicular direction retains the properties typical of a flat plate.

Fuel Distribution System. The Fuel Distribution System includes fuel nozzle housing, a recirculation plenum system, ejector, prereformer and an array of tubular manifolds connected to vertical risers penetrating the SRB's assemblies. An isometric view of the Fuel Distribution System is shown in Figure 3.21.

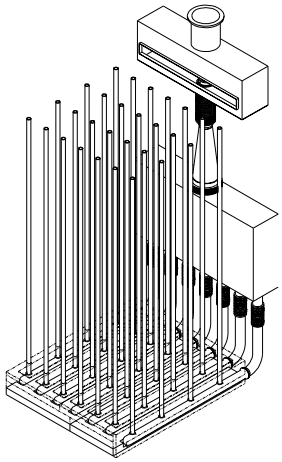

Figure 3.21 — Fuel Distribution System.

Fresh fuel is injected through an ejector nozzle that entrains depleted gas extracted from the upper zone of the fuel cell substack. This fuel mixture is directed to a pre-reforming section where partial reformation occurs within a catalytic bed.

The fuel stream then exits the pre-reformer and is manifolded through a piping network connected to horizontal manifolds installed at the base of the substack. These manifolds are coupled at the periphery of the stack by a quick connect flange assembly.

Each manifold includes a number of vertical risers that direct the fuel to the top of the in-stack reformer internal cavity. The preponderance of fuel reformation occurs in this area and a hydrogen-rich stream is fed at the base of the stack to the exterior of the tubular fuel cells. Complete reformation is finally achieved at the closed end of the fuel cell.

In-Stack Reformers. The in-stack reformer concept was developed to improve the SOFC system efficiency by reducing the airflow pumping requirements necessary to maintain cell axial temperature distributions within an acceptable range. Additionally, lower airflows reduce the required effectiveness (surface area) of the internal and external recuperators.

The SRB concept provides a large surface area for catalytic activity and heat transfer required for hydrocarbon reformation. It removes thermal energy uniformly along the entire cell length thereby resulting in sufficiently flat axial temperature distribution which helps maintaining acceptable axial temperature gradients within the substack. Moreover it has a much lower pressure drop than a conventional packed bed type external reformer.

The in-stack reformers each consist of a catalytically active inner assembly surrounded by a nickel foil liner, an outer board assembly and an embedded riser tube. Heat is radiated from the adjacent cell bundle region through the porous alumina outer board to supply the energy required for the endothermic reformation reaction.

As explained in the previous section, the in-stack reformers accomplish 85 to 100% of the reformation depending on the generator operating point.

The following is a summary of functional requirements of the in-stack fuel reformation system:

- control the cell axial temperature distribution to minimize voltage loss and maintain an acceptable axial temperature gradient.
- minimize the impact of prereformer catalyst replacement on system availability.
- provide adequate structural support for the upper air plenum and air feed tubes.
- assure electrical isolation to avoid short circuits within the stack or flash-over at the maximum voltage potential in open circuit.
- maintain reformer pressure drop consistent with the capability of the recirculation ejector.
- maintain adequate fuel flow distribution uniformity within the cell stack.
- minimize stack plus reformer size and weight.
- minimize reformation cost.

Air Supply System. Process air is introduced at the top of the generator submodule into an array of air plenums. Air flows from the air plenums into the air feed tubes, which are coaxial with the fuel cells and convey the air to the bottom of the cell. The air subsequently flows upward through an annulus between the feed tube and the cell inner surface.

Spent air exiting from the open end of the cells enters the combustion zone and reacts with spent fuel to completely consume the remaining fuel. Because the air feed tubes cross the combustion zone in a manner similar to a gas-to-air heat exchanger, incoming air is heated by the exhaust gas exiting the cell stack. The exhaust is directed to an upper dome prior to being manifolded to an external common exhaust duct.

High-pressure exhaust gas is collected from all submodules and is conveyed to the gas turbine through insulated piping. The turbine drives the compressor for compressing air that is delivered to the fuel cells.

Internal Thermal Insulation Package. To minimize heat losses from the SOFC stacks and at the same time maintain the pressure vessel wall temperature within reasonable limits, it is necessary to embed all the internals in thermal insulation without impairing the capability to easily service and replace internal components including the generator stack.

Typically, stack insulation within the stack liner is constituted by high purity alumina which exhibits excellent chemical stability at high temperature in both reducing and oxidizing atmosphere.

All elements of the stack insulation structure are typically vacuum formed by utilizing alumina fibers and binders in specific ratios to yield the desired thermal and mechanical properties. These elements include fuel manifold support boards, fuel distribution boards, in-stack reformer outer boards, stack end boards, lower/upper-positioning boards, recirculation and combustor boards.

The insulation package external to the stack liner consists of a number of highly efficient thermal insulation blocks and panels interlocked to form an effective thermal barrier system between the cell stack operating at 1000°C (1800°F) and the pressure vessel at ambient air. This insulation material is fitted between each substack and around all main manifolds and piping spool pieces.

The insulation blocks and panels are constructed with silica material that has a microporous structure and is reflective to thermal radiation.

An additional layer of low density fiber material is installed between the ceramic cell stack and the composite blocks to form a compliant layer capable of accommodating cyclic thermal differential expansion while offering effective bypass gas sealing and adequate lateral load support.

PSOFC Module Description. The pressurized SOFC generator module includes twenty substacks (576 cells) electrically connected in series/parallel to the module terminals. Advantages of this type of construction include ease of assembly, flexibility in power output requirements, better serviceability and substack replacement capability.

The substacks are installed within a pair of horizontal pressure vessels containing a supporting structure designed to provide easy access to the internals and easy assembling and replacement of the submodules without interference with the installed internal components.

Pressure Vessel. The pressure vessel, as shown in Figure 3.22, is a horizontal cylindrical shell and is supported by two saddles anchored to the shipping container structural frame.

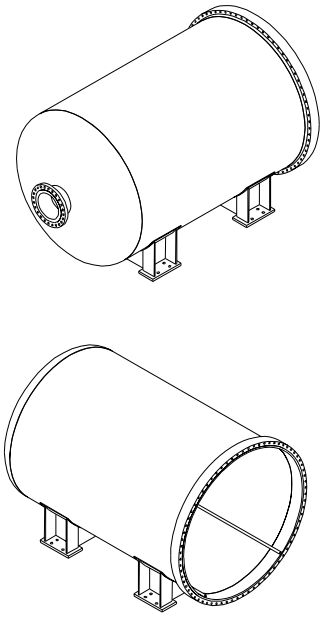

Figure 3.22 — Pressure vessel isometric views.

Pressure bearing components are required to meet construction codes such as the American Society of Mechanical Engineers (ASME) B31.1 piping code or the ASME Boiler and Pressure Vessel (BPV) Code. The allowable stresses for materials currently approved for construction under the rules of Sect. VIII, Div.1of the ASME BPV Code are provided in various Code Cases or in Sect. II, Part D.

The design of the components is in compliance with the ASME BPV Code, Section VIII, Division 1. The cylindrical shell material is SA-516, Grade 70 carbon steel which provides a minimum tensile strength 480 MPa (70,000 psi). The cylindrical shell thickness is determined by the tangential stress due to the design pressure. Since the maximum longitudinal stress (PR/2t) is only half of the maximum tangential stress, one-half the shell thickness is available for the longitudinal bending stress due to weight at the mid-span or in the plane of the saddles, assuming the vessel to behave as its own carrying beam.

As shown in Figure 3.22, two saddles including four legs and stiffener plates support the pressure vessel. The saddles are welded to the outer shell of the vessel with a 120-degree contact angle, and they could be anchored to a concrete slab in the field. The saddle reactions are highly concentrated and induce localized stresses in the shell, which are within the allowable stress conditions specified by the ASME Code.

The ASME flanged and dished head is cold formed from the same material as the pressure vessel. Each head will include one large central air inlet or exhaust outlet nozzle and smaller penetrations for the electrical DC power leads or for internal instrumentation cables.

The shell flange as shown in Figure 3.22, has an outer diameter of approximately 3.5 m (137 in.) and a length through the hub of 280 mm (11 in.) and is forged from SA-105 carbon steel material. Seventy-two 38 mm (1.5 in.) diameter radial holes are drilled through the flange for the bolts. The overall weight of each flange is approximately 2450 kg (5400 lb).

Bolting material for pressure connections must conform to the specifications listed in the ASME Code. Specifically, for this design, SA-193 Grade B7 (1 Cr-1/5 Mo) ferritic steel bolts have been selected. To minimize galling when the bolts are tightened, fasteners are made up with a thread lubricant such as Molykote paste. The proposed

bolting configuration includes 72 bolts with a 35 mm (1.4 in.) bolt diameter in a bolt circle of 3.4 m (134 in.).

Two of these pressure vessels bolted together at their flanges, as shown in Figure 3.23, form the basic building block of the power plant.

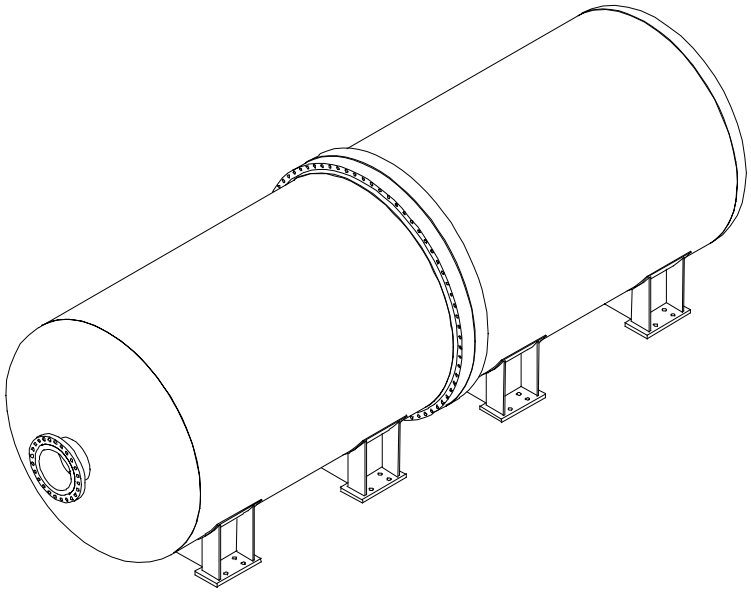

Figure 3.23 — PSOFC generator module isometric view.

A detail drawing of the pressure vessel and associated Bill of Materials is shown in Figure 3.24.

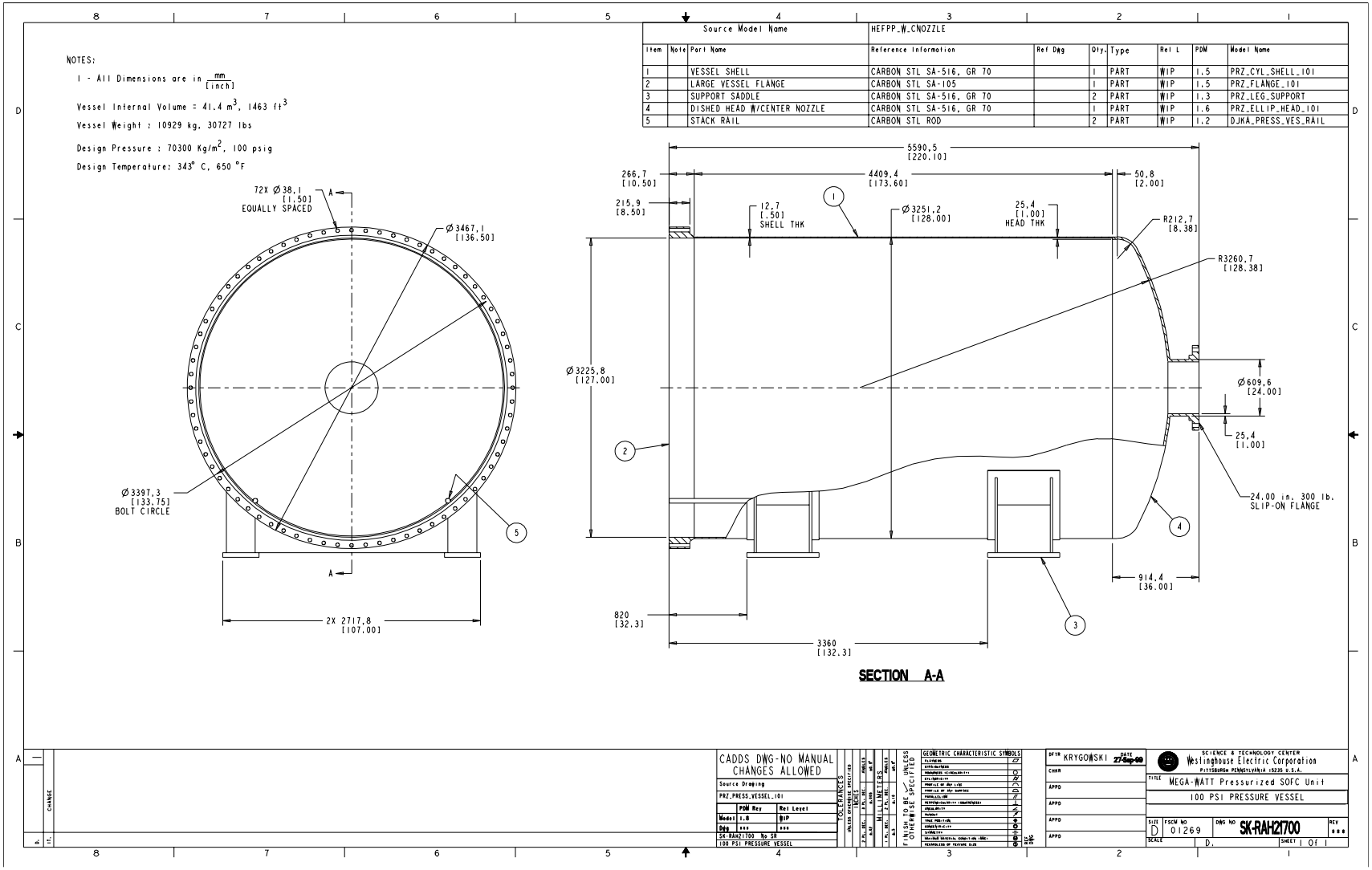

Figure 3.24 — Pressure vessel detail drawing.

Internal Sub-module Supporting Structure. As shown in Figure 3.25, the pressure vessel incorporates internally a supporting structure that is embedded in high temperature insulation material. This supporting structure is composed by two tubular steel side members separated by a series of equally spaced high density ceramic boards over which a steel deck is finally installed.

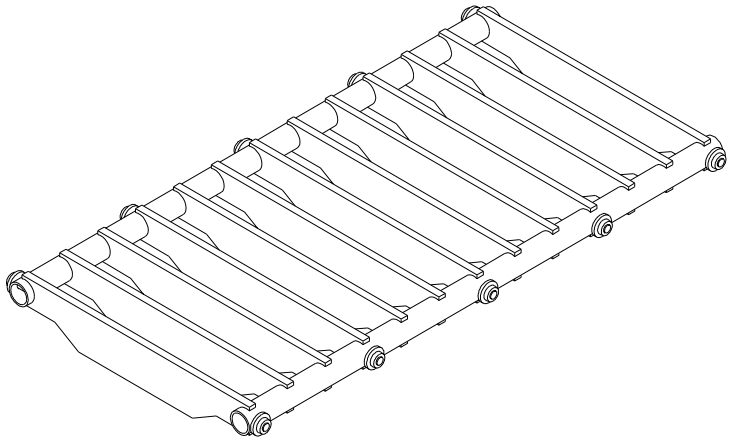

Figure 3.25 — Stack support car.

The tubular members include a series of high temperature roller assemblies including a wheel, axle box; die steel caged roller bearing and high load rating axle. These wheel assemblies are typically used in furnace and kiln cars for a variety of heat treatment processes.

This rolling structure provides a convenient open deck for stack assembly, support for piping, ducting and electrical instrumentation without interfering with the assembly/disassembly of the stacks. Once the internals are fully assembled on the support structure, the entire assembly is rolled into the pressure vessel over two rails welded to the shell wall. Once in position, the wheels are locked and secured.

This method of supporting and transporting the stack submodules is particularly advantageous for in-situ stack replacements or quick field installation in the event that the pressure vessels are procured locally or are already installed at the power plant.

A complete assembly of the Module internals, including the SOFC stacks, ducting and supporting structure is shown in Figure 3.26.

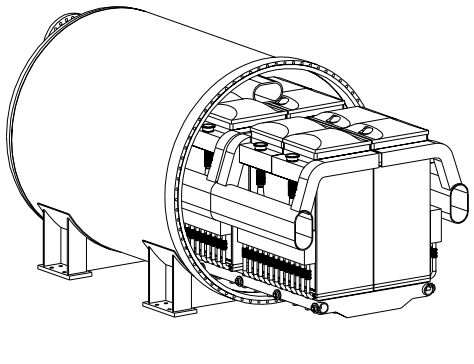

Figure 3.26 — Isometric view of Module with internal components.

Internal Air/Exhaust Ducting. When the substacks are inserted and positioned within the pressure vessel, they are connected to a common central air feed manifold by utilizing individual spool pieces connected to the inlet nozzle of each substack. The central manifold uniformly distributes the incoming pressurized process air to the individual substacks. The air manifold is positioned longitudinally within the pressure vessel, is supported by the ceramic frames and is embedded in the same insulation material surrounding the supporting structure. The final connection of the air manifold is made in correspondence to the side flanged cover nozzle through an expansion joint/adapter.

The exhaust gas flow from each substack is directed to an exhaust collecting plenum overhanging each substack and is subsequently manifolded into a central duct exiting through the exhaust outlet nozzle.

The air ducting operates at a maximum temperature of 760°C (1400°F) and the exhaust ducting temperature does not exceed 870°C (1600°F). Because the internal differential pressure between process air and exhaust is less than 60 mbar (0.9 psi) as a result of only frictional losses and generator pressure drop, ducting rather than piping is utilized internally. Externally, all piping is fabricated to withstand a 10 barg (150 psig) design pressure.

Fuel Inlet Piping. The fuel inlet piping will operate at a pressure of 3.5 to 5 bar (50 to 70 psi) differential inside the pressure vessel and up to 12 to 14 bar (180 to 200 psi) externally. The final pressure will be determined on the basis of the selected generator operating range, fuel composition and gas turbine selection.

Electrical Interconnections. Internal electrical interconnections between stacks are accomplished through utilization of a main DC bus bar and flexible cable connectors clamped to each stack power lead.

High reliability electrical feed-throughs are utilized on the pressure boundary of the module in order to guarantee sound electrical connection between the internal stacks and the external power conditioning system.

Generator Instrumentation. The SOFC generator module is equipped with a variety of instrumentation providing for automatic control with manual capability for plant operation, monitoring and diagnostics.

The generator stack instrumentation consists primarily of DC voltage taps and cell stack thermocouples. Within the cell stack, there are a number of voltage taps monitoring the progressive buildup of accumulated cell voltages with the first tap near ground potential and the last at the maximum DC voltage. The stack external terminal voltage is also monitored as well as the main generator module terminals.

Several thermocouples are embedded within each cell stack at different elevations to monitor and control the temperature of the generator stack.

A number of pressure taps may be included into each stack fuel supply system to monitor differential pressures around the fuel ejector systems and to provide gas sampling as required.

3.2.2 Gas Turbine System

3.2.2.1 Introduction

Rolls-Royce Allison (RRA) subcontracted to Siemens-Westinghouse to examine the design of components relating to a turbogenerator for the bottoming cycle of a 20 MW SOFC power generation plant. RRA issued a preliminary report defining the geometry and performance of the intercooled compressor system and gasifier (HP turbine) and free power turbines (LP turbine) required. Subsequently, Siemens Westinghouse has since determined that a better system would be rendered by placing all the turbo machinery on one shaft.

In the original free power turbine configuration, the free power turbine speed was in no way compromised by matching to compressor requirements and was allowed to rotate at about 20% lower speed than the compressors, yielding an optimum low stress design. Rolls-Royce Allison has examined the possibilities for the single shaft machine and finds that it is appropriate to leave the compressor and HP turbine stage designs unchanged and use an unshrouded low aspect ratio second stage rotor blade in order to preserve conservative stressing.

To provide a single reference document for the RRA subcontract results, the preliminary compressor and turbine data, issued in October 1998, are reproduced herein with corrections and updates where appropriate. Other topics briefly discussed include the startup combustor, which energizes the turbines whilst the fuel cell stack exit temperature is too low, electrical system efficiency and general arrangement of the "turbogenerator."

3.2.2.2 Plant Design Change

The original Siemens Westinghouse configuration called for an intercooled compressor driven by a gasifier turbine, followed by a power turbine, on its own shaft, driving a generator. A fuel cell stack added the heat necessary to drive the first turbine and a second stack reheated the working fluid between the two turbines. Siemens Westinghouse subsequently requested that the design be reconsidered, and adjusted where necessary, to be appropriate to placing all the turbomachinery on one shaft, without cycle change. Advantages of this configuration potentially include:

- Simpler mechanics (fewer total bearings)
- Better plant control due to ability to force the system
  - flow level to the optimum value by adjusting generator loading
- More freedom in cycle choice because the pressure level
  - level between stacks is no longer dictated by balancing
  - the first turbine work with total compressor work

A disadvantage of the system arises from the fact that the flow from the first turbine exit does not pass straight to the second turbine inlet, because is has to be diverted to be reheated in the second stack. The challenge for this system is it tends to increase the shaft length required to accommodate low loss ducting, hazarding shaft dynamic characteristics.

3.2.2.3 Design Approach

The Siemens Westinghouse cycle uses two fuel cell stacks in flow series in which hot air from the first stack powers the HP turbine and the second stack reheats the working fluid prior to entry to the LP turbine. The compressor system is intercooled at mid-point, enabling a slightly higher-pressure ratio to be used whilst retaining the correct heat balance around the cycle.

Though axial compressors are often more efficient than radial stages, this ceases to be true when the pressure ratio is low and the exit flow has to be diffused to near-zero velocity prior to the next flow process, as is the case for both compressors in this application (the first stage feeds to the intercooler, the second stage feeds to the recuperator). For the defined duties, it is clear that two low cost radial compressor will serve the purpose well. Where radial compressor stages are used in aero engines, they are of much higher stage pressure ratio.

There is no strong merit in considering a radial turbine because these really only come into their own as a means of reducing cost if one stage can replace two axial stages. In the proposed cycle, flow is reheated between turbine stages, requiring them to be separate, and each has a duty easily accomplished in a single uncooled axial stage.

The HP turbine stage geometry is somewhat like an aero HP turbine stage but runs at much lower temperature and is therefore not cooled and does not use the same high cost super-alloy. The LP turbine stage is determined to be best satisfied by a low aspect ratio unshrouded rotor blade that is not like a lightweight aero stage design.

During steady state running, the electrochemical fuel cell process keeps the stack and its throughflow at high temperature. Also, non-utilized fuel is reacted with residual oxidant in the exit section of the stack, raising gas stream temperature high enough to drive the turbine, approximately 870°C (1600°F). When the system is being started however, and the fuel cell stack is at ambient temperature, no galvanic action can take place and thus no heat is added or fuel burned within the stack. During this period, though the fuel cell is fed with hot pressurized air at inlet during this period, its exhaust is at low temperature and too cool to drive the turbine. A combustor burning natural gas is therefore required for system startup and is placed in the exhaust stream just before entry to the HP turbine.

3.2.2.4 Compressor Selection

The two compressor stages are very similar in duty, substantially differing only in required corrected flow size. In radial stages, the pressure ratio dominates the level of impeller rim speed required for optimum loading and efficiency. The axial inlet diameter is determined by:

- Good level of inlet air velocity/blade speed (for favorable aerodynamics)
- Avoiding excessive inlet tip relative Mach number
- Keeping the entry axial Mach number low enough to limit duct losses

For a given rim speed and initial area allowance for bearings, too high a value for RPM raises the impeller inlet tip relative Mach number and may lead to a need to reduce inlet radius, cramping the bearing design and increasing axial Mach number.

Noting that both stages have the same pressure ratio and similar inlet temperature is, it follows that they have similar impeller rim diameters. Inducer inlet inner radii have been held equal, which is compatible with most mechanical arrangements. Diffusion to low velocity is required at exit from both stages and so the performance is quoted at a nominal 0.15 outlet Mach number, i.e. including diffuser losses.

The rim speed of the two impellers is approximately 365 m/s (1200 ft/s), which is compatible with the use of aluminum or steel rather than relatively expensive titanium alloy. Compressor design point performance is summarized in Table 3.3 below, and compressor performance maps are provided in Figure 3.27 to Figure 3.30. Note that RC denotes pressure ratio and the curve parameter is shaft speed in percent.

Table 3.3 — Radial Compressor Stage Design Point Data

Stage	Inlet Temp °C	Pressure Ratio	Airflow kg/s (corrected)	Adiabatic Efficiency	Speed RPM
1	16	2.47	18.5	0.864	10,600
2	23	2.48	7.7	0.864	10,600

* *Compressor corrected flow* = $\frac{W\sqrt{(T/T_{ISA})}}{(P/P_{ISA})}$

** *Definition of efficiency*

Adiabatic efficiency = (Ideal rise of enthalpy from inlet to outlet pressure)/Unit work done

Outlet is defined as total pressure after diffusion to 0.15 Mach number

Working fluid is air with zero relative humidity

Windage is included in radial stages. Bearings not included.

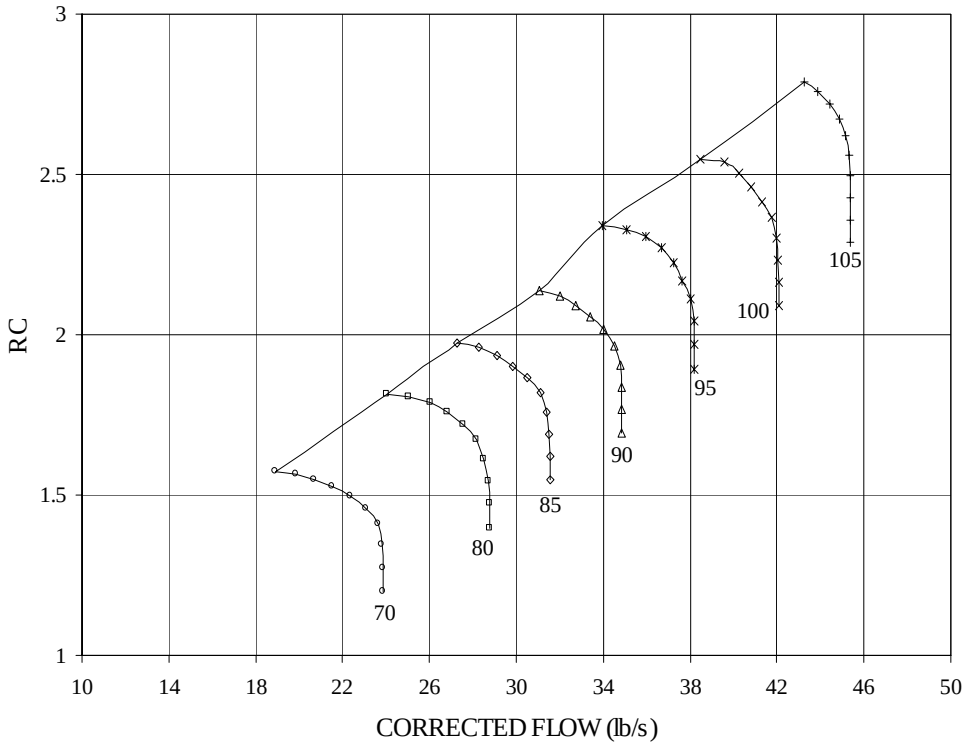

Figure 3.27 — Compressor performance map, first stage.

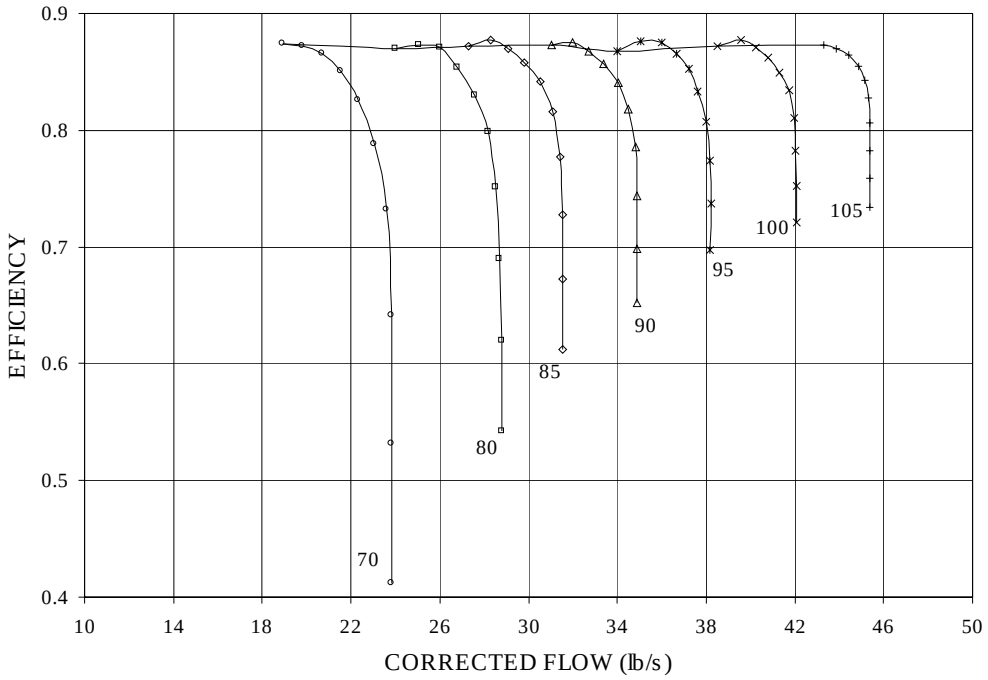

Figure 3.28 — Compressor efficiency, first stage.

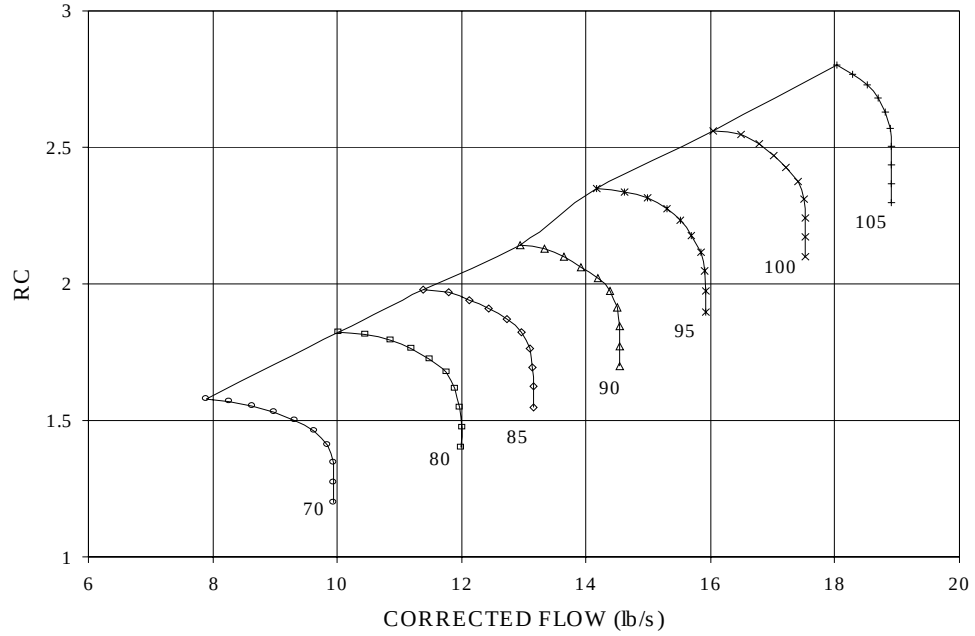

Figure 3.29 — Compressor performance map, second stage.

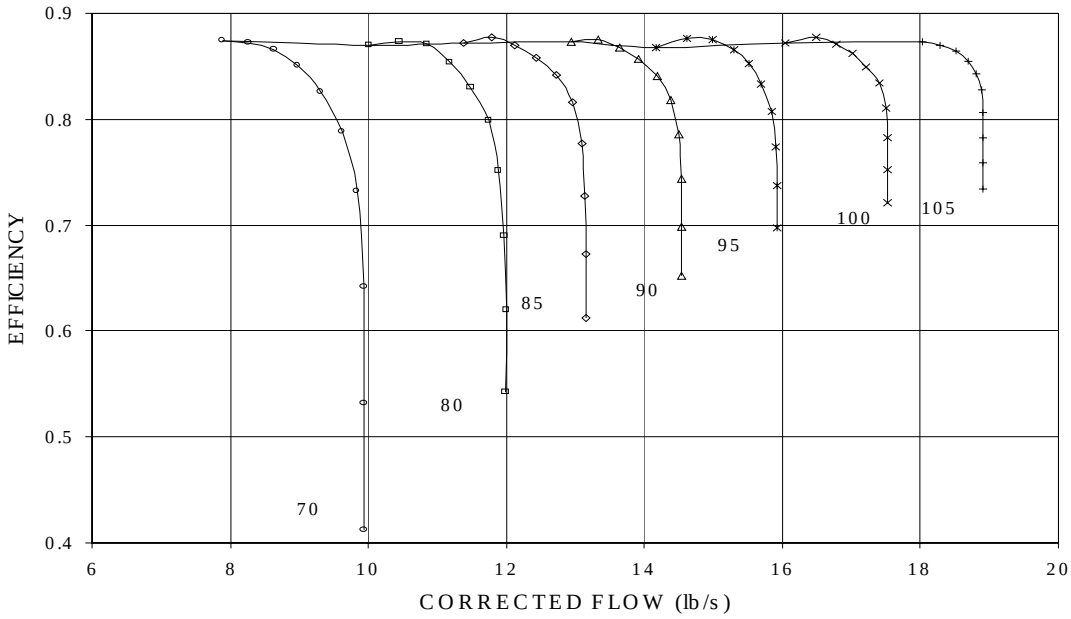

Figure 3.30 — Compressor efficiency, second stage.

In a high-pressure ratio multistage compressor, part speed operation is compromised because the working fluid is no longer fully compressed. This leads to the situation where the last stage is now too small to accept all the flow the first stage would pass when working at its design incidence. In consequence, the last stage works at negative incidence relative to design and the front stage works at positive incidence, tending towards stall. In a normal compressor, this mismatch is ameliorated by the fact that the temperature at entry to the last stage is falling with pressure ratio and its capacity therefore increases a little. As a result, for a simple 2.5 x 2.5 = 6.25 nominal design pressure ratio, given the relative flexibility of radial stages, it might be possible to handle the whole range of operation without variables.

In our case, intercooling prevents this capacity increase and the part-speed movement towards stall is much more rapid. The consequence is shown in Figure 3.31, which is the stacked map for the two-stage compressor system with the intercooler working at fixed effectiveness. It will be seen that the stall line is very steep such that stall will be encountered with very little speed reduction (operating line will pass through design point and run nearly parallel to last stage stall line).

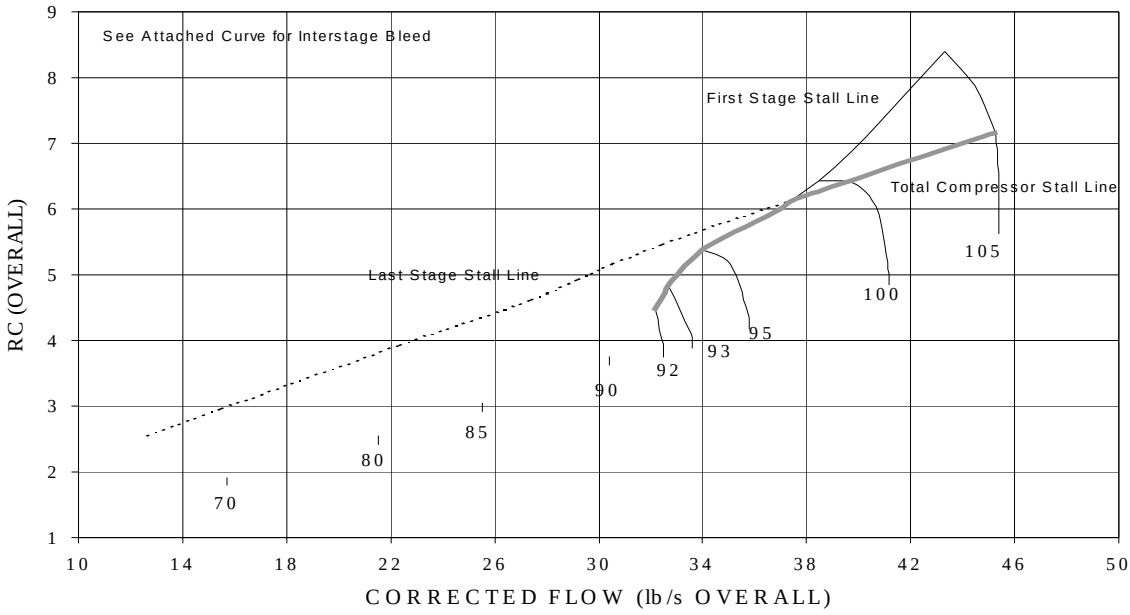

Figure 3.31 — Overall compressor performance map.

To preserve part speed stability, interstage bleed will be required. Figure 3.32 shows that the stall line can be recovered to a good level using an interstage bleed scheduled to pass the amount of flow shown in Figure 3.33. This bleed impacts on plant overall efficiency at part power.

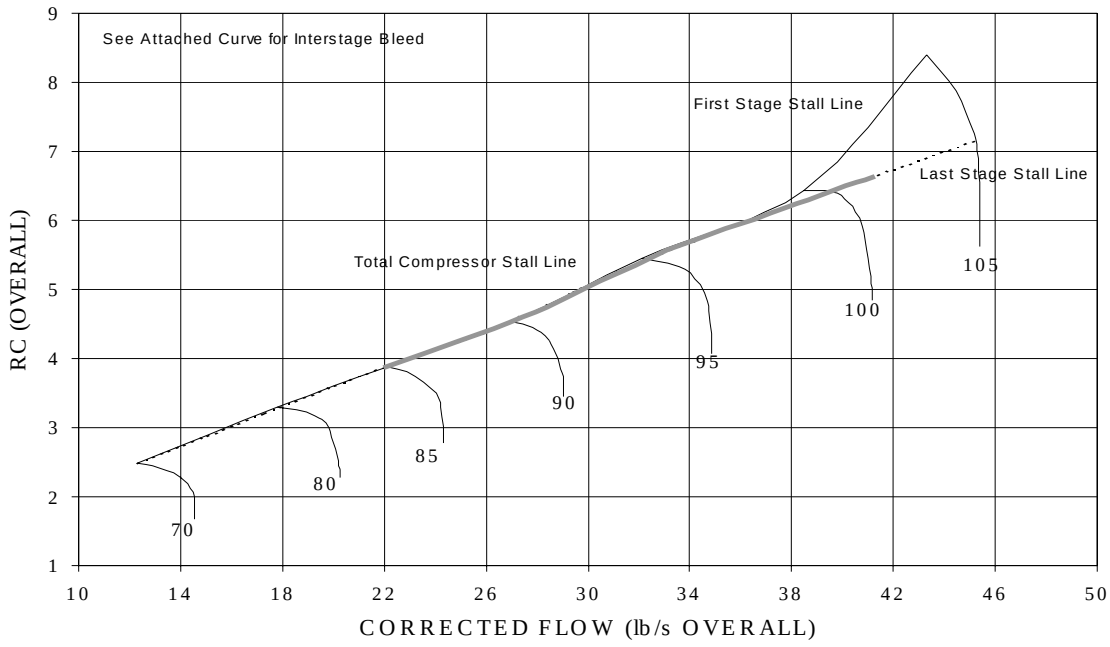

Figure 3.32 — Overall compressor performance map.

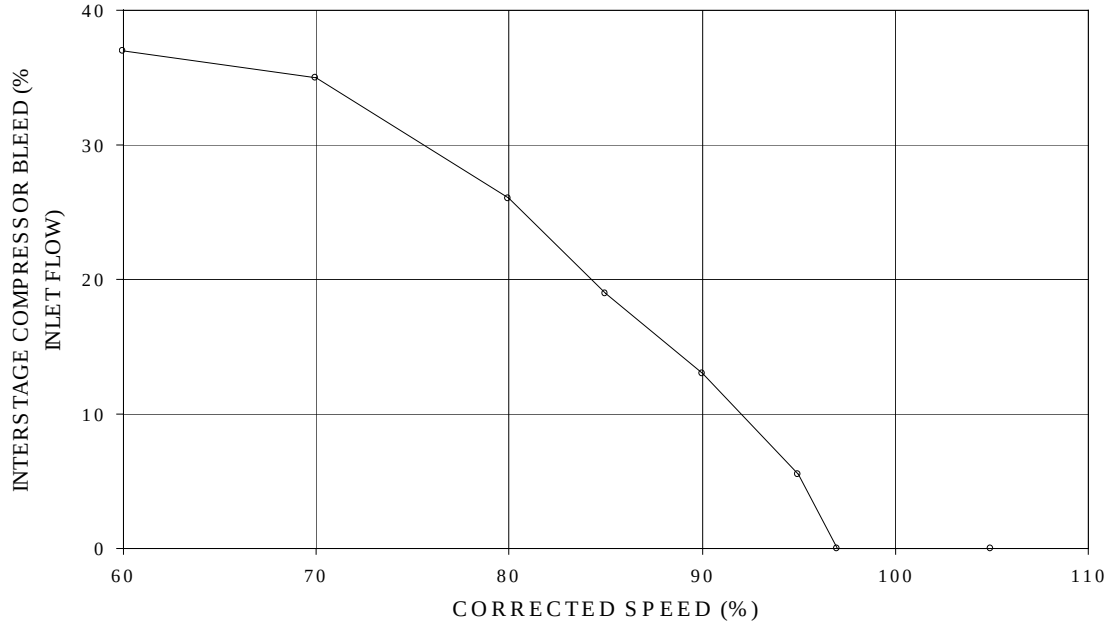

Figure 3.33 — Compressor bleed schedule.

3.2.2.5 Intercooler Selection

There are several possible configurations for the intercooling system. Air liquefaction plant intercooled compressor systems generally use air-to-water tube-in-shell heat exchangers adjacent to the compressors and then the heated water is passed to a large natural convection-cooling tower, or to a dry, forced-connection heat rejection unit, dumping the heat to atmosphere (in some plants this heat could gainfully be transferred to boiler feed water). This scheme is compatible with our observation that the potentially lower cost approach of using water as the final heat sink is usually rejected by customers who, almost universally, insist on an atmospheric sink, due mainly to permitting requirements.

Rolls-Royce Allison have studied intercooling systems for gas turbines and found that the ducting and heat exchanger pressure losses for the above systems tend to be 5%-8% in addition to the compressor exit diffusion loss. The parent company, Rolls-Royce plc, has developed a Naval engine (the WR21) which uses a close mounted, near axisymmetric, heat exchanger array with about half this loss. The geometry is well suited to the gas path of radial stages. The drawback is that the heat exchanger modules have to be super-compact, with very small matrix passages. This results in their being expensive, sole-source and more subject to blockage. They are probably not cost-effective in this application.

3.2.2.6 Turbine Selection

In most cases, the highest efficiency configuration is served by the use of tip sealing shrouds on the rotor blades to limit tip clearance losses. The presence of a tip shroud implies a maximum tip velocity of about 460 m/s (1500 ft/s) to limit shroud cantilever and blade airfoil direct stresses. When the LP turbine was a separate stage, it was possible to run it a little slower than the other stages to keep tip speed down for comfortable mechanical loading whilst having the speed high enough to keep turbine aerodynamic loading low enough for high efficiency.

Full use of the highest permissible tip speed tends to lead to high hub/tip radius ratio that is undesirable in being very sensitive to tip clearance and is also inclined to reduce efficiency due to more dominant wall effects. The first stage was restrained not to ex-

ceed hub/tip radius ratio of 0.875. To ensure favorable design geometry, the flow coefficient (axial velocity/blade speed) was also kept above 0.3.

The original free second stage, which was a normal shrouded design, has been forced up by about 20% RPM for the single shaft. Blade hub and fixing stresses relate to the term AN^2, chosen originally to be to be 4×10^{10}. "A" represents the axially resolved annulus area in square inches at exit from the last rotating row and "N" is the rotational speed in RPM. The product, AN^2, has the dimensions of velocity squared and is a good measure relating to the maximum turbine tensile stress. "A" is set by the requirement to minimize outlet losses by reducing exit axial Mach number. Increasing the RPM from 8185 to 10,600 would have brought AN^2 up from 4 to 6.7×10^{10}.

This is too high for uncompromised aerodynamics and mechanics together and it was chosen to change to an unshrouded rotor blade to keep stresses low and to decrease the tip radius. The tip radius is reduced to bring the stage flow coefficient into an optimal range while preserving a low exit axial Mach number but the tip speed is 490 m/s (1600 ft/s), i.e. still in the range mechanically requiring an unshrouded design. By itself, the removal of the shroud reduces efficiency due to tip leakage effects, but the increased blade speed serves to decrease aerodynamic loading that has a slight positive effect on efficiency. Though the Total-Total efficiency actually improves a little (Table 3.4), the effective value after diffusion decreases is almost unchanged due to a small increase in exit dynamic head and consequent diffusion loss. The LP turbine stage exit diffuser is good enough to assume a 50% dynamic head loss.

Table 3.4 — Axial Turbine Design Point Data Summary, 850°C Entry Temperature

Press Ratio	RPM	Airflow kg/s (corrected)*	Adiabatic Efficiency**	No. of Stages
1st stage 2.066	10,600	7.1	90.7	1
2nd stage 2.096	10,600	17.5	92.3	1

** Turbine corrected flow* = $\frac{W\sqrt{(T/T_{ISA})} \times F}{(P/P_{ISA})}$

where $F = \sqrt{(\theta')} / \delta'$

$\theta' = \frac{2 \times R_{gas}}{62.23} \times \gamma / (\gamma+1)$

$\delta' = 0.3698\, A \times \gamma / (\gamma+1)$

$A = (2/(\gamma+1))^{\gamma/(\gamma-1)}$

R_{gas} *typical = 53.3 ft-lbf/lb-°R*

F typical value is 1.00 to 1.04

*** Adiabatic Efficiency = Work done/(Ideal fall of enthalpy from inlet to outlet pressure)*

Outlet is defined as delivery at 0.2 Mach axial number exit
Working fluid as defined for cycle
No windage or bearing loss

Turbine performance maps are provided in Figure 3.34 to Figure 3.37, and the single-shaft arrangement of the major gas turbine components is depicted in Figure 3.38. Note that the curve parameter in Figure 3.34 to Figure 3.37 is shaft speed in percent.

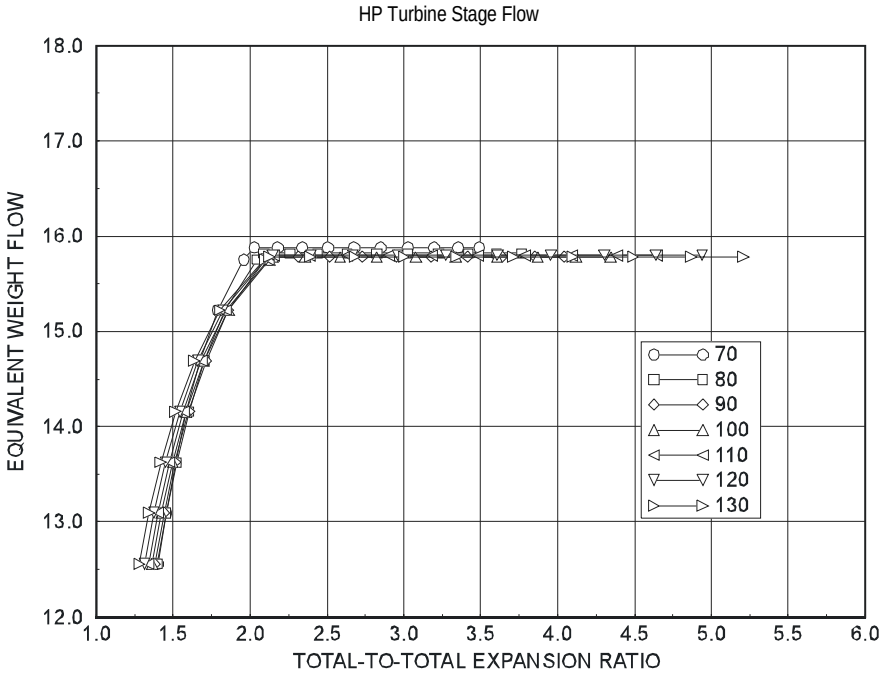

Figure 3.34 — HP turbine stage performance map.

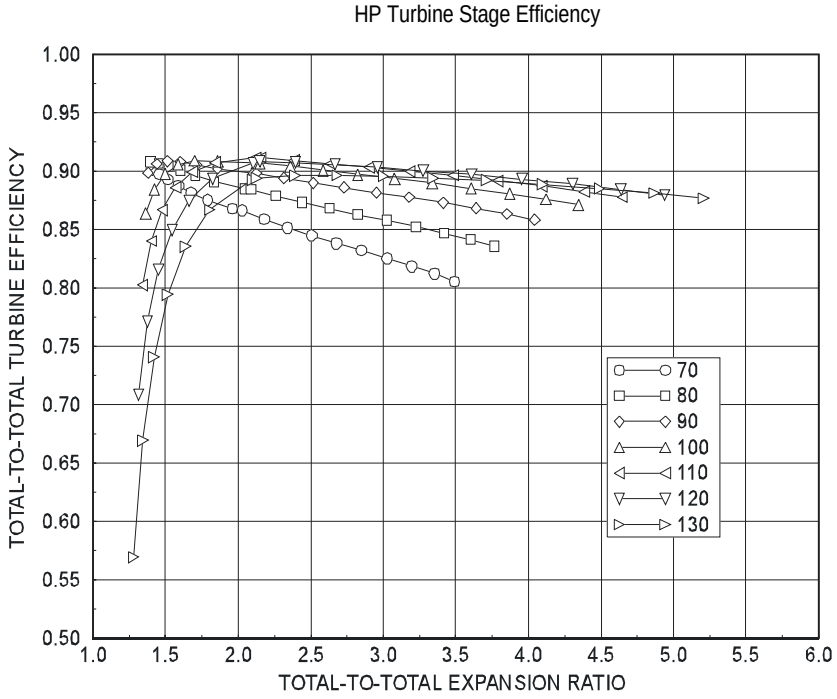

Figure 3.35 — HP turbine stage efficiency.

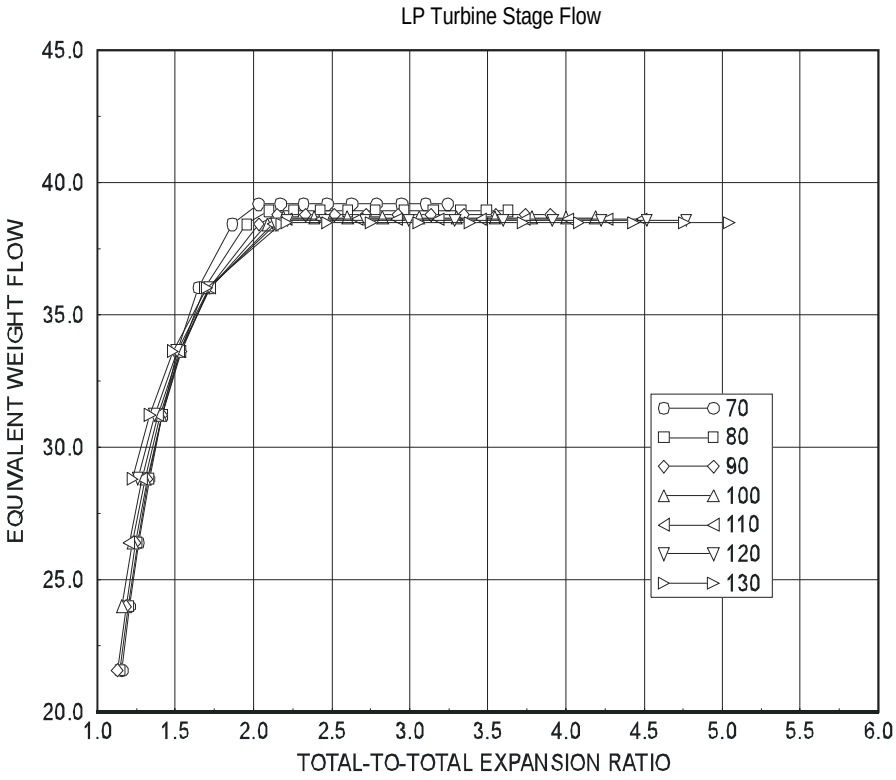

Figure 3.36 — LP turbine stage performance map.

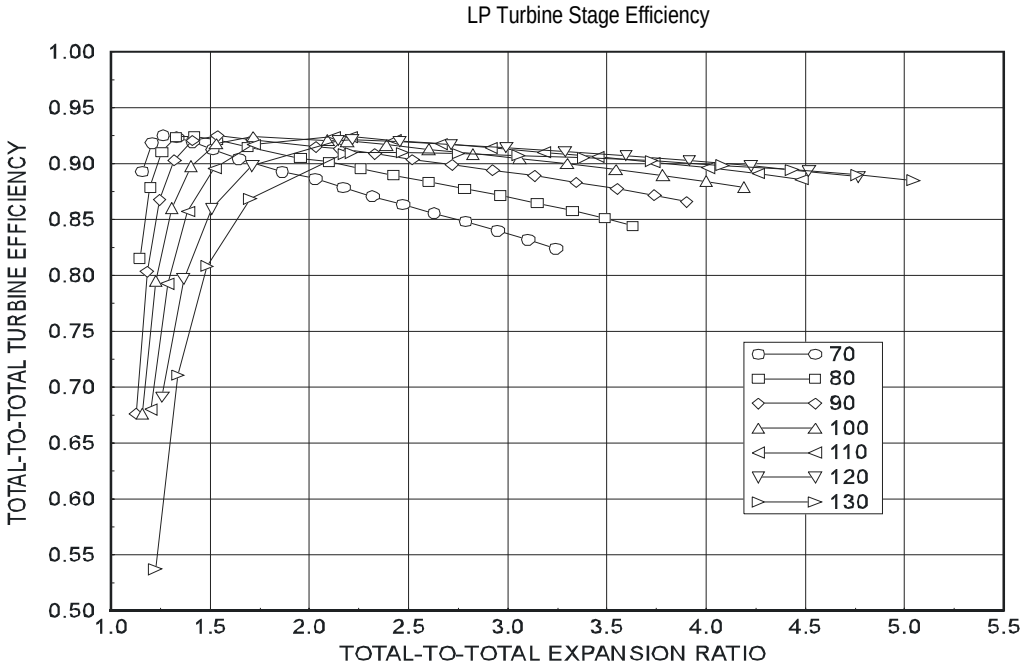

Figure 3.37 — LP turbine stage efficiency.

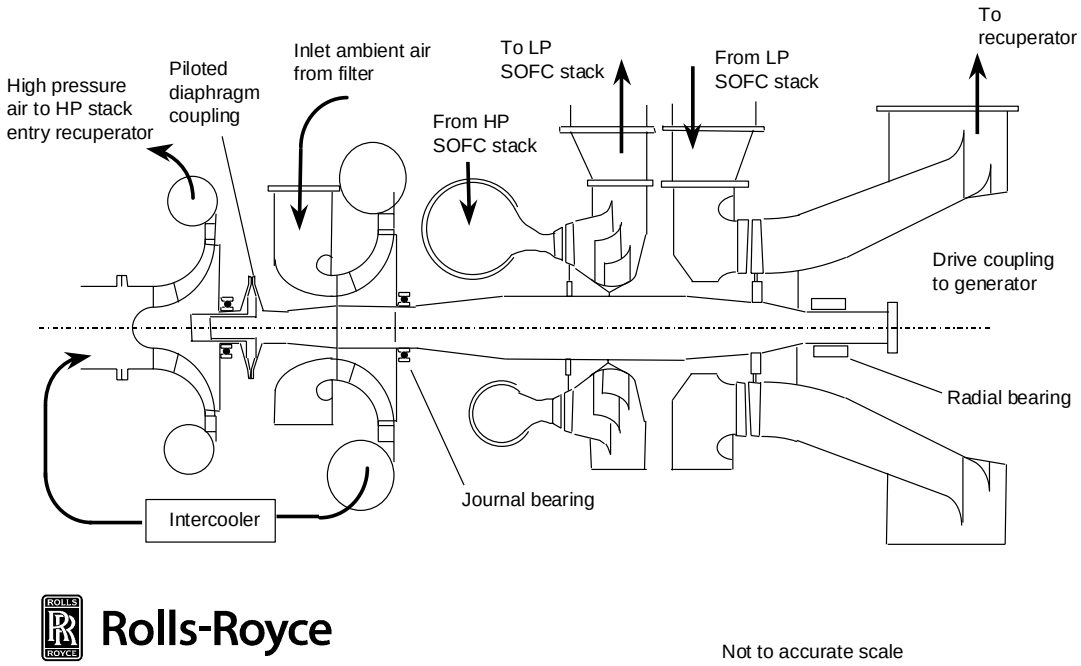

Figure 3.38 — Turbomachinery arrangement for Siemens Westinghouse 20 MW HEFPP Fuel Cell Plant.

More detailed views of the compressor air inlet sections are provided in Figure 3.39 and Figure 3.40.

To reduce weight in aero engines, and to minimize the amount of high cost alloy used in large turbines, it is frequent practice to use high aspect ratio turbine blades. Tip shrouds are essential to such blades because, without them, they are liable to a wide range of resonant vibration and flutter conditions, leading to fatigue failure. It is therefore important to ensure that the unshrouded blades are sufficiently low aspect ratio to have good vibration characteristics.

Taken too far, this can result in very pronounced individual blade pressure fields that also require large axial gaps between airfoil rows to prevent blade passing order vibration. Excess axial gaps increase wall friction losses and may compromise shaft dynamics, and the turbines have been laid out with this requirement. Unshrouding the LP turbine stage has decreased its total blade numbers and simplified manufacture, leading to a cost saving, which is incorporated in Table 3.4.

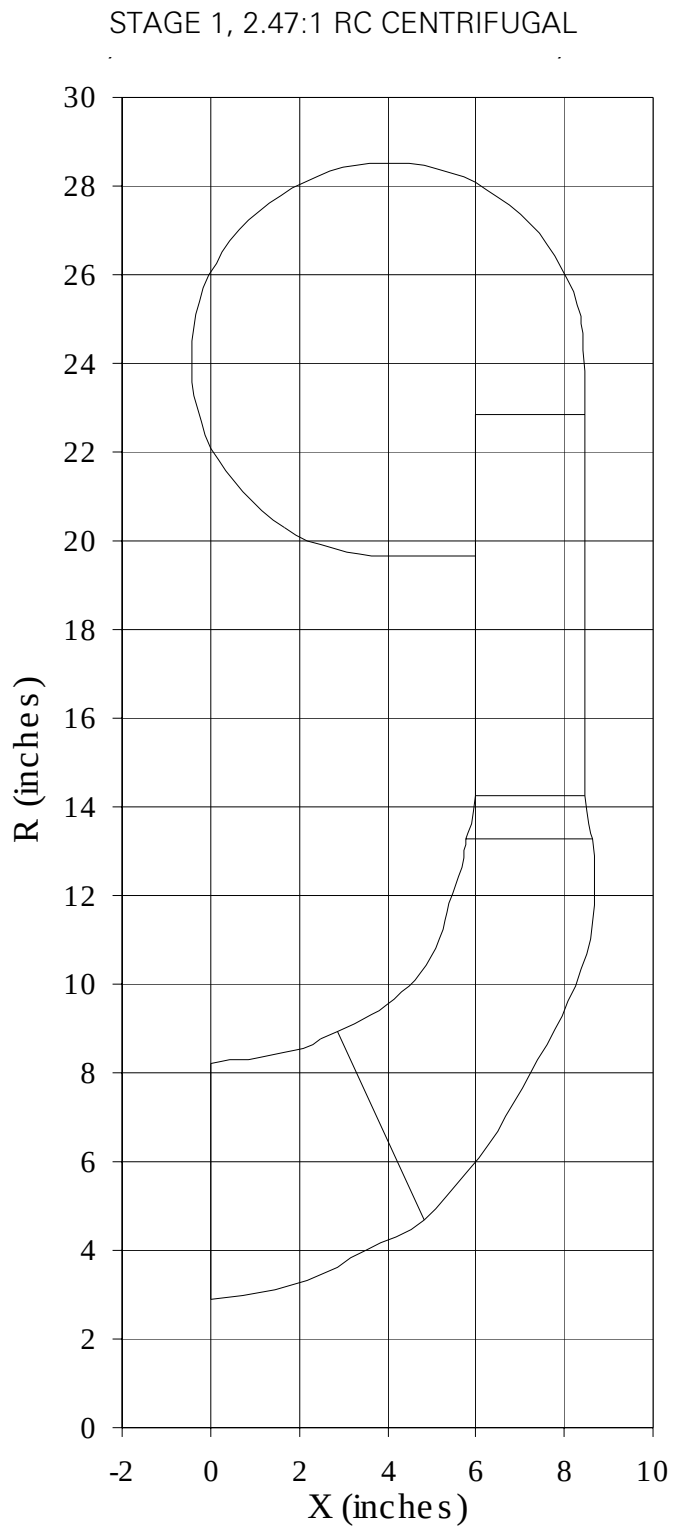

Figure 3.39 — Compressor inlet configuration, first stage.

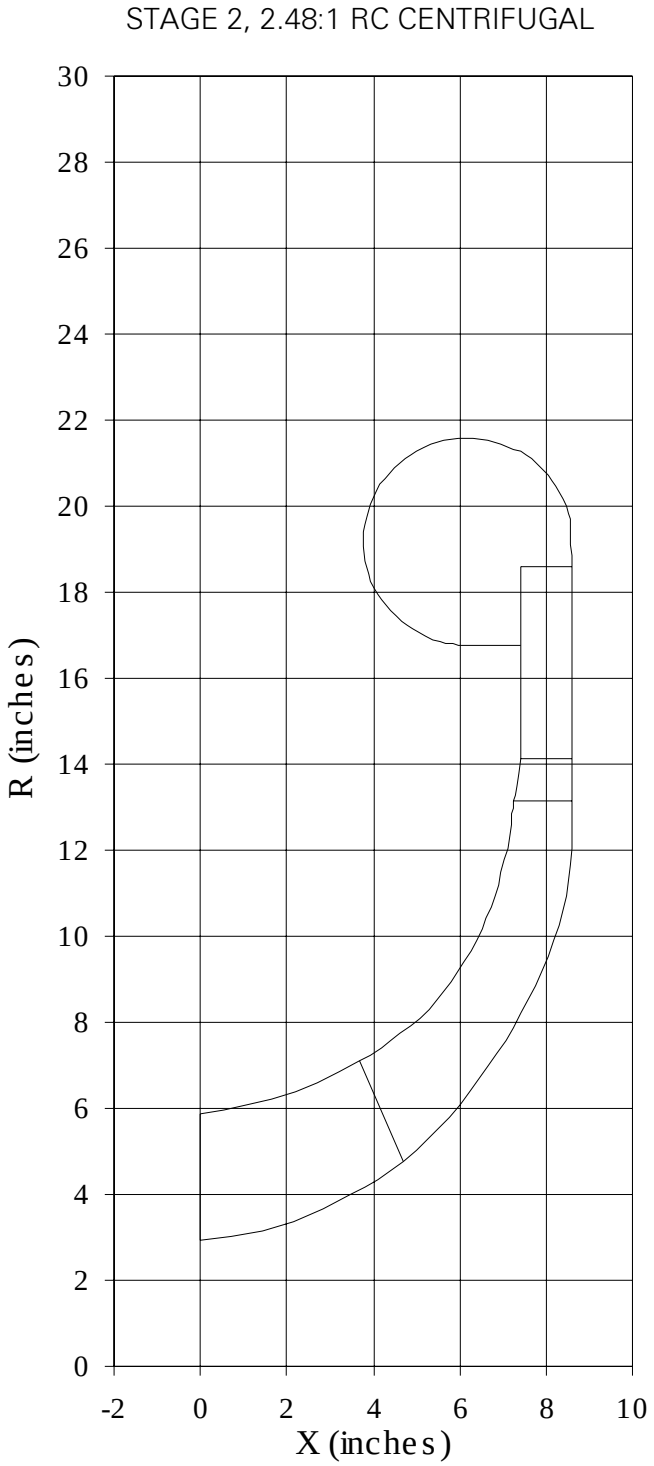

Figure 3.40 — Compressor inlet configuration, second stage.

The geometry proposed is based on general experience, from which we recommend a compromise 40 to 50 airfoils in a row for weight insensitive applications. These relatively low numbers favor cost minimization for the relevant size of turbine. There is insufficient time in this feasibility study to create a model of these blades and demonstrate analytically that the proposed geometry would be correct.

The exit axial Mach number from both turbines at design point is only about 0.2 corresponding to an exit dynamic head about 3% for the HP turbine and 4% for the LP turbine stages. The HP turbine stage has a compromised diffuser and a pressure loss of 3% should be assumed.

Note: Continued cycle optimization caused some final parameter values to differ somewhat from those reported in the above narrative. For example, the final compressor ratio is 7:1, vs. 6:1, which increased slightly the pressure ratio across each compressor stage. In addition, the LP turbine is loaded more heavily as a result of the HP turbine expansion ratio optimization. This resulted in a reduction of the LP turbine efficiency from 92.3% to 91.3%, the value used in the final power system performance estimates.

3.2.2.7 Combustor Selection

While the stack exit temperature rises from ambient to its full steady state value, the delivery temperature from the combustor is held constant, requiring progressively less fuel to be burned. Combustor stability is therefore required over a substantial range of fuel flow. The simplest, low cost, way to enable wide stable range for a gas combustor is to create a primary burning zone in the combustor in which the fuel richness varies from lean to greater than stoichiometric. This ensures that the gas flow can be turned down substantially before the whole volume capable of supporting a stable flame disappears.

The disadvantage of his approach is that it produces locally very high temperature and starts to generate NOx. However, as the combustor is only fueled for a short time, it is probably not required to have ultra-low emissions. Drawing a balance between emissions and turndown, typically leads to a stable turndown range of about 1:4. If a greater range of turndown is required (to smooth the transition from combustor heating to galvanic heating) a relatively convenient arrangement is to select a combustor with

multiple liners and progressively shut them down to extend range, e.g. 3 liners would give 1:12 turndown. It would be convenient to use an existing developed gas turbine combustion system. To avoid complicating the hot ducting, the combustor is always in the main flow path even when it is not fired so material changes would probably be necessary for non-liner parts to be compatible with the high inlet temperature relevant to normal plant running. Durability of the system will be aided by the fact that the combustor will use the same desulphurized natural gas fuel that is consumed in the fuel cell.

Sizing the combustors is affected by the fact that their highest-pressure loss condition is when they are unfired and the system is up to full temperature. Clearly the pressure loss should be small at this condition to favor high plant efficiency and so the combustors should be sized to the full 870°C (1600°F) flow of the HP turbine stage. This corrected combustor flow level is about 7.3 kg/s (16 lb/sec) [compare with 6.8 kg/s (15 lb/sec) nominal for the 9-liner system of the Pratt & Whitney FT8 or 12.7 kg/s (28 lb/sec) for the 8-liner Rolls-Royce Avon industrial engines. Note that these figures are around 20% above their effective value because turbine cooling bypasses the engine liners].

In turbine engines, an important function of the combustor pressure loss is to give a positive pressure difference to turbine blade cooling film feeds and this is consistent with a typical design loss level of about 4% total pressure. In our application, no turbine blade cooling is required and the design pressure loss should be lower. Noting that pressure loss is proportional to velocity squared, the Avon system would give about

$$4 \times \{16 / (0.8 \times 28)\}^2 = 2\% \text{ pressure loss, which is a good level.}$$

The design of a combustion system can also be approached more fundamentally. To have good control of the combustion zones by conventional jet penetration, it is appropriate to design for a pressure loss function

$$PLF = 15$$

i.e., a total pressure loss of 15 x the dynamic head based on total chamber flow area. We therefore require an entry dynamic head only $1/1000^{th}$ of the total pressure to have a 1½% loss. Loss variation away from design point will be in proportion to this entry dynamic head squared. If the combustor liner system is contained within a single cy-

lindrical outer casing, the radius required to achieve this dynamic head level is approximately 380 mm (15 in.).

The length of combustor is dictated by the uniformity of temperature required at delivery (presumed close to turbine inlet). Fair practice is to aim for the value of

$$\frac{\text{T max local - T average}}{\text{Combustor temp rise}} = 0.2$$

if cylindrical combustor liners are used, this requires 2½ diameters for burning and mixing.

If only a single liner was used, the required length would be 1.5 to 1.8 m (5 to 6 ft) which seems a bit bulky. The length can be reduced by filling the same outer case with a group of smaller diameter cylindrical liners having the same total area, e.g. three 432 mm (17 in.) diameter liners, which would require a length of only 1.1 m (3.6 ft). If the flow is delivered to an annulus rather than to cylindrical liners, the length can be further reduced to 0.6 m (2 ft). This compactness of the arrangements again points to the use of existing gas turbine systems.

The fuel nozzles can be of simple "showerhead" form with low-pressure drop. Natural gas is much easier to feed than kerosene because it does not require atomization. Premixing to attenuate emissions would detract from turndown capability.

Running at 870°C (1600°F), all the combustor and associated ducting will have to be contained in a thermal blanket, mainly to prevent overheating adjacent plant items.

3.2.2.8 Turbomachinery General Arrangement

Intercooled radial compressor sets, which feature 2 to 6 stages, with the relevant 1 to 5 intercoolers, are offered industrially by such manufacturers as Atlas-Copco. The cost of these units varies with detailed specification, including the issue of whether the compressors have to be customized. Referring to Atlas-Copco sales literature indicates that they might require a 3-stage unit or possibly a customized 2-stage unit to meet the required pressure ratio. An intercooled, motor-driven Atlas-Copco compressor system is depicted in Figure 3.41.

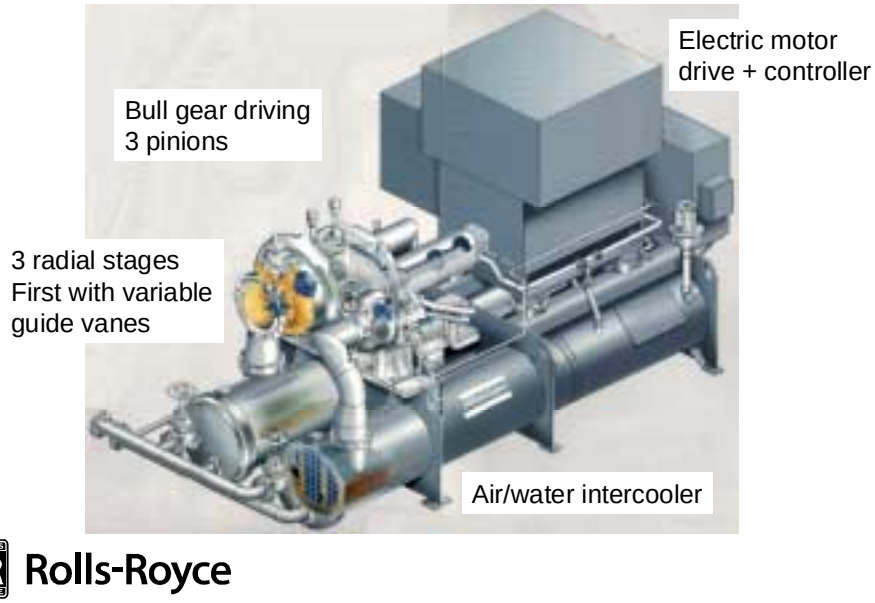

Figure 3.41 — Example of multistage intercooled compressor set industrial process equipment by Atlas-Copco.

If this approach were adopted for the proposed HEFFP plant, a generator would replace the motor and the two turbine stages would be required to drive direct into the bull gear through a small pinion. In the long term, this is a rather expensive system without the possibility of eliminating lubricating oil. The mechanics of this arrangement would be slightly less satisfactory than the balanced multiple compressor system because the compressor and turbine gear tangential loads work in the same direction when their radial loads are opposed.

The aerodynamic designs put forward in this report are directed towards the single shaft configuration illustrated in Figure 3.38. Briefly, the features of this system are:

- The high-pressure compressor stage, being smaller, is placed on the end of the single system shaft. This aids the achievement of good shaft dynamics and permits the use of a simple cylindrical intake for this stage.

- The intake for the second compressor, having only a small internal pressure difference relative to ambient, can be a fabricated sheet metal box.

- Both compressors use radial vanes and an exit volute to diffuse the delivery flow into a pipe.

- So that both compressor impellers may be run at minimum clearance, they are both axially located by ball bearings a no-compromise high efficiency arrangement. To avoid conflict between the two, the compressor stages are joined with a piloted diaphragm coupling. This is a rather complex and expensive arrangement and more detailed study could show that relaxing to one ball bearing and a solid drive could be more cost-effective.

- The exhaust from the HP turbine stage must be turned for radial removal in a short axial length in order to minimize shaft length. The form of diffuser illustrated has been used in RRA small gas turbine practice for many years. It can be expected to lose nearly one dynamic pressure head (5%).

- The exhaust from the LP turbine stage is handled in a very conventional low loss diffuser, probably experiencing no more than 3% pressure head loss.

- The intercooler is of the tube-in-shell variety used on industrial process compressor sets.

- The combustor outline is based on the use of a Rolls-Royce Avon outline. Material for the outer casing and some other parts would have to be upgraded to Inco 718 or similar.

Keeping an eye on the future content of the powerplant, it is considered quite likely that the most attractive and cost-effective plant will be based on

- Direct drive alternator (5 MW @ 10,600 rpm). Motors of similar speed and power ratings are entering service.

- Power conditioning to 60 Hz grid connected output (in distributed generation).

- Oil-free bearings. Magnetic bearings are considered to be the most suitable. Their use will often be incompatible with using aeroderivative parts due to their rather large working area requirements.

It is expected that magnetic bearings direct drive alternators and inverters will all be introduced in more conventional gas turbine gensets. Part of the development process will be to bring the integrated system cost to a level competitive with, and therefore similar to, the current oil-lube bearing, gearbox and low speed synchronous alternator systems.

There are three recuperator types that can be expected to give good service

1. The traditional robust "chemical industry" tube-in shell design. For this flow class, typical practice has been of cylindrical units about 9 m (30 ft) long. They have normally been sized to considerably less than the 90% effectiveness level intended here.
2. Compact plate-fin designs, very much smaller than the tube-in-shell units, even when configured for 90% effectiveness. Past experience with this class of unit has been unsatisfactory due to unsubtle mechanical designs that permitted severe thermal stresses to prevail, leading to early failure in cyclic use. Northern Research Engineering Corporation (NREC) has recently reengineered this type and offers a unit that may well be satisfactory.
3. Primary surface recuperators have been developed over a very long period of time by Solar. These are even smaller than the compact plate-fin designs and have many features specifically included to avoid cyclic thermal stress problems. Solar have succeeded to the point where they offer these recuperators in their Mercury 50 product. In fuel cell plant application, relatively few temperature cycles are expected and the greater concern with these thin foil based units is long term creep closing down pathways and increasing flow resistance. The fuel cell plant temperatures are close to normal for these units.

Given that a recuperator effectiveness of at least 90% is specified for this application, it is suggested that the unit needs to be of compact form. We have examined an NREC-type arrangement based on individual cores of the dimensions shown below.

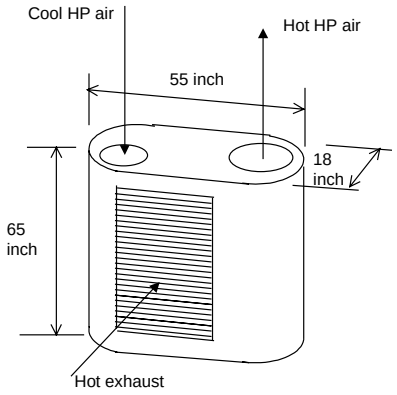

In order to reach 90% effectiveness for the 18 kg/s (40 lb/s) flow, we estimate that 5 of these cores will be required. On the exhaust side, the five cores are arranged in flow series, but on the air side a parallel configuration is employed, with the cores receiving cool air from and delivering hot air to common manifolds.

3.2.2.9 Gas Turbine Equipment Cost Considerations

The cost of turbomachinery depends strongly on its detailed design, particularly whether it is prepared for purely industrial purposes or for multipurpose duty including commercial aviation. In the most active sections of the industrial market, tight competition and purpose-designed industrial machinery tends to set the acceptable price level for units produced in substantial volume. At the flow required for the 20 MW fuel cell plant 18 kg/s (40 lb/s), a representative price for a complete simple cycle gas turbine is about $150/kW at 1090°C (2000°F) turbine inlet temperature. Total generating set price is $400/kW; i.e. the balance of plant costs $250/kW, which is more than the engine.

The special configuration turbomachinery required for the fuel cell plant will be more expensive than normal competitive industrial turbines because

- The low turbine inlet temperature of 870°C (1600°F) reduces output to only about 70% of "normal" power. This alone scales turbomachinery cost to $214/kW.
- Extra duct features required for intercooling and stack feed and return increase cost.
- The relatively small production volume does not justify so much production tooling. This and the extra duct features are assessed as doubling the cost to $428/kW.
- In practice, program development cost recovery may also place a significant charge on each unit. This term has been ignored.

The balance of plant cost should largely remain in proportion to power output, thus the generating set skid is expected to cost (428 +250) = $678/kW. Given an output of 3.8 MW, the skid cost is $2.58 M.

The turbine-based system cost in this plant includes two other substantial items, the intercooler and the recuperator.

We have examined intercoolers in other programs and consider that for this radial compressor application, only requiring moderate exchanger effectiveness, the most practical and quite satisfactory arrangement is a conventional water cooled tube-in-shell heat exchanger. Though the primary intercooler is not very expensive, in most arrangements a large water-air secondary heat exchanger is required. This can be forced or natural ventilation and, in combination with suitable ducting and plumbing, tends raise the price of a suitably sized system to around $0.2 M.

There is little data available to us defining the price of modern compact recuperators but what we have suggests an allowance of $0.83 M for the heat exchanging cores and $0.2 M for associated ducting.

The cost of the turbine skid plus intercooling and recuperation is thus $ 2.58 M + $ 0.2 M + $1.03 M = $ 3.81 M or $ 1000 / kW.

Intercooling and recuperation introduce additional maintenance requirements and it is considered that this will double running maintenance cost from a representative industry value of $ 0.005/kWh to $0.01/kWh.

3.2.3 SOFC Power Conditioning System

This project involved no task for the development of a power conditioning system (PCS) concept. For the power system performance estimates, the PCS efficiency, pertaining to the process between the SOFC DC terminals and the utility AC grid, was assumed to be 94%. This is consistent with current Siemens Westinghouse studies of mature power generation products to be offered circa 2010. The PCS equipment was costed at $120/kW DC.

The 20 MW PSOFC generator plant will be made up of nine electrically independent operating PSOFC generator modules rated at approximately 2 MW, and one 4 MW Gas Turbine generator. Each 2 MW PSOFC module should have its own power conditioning system (PCS) to process the dc power. The power conditioning systems should be located immediately outside each of the nine pressure vessels. By converting the dc power to ac at the PSOFC pressure vessel, the length of the high current dc bus duct, and the number of high current dc electrical components (breakers, etc.) can be minimized. Medium voltage ac components are more readily available, smaller, and less costly than low voltage, high current dc components.

One gas turbine alternator, nominally rated at 4 MW, will provide the additional power to the system. The turbine system supplies compressed air to all nine PSOFC modules. The GT unit will be supplied with the gas turbine, the alternator, and the power conditioning system as a single unit. As such, no other power conditioning will be required. The unit will export power directly to the 13.8kV bus.

Operator control of the PCS systems will be provided through standardized interface ports. Interface ports for operation and system status/diagnostics will be made available at the control panel provided. Each PCS system should provide status readouts at the control center for operator review and intervention, if necessary.

The PCS should be configured to supply continuously adjustable current between 0 and 100%. The output power factor will also be adjustable from leading to lagging power factor. The PCS should be designed to tolerate some level of phase imbalance. The PCS will manage the export power based on the set points transmitted from the PSOFC control. In the event of a complete utility disconnect, one or more of the PCS systems will enter a stand alone operating mode. This mode of operation is required to maintain PSOFC auxiliary equipment in the event of loss of utility power, to avoid complete plant shutdown, until utility power is restored. However, the PCS units should be configured for bi-directional power flow, should utility power be required to support the PSOFC auxiliary system power bus.

Figure 3.42 is a simplified block diagram of the major electrical components of the 20 MW power plant, and shows the PCS system configuration. Only two of the nine parallel modules are shown. Included in the PCS system is the DC to AC inverter, and a step-up transformer. The DC to AC inverter converts the high current DC power into 480V, three phase ac for distribution. The transformer boosts the voltage for greater distribution efficiency and reduced bus conductor requirements. The nine parallel connected PSOFC PCS systems feed into a common ac bus for electrical distribution.

3.2.4 Instrumentation and Controls System

The PSOFC modules and auxiliary equipment will be equipped with instrumentation and controls that provide for automatic operational control, and with manual capabilities for plant operation. The instrumentation and controls (I & C) systems also provide for monitoring, data collection, and diagnostics. The I & C systems will be categorized into generator module instrumentation and auxiliary system instrumentation and control. Each of the nine PSOFC modules will have complete and independent I & C systems for individual control of each sub-system. Each I & C system will allow for remote operation with the operating data consolidated and provided with data displays at the main operator interface panel.

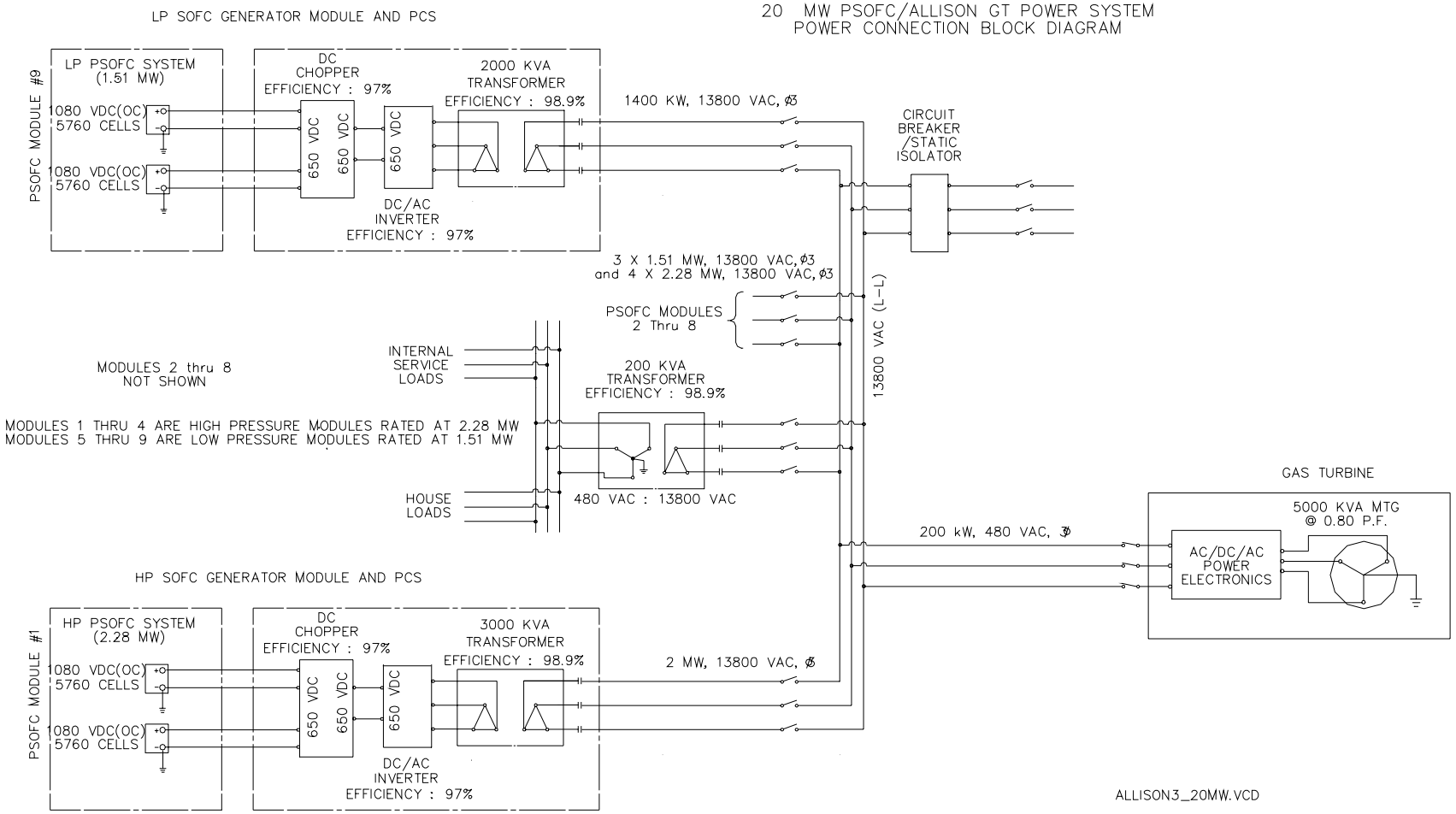

Figure 3.42 — Power Connection Block Diagram.

3.2.4.1 Hardware

PLC. The heart of the instrumentation and controls system is the programmable logic controller (PLC). The PLC provides safe, reliable, and steady operation of the PSOFC system over the entire operating range of the PSOFC generators. The controllers will scan inputs, execute preprogrammed logic, and set the state of outputs based on the control strategy. Depending on the final control architecture, one PLC could serve each PSOFC sub-system, with an additional PLC serving as a master controller.

Input/Output Modules. The I/O modules will link the instrumentation signals to the PLC. Thermocouples, voltage sensors, and current sensors will provide raw analog data through the I/O modules. The PLC converts the signals to digitized engineering units for display, or it provides an appropriate output response to various system actuators.

Communication Modules. The communication modules will link the master PLC to one or more PSOFC Control/Data computers. In addition, the communication modules will provide the control signals to the PCS for power control.

Electrical Control Hardware. The electrical control hardware is composed of those components that gather the input and output signals and respond to the needs of the main PLC process controller. Power supplies, signal conditioners, relays, current and voltage sensors, etc., comprise the electrical control hardware. These components form the control circuits that implement the commands from the PLC. The electrical control hardware also provides for continuous control of auxiliary devices such as blowers, valves, and the PSOFC generator/GT electrical loading. The components will be packaged for efficient space utilization and convenient maintenance access.

Operator Interface. An operator interface computer will be supplied as part of the I & C system, to provide a display of the critical PSOFC generator parameters, and to allow for operator input of some control parameter setpoints. The operator interface will consist of a computer with keyboard. A graphics display monitor, a large capacity hard drive, and a printer. Provisions for alarm monitoring/logging, operator input for state transition, manipulation of remote alarm action and control parameter setpoints will be incorporated into the operator interface.

3.2.4.2 Software

The instrumentation and controls system is a PLC based system that stores and uses information about the status of the PSOFC generator, the gas turbine systems, and the support systems. Data is read continuously and updated by the control software. Some of this data is also directed to, or taken from, the operator interface. The system software responds to the data, and controls the state of the generator. The system detects alarm conditions, and controls both modulating and discrete devices.

The PSOFC generating system will have a table of pre-defined operating states. For example, Pre-Op, Purge, Heat, Load, Run, Cool, Stop, and Sstop are typical PSOFC system states. The control system software contains the logic that determines the operating state of the PSOFC generators and all valid transition states. The control system will allow the operator to transition from the present state to a valid transition state only.

Discrete control logic will be used to change the states of control solenoid valves, and to provide valve status information to the operator.

Analog control logic will be set site alarm limits, and detect out of limit alarm signals. Response to the alarm signal will depend on the severity of the alarm. All alarms warn the operator. Others may result in a shutdown of the system.

Operator interface software package will be provided for supervisory control and data acquisition.

3.2.5 Electrical Distribution System (EDS)

The PSOFC/GT electrical distribution system links the PSOFC modules and the gas turbine systems to the PCS, and the PCS to the utility ac power grid. Included in this link are the bus leads, all of the power monitoring equipment, disconnect switches, and protective devices. A step up transformer is supplied as part of the PCS to elevate the output voltage before it is routed to the switchyard. At this switchyard additional step-up transformers raise the voltage as necessary for export to the utility grid. The disconnect switches will be strategically located for safe operation and maintenance of the PSOFC generating plant. Fault detection equipment will be provided, to sense utility grid under voltage, over voltage, and off frequency conditions.

There is also a requirement in the electrical distribution system for a 480 vac, 60 Hz bus. The bus will be fed by a step down transformer from the primary bus. The 480 vac bus is required to supply three-phase power for the PSOFC system auxiliary equipment, and for backup (UPS) power supplies. The electrical distribution system will have service breakers for individual sub-systems, for maintenance and for electrical protection capability in the event of a sub-system fault. A power distribution panel will be located within the PSOFC system to distribute the power to the internal system loads.

The electrical power from each of the PSOFC modules can be exported to the utility grid via a 13.8 kV bus if the adjacent grid lines are at this voltage. Otherwise, step-up transformers in the switchyard are used to match voltages. A static isolator will be provided between the high voltage bus and the grid interconnection to allow for quick disconnect, in the event of a fault, either on the utility grid, or on the PSOFC generating system. Individual PSOFC sub-modules will be protected by three phase circuit breakers.

The performance of the electrical distribution system is closely monitored and controlled by the instrumentation and control system. The I&C system provides the supervisory functions for power flow and fault conditions for each PSOFC sub-system and the gas turbine systems. The major power components of the electrical distribution system are shown in Figure 3.42.

3.2.6 Fuel Processing System

The supply of natural gas is assumed to be within the conventions of the U.S. distribution system. In the U.S., the distribution mains range in size from 0.508 m. (20 in.) to 1.07 m. (42 in.) and contain gas at 13.8 barg (200 psig) to 103.4 barg (1500 psig). Compressor stations are normally located 80 km (50 miles) to 100 km (60 miles) apart and occasionally as far as 290 km (100 miles). Gas flows in the mains at 24 km/hr (15 mph or 22 fps). The natural gas is reduced in pressure at the local natural gas supply utilities. These utilities add an odorant and distribute the gas through lines at about 4.1 barg (60 psig). The pressure at residential customers varies from 4 barg to 17 mbarg (60 psig to ¼ psig). The most commonly used gas piping is rated to operate at 6.9 barg (100 psig). For this study, it is assumed that the supply of natural gas at the plant site

is at 1.03 barg (15 psig) and contains a sulfur-based odorant. The gas line size needed for a 20 MW plant is 30.5 cm (12 in.) at 1.03 barg (15 psig) supply pressure.

On the plant site, the natural gas is filtered in an automatic duplex inlet filter. One side of the filter is on standby while the other side performs the filtering. When the differential pressure across the filter reaches the set pressure corresponding to a dirty filter element which needs to be changed, the automatic duplex filter uses the gas supply pressure for the motive force to actuate the three way valves and divert the flow through the standby side. A dirty filter indication is sent to the control system and filter element changing is scheduled. Filter element changing is performed with the unit on line and fuel flow is not interrupted.

The natural gas enters the inlet of one 100% capacity natural gas compressor. The compressor discharges to an accumulator which provides a pulsation dampening function as well as a reservoir of natural gas at compressor discharge pressure to ride through supply interruptions when the compressor stops and goes off line when the accumulator high pressure set point is attained. The compressor operates on accumulator pressure control, starting on low pressure and stopping on high pressure. The compressor design flow rate is set slightly higher than the maximum plant fuel consumption rate. During normal plant operation, the compressor will be idle about one fourth of the time.

From the natural gas accumulator, the fuel passes through a gas recuperator. Hot natural gas from the outlet of the desulfurizer system exchanges heat with the cooler natural gas leaving the natural gas accumulator. This preheated natural gas then leaves the gas recuperator at a temperature near 378°C (710°F).

The natural gas desulfurizer includes two 100% capacity each adsorbent containing vessels operating in series. At the entrance of the first vessel, a very small quantity of hydrogen, about 1% (by volume) of the fuel flow, is mixed with the natural gas. The gas mixture is electrically heated to raise its temperature to near 400°C (750°F). Each vessel includes an electrical gas heater under automatic temperature control to ensure that the zinc oxide bed and natural gas are at suitable temperature for effective sulfur removal.

The gas mixture first comes into contact with a cobalt-molybdenum catalyst where conversion of the complex sulfur compounds into H_2S occurs. The gas then passes into a bed of zinc oxide adsorbent. The adsorbent is ineffective for sulfur removal at ambient temperatures, but is very effective at temperatures above 277°C (530°F). Pre-heating of the natural gas/hydrogen mixture in the gas recuperator followed by supplemental electrical heating in a gas heater to the optimum operating temperature of 400°C (750°F) permits use of minimum sized adsorbent beds.

Sulfur removal effectiveness is periodically (monthly) checked after drawing a sample from the line between the two-desulfurization vessels. When the sample shows detectable sulfur, the valves are realigned to isolate the first vessel and pass the flow through the second vessel. After the zinc oxide adsorbent is replaced, the vessel is put back into service and aligned as the second in series. In this manner the adsorbent is fully consumed while ensuring that continuous desulfurization of the fuel occurs.

3.2.7 Gas Supply Systems

The plant includes both nitrogen and hydrogen generating equipment. The nitrogen is stored in pressurized cylinders until needed. The hydrogen is produced as demanded and not stored, thereby reducing fire protection concerns.

3.2.7.1 Nitrogen Supply System

The inlet to the natural gas compressor accumulator has a connection to a nitrogen purge system. The nitrogen supply system is normally isolated from the natural gas supply and is activated under two conditions:

- Emergency or safety stop (SSTOP)
- Maintenance of natural gas system components

When activated, the nitrogen purge system connection isolation valve and gas vent valve both automatically open. Nitrogen gas from a pressurized tank flows through the accumulator, gas recuperator, desulfurizer vessels and outlet duplex filter to the vent.

This dilutes and forces the natural gas out of the system until a nonflammable concentration of gas remains.

SOFC Cover Gas. The SOFC stacks require an inert or reducing environment on the fuel side of the cells when the temperature approaches and exceeds 600°C (1100°F). During normal operation, a reducing environment is maintained by reformation of the natural gas fuel by recirculation of a portion of the spent fuel back into the fuel ejector where it passes through the pre-reformer and is distributed into the in-stack reformers. Here steam reformation converts the methane and higher hydrocarbons to hydrogen and carbon monoxide.

During startup when the stack temperature is low and fuel recirculation will not support methane reformation, a nonflammable, inert nitrogen cover gas is used to provide the required atmosphere. A commercially available nitrogen generating system produces this cover gas. This system uses a selective membrane to separate nitrogen from the other constituents of air. This nitrogen cover gas system operates at plant startup and also when the plant is shut down.

A pre-packaged, skid mounted nitrogen generation system produces nitrogen gas whenever demanded by the low-pressure control in the nitrogen storage accumulator. The system stops when high pressure in the accumulator is attained. During normal plant operation there is no need for nitrogen. The nitrogen is available upon demand for plant start or cool down. The nitrogen generating equipment may occasionally operate to refill the accumulator if there are any leaks. The nitrogen system is sized to produce in seven days a sufficient quantity of nitrogen to support an unplanned emergency plant shut down. The storage accumulator has provisions to be filled with nitrogen from an external source, if necessary.

The nitrogen production is in commercially available equipment that consumes electricity and compressed air to generate nitrogen gas. The nitrogen is separated from the compressed air through a selective membrane. The nitrogen is 98% pure. Nitrogen flows under its own pressure from the accumulator without the need for additional pumping. When used as a cover gas for the SOFCs, some excess hydrogen (about 2% by volume) is added to scavenge the residual oxygen which remains in the nitrogen.

3.2.7.2 Hydrogen Supply System

A pre-packaged, skid mounted hydrogen generation system produces hydrogen continuously during plant start and normal operation. During normal operation the hydrogen is mixed into the natural gas to form a mixture which is about 1% hydrogen. This mixture is heated and delivered to the cobalt-molybdenum catalyst in the fuel desulfurization vessels. During plant start when fuel is supplied to the SOFC generators the hydrogen is also needed for catalysis of the natural gas.

The hydrogen production is in commercially available equipment that consumes electricity and electrolyzes water to generate hydrogen gas. This gas is drawn form the electrolysis chamber and immediately compressed. Hydrogen is produced as needed for desulfurization of natural gas. The hydrogen generator is sized to provide 100% of the hydrogen needed for catalysis of sulfur compounds in natural gas on the cobalt molybdenum catalyst.

3.2.8 Balance of Plant (BOP) Equipment

3.2.8.1 Startup Boiler

A natural gas heater boiler is supplied to provide a source of steam for plant start up. This commercially available, prepackaged, skid mounted boiler is a self-contained complete system with all-auxiliary components and instrumentation. Integration into the SOFC plant requires connection of natural gas and demineralized water piping and electrical power cable. The steam outlet is piped to the SOFC vessels and the boiler blowdown line is piped to a drain.

Boiler operation is manually controlled for the short time that it is needed. The boiler is used only for plant startup and is drained and laid up dry for a prolonged period of inactivity during normal plant operation.

3.2.8.2 Auxiliary Air Compressor

The auxiliary air compressor system includes an internal combustion engine driven compressor, inlet air filter, compressed air filter/dryer and air accumulator plus the necessary engine starter, instrumentation and controls. The dual fuel engine can use either natural gas or propane gas. The primary engine fuel is the normal natural gas supply.

In the event of loss of natural gas supply, the engine automatically switches over to use propane from a pressurized tank that contains liquid propane.

The compressor operates to fill an air accumulator. The compressor engine starts and stops based upon pressure control signals from the air accumulator. The auxiliary air compressor is sized to continuously provide all of the necessary airflow required to protect the airside of the SOFCs after a shutdown. This flow of air-cools the stacks from normal operating temperature to less than 260°C (500°F) in about three hours.

The compressed air accumulator provides a pulsation dampening function at the compressor outlet and permits supply of an uninterrupted source of auxiliary air when the engine has an interruption due to automatic fuel supply changeover.

3.2.8.3 Water Treatment and Storage

Potable water is taken from a local source, filtered, deionized and stored in a day tank. The day tank is sized to provide the water needed by the hydrogen generating system and startup boiler system during a normal plant start. The day tank is automatically filled on level control. Municipal water supply pressure is used to fill the tank.

The potable water system includes a pump to transfer the deionized water from the day tank to the hydrogen generating system and startup boiler.

3.2.8.4 Process Air Piping

The design of the process air piping from the main compressor to the SOFC vessels and back to the turbines has to satisfy several criteria. To satisfy these criteria, the process air piping is internally and externally insulated.

- The piping wall temperature should be less than or equal to 371°C (700°F). This criterion allows the use of standard piping material instead of higher cost alloys rated for high temperatures. All standard piping steels suffer no loss of strength until the working temperature exceeds 400°C (750°F).

- The external insulation jacket surface temperature is less than the OSHA 29CFR1910.107(l)(7) limit of 65.6°C (150°F). Conventional jacketed, mineral wool is suitable for this application.

- The speed of the air inside the inner insulation is less than 30 m/s (100 ft/s). This air speed does not require an internal protective liner for the insulation and permits the use of less expensive, commonly available insulating materials without concern for erosion of the surface. Vacuum formed alumina-silica fiber insulation was found to have good thermal resistance and appropriate abrasion resistance.

To satisfy the piping criteria, the internal insulation is approximately 19.4 cm (7.63 in.) thick and the external insulation is 7.6 cm (3 in.) thick.

3.2.9 Plant Operation

Plant operations are summarized in the following sections. These summaries include normal plant startup, normal operation, normal shutdown and emergency shutdown.

3.2.9.1 Preparations for Normal System Start

The following services are available:

- Natural gas compressor is operational and gas supply pressure is in range
- Auxiliary air compressor is operational and compressed air accumulator pressure is in range
- Demineralized water day tank is filled to required level with deionized water
- Nitrogen system accumulator pressure is in range
- Hydrogen system is operational

System Configuration:

- Initial system status — unpressurized at ambient temperature
- Fuel piping — fuel supply control valves for all SOFC modules are closed. Fuel supply control valves for both air heaters are closed. Combustor fuel supply is off. Desulfurizer vessels' vent to atmosphere is closed.
- Vessel fuel vent system piping — fuel vent system isolation valves from each SOFC module are closed.
- Auxiliary air compressor piping — Isolation valves to SOFC module air supply headers are closed.

- Cover gas piping — Isolation valves to both SOFC module fuel supply headers are closed.

Operator Actions Sequence. Start turbine air compressor motor. When airflow through turbine is established, fire the combustor to bring the turbine/compressor assembly up to normal speed. Allow the turbine/generator to free wheel as the flow of air passes through the LP SOFC modules to the LP turbine inlet.

Fire the air heater on the HP SOFC module inlet header. Control firing to limit the air heater exit air temperature to 500°C above the lowest temperature HP SOFC vessel stack.

Fire the air heater on the LP SOFC module inlet header. Control firing to limit the air heater exit air temperature to 500°C above the lowest temperature LP SOFC vessel stack.

When the highest temperature HP SOFC module stack reaches 500°C, open the cover gas system supply isolation valves to admit inert gas into the header which feeds the HP SOFC vessels.

When the highest temperature LP SOFC module stack reaches 500°C, open the cover gas system supply isolation valve to admit inert gas into the header that feeds the LP SOFC vessels.

Begin adding steam to the SOFC generators, via the fuel supply system, when combustion zone temperatures reach 600°C.

When the SOFC vessels reach 675°C stack temperature, begin to draw current. Start low fuel flow. Slowly increase the power being drawn from the stack. Fuel flow increase will automatically follow current increase.

Isolate cover gas system from the SOFC module headers when the current from each stack reaches 300 A. Fuel reformation and recirculation is sufficient to maintain a self-sustaining reducing atmosphere in the fuel region.

Begin to load the turbine generator. Increase the power drawn as the temperature increases in order to maintain airflow (shaft speed) at design value(s).

Turn off air heaters when the current from each stack is approximately 460 A. At this time the recuperated air temperature is self-sustaining.

Turn off the turbine combustor.

3.2.9.2 Normal Operation

The plant run state is entered when the stack temperature achieves 850°C and the current draw is 300 A from each SOFC module. During normal operation, the operator has control of:

- Fuel utilization
- Current
- Stack temperature

Setting the control system set points for any two of these parameters determines the third.

The plant is expected to operate unattended for 50 weeks with periodic remote monitoring and control adjustments made via telephone modem access for a remote location. At the end of the scheduled normal time, operators return to the site to supervise a normal shutdown.

While most maintenance will be performed during the annual scheduled plant outage, some activities may need to be performed during normal operation. The replacement of natural gas desulfurizer adsorbent will normally be performed during the annual maintenance period. In the event that the first bed in series does not last until the end of the 50 weeks of operation, it is isolated and all flow diverted through the remaining bed. After the bed has cooled and the adsorbent replaced, it is put back on line as the second in series. Similarly, the duplex filters on the inlet and outlet of the desulfurizers will normally last for years before developing enough filtrate cake to produce the pressure drop to trigger automatic change over. The duplex filter changes position to pass flow through the standby filter when across the filter media increases to the dirty filter set point. Spent filter elements will be changed as the need arises.

3.2.9.3 Normal Shutdown

Start Cover Gas System. When cover gas system is fully operational, the turbine AC generator is unloaded.

Shutting down the SOFC modules is accomplished with simultaneous control actions to:

- Stop natural gas flow to the modules
- Start cover gas system flow to the modules
- Unload current to ~35 A per stack and transfer power to stack energy dissipaters

The turbine will continue to rotate and produce compressed air flow, running on the stored heat from the SOFC modules. After system cooling has proceeded and the turbine/ compressor approaches stall, the generator will be used as a motor to drive the compressor. An alternate, but slower, way to cooling the plant is to open the auxiliary air supply isolation valve to permit flow of air into the HP SOFC modules from the auxiliary air system.

Stop flow of cover gas system when the stack temperatures are lowered to 500°C.

Continue supply of auxiliary air until stack temperature is reduced to100°C.

Automatic Stop Conditions. The plant will automatically enter STOP when any of the following conditions are sensed:

- Low generator voltage
- Low generator current
- High stack temperature for 10 minutes
- Low UPS battery voltage

The sequence of automatic shutdown actions is the same as if the shutdown were initiated by manual control action.

3.2.9.4 Normal Maintenance

At the end of a normal run time, the plant is shut down for normal maintenance. The maintenance period is two weeks. During this period the activities include:

- inspection of turbine and generator rotating parts
- lubricating oil changes
- air filter element replacement
- instrumentation and control system calibrations
- repair or replacement of failed or improperly operating components
- fire protection system inspection and testing

3.2.9.5 Emergency Operations

To accommodate the occurrence of abnormal situations, the plant control system is equipped to automatically take control actions. The priorities for automatic emergency control actions are 1) personnel protection and 2) property protection. The extent to which emergency conditions are accommodated is indicated in Table 3.5.

It is assumed that no two failures occur simultaneously.

Table 3.5 — Plant Emergency Situations

Plant Mode	Control Sequence			
	Loss of Grid	**SOFC Failure**	**Turbine or Generator Failure**	**Cover Gas System Failure**
Startup	Start auxiliary air compressor Enter aux. air stack cooling sequence Maintain cover gas flow until stacks are less than 500°C	Enter normal stop sequence	Start auxiliary air compressor Enter aux. air stack cooling sequence Maintain cover gas flow until stacks are less than 500°C	Depressurize Vent Fuel Side Start primary air cooling sequence Reestablish purge with nitrogen
Normal Operation	Divert turbine/generator power to resistance banks, SOFC to open circuit.	Enter normal stop sequence	Start auxiliary air compressor Enter aux. air stack cooling sequence Start and maintain cover gas flow until stacks are less than 500°C	N/A
Normal Shutdown	Start auxiliary air compressor Enter aux. air stack cooling sequence Maintain cover gas flow until stacks are less than 500°C	Continue normal shutdown sequence	Start auxiliary air compressor Enter aux. air stack cooling sequence Maintain cover gas flow until stacks are less than 500°C	Depressurize Vent Fuel Side Start auxiliary air compressor Purge with nitrogen

3.3 Power System Installed Cost and Cost of Electricity Estimates

Table 3.6 summarizes the development of the power system installed cost, and in Table 3.7, the system COE estimate is developed. Mature-product conditions (circa 2008) were assumed. SOFC power conditioning equipment was costed at $120/kW. Balance-of-plant equipment costs were obtained from potential suppliers; supply rates consistent with 10 to 100 power systems/year were assumed. The transportation cost estimates were developed consistent with Siemens Westinghouse transport experience with recent SOFC demonstration units; the transport distance was 500 miles per the design requirements. The site preparation, project management, and equipment installation cost estimates were developed by ICF Kaiser Engineers, Pittsburgh, PA, under subcontract. Input for the COE analysis is identified in Table 3.7.

Table 3.8 provides the COE estimate for the conventional power generation technology, a 20 MWe-class gas turbine/steam turbine combined cycle. For the reference fuel cost, $3.00/MMBtu, the HEFPP COE estimate is higher than the conventional-technology

COE estimate by approximately 3%. Better COE performance is achieved when the HEFPP system operates in a higher-fuel-cost environment. For example, with $6 fuel, the HEFPP COE estimate is less than the conventional-system COE by approximately 7% (66 mills/kWh vs. 71 mills/kWh), and for $9 fuel, it is 13% less (83 mills/kWh vs. 95.0 mills/kWh).

Table 3.6 — Power System Installed-Cost Estimate

Installed Equipment Costs						
	Equipment	**Freight**	**Installation**	**Totals**		
SOFC Generator	8,890,422	31,500	47,365	8,969,287		
Gas Turbine System	3,960,682	3,500	59,347	4,023,529		
SOFC Power Conditioning System	1,988,520	15,750	24,374	2,028,644		
Instrumentation, Controls, and Electrical Cabinets	877,542	7,000	199,520	1,084,062		
Switchyard and Electrical Distribution	959,600		237,980	1,197,580		
Fuel Supply System	167,091	1,750	10,000	178,841		
Hydrogen Supply System	89,779	1,750	10,000	101,529		
Purge Gas Supply System	120,520	1,750	10,000	132,270		
Auxiliary Air Supply System	179,723	1,750	6,510	187,983		
Startup Boiler System	74,884	1,750	1,316	77,950		
Piping and Insulation	1,608,054	15,750	317,649	1,941,453		
Site Buildings				36,159		
Totals	**18,916,818**	**82,250**	**924,061**	**19,959,288**		
Project Cost Summary						
Installed Equipment						19,959,288
Project Management, Engineering, and Permitting						919,369
Site Preparation						412,994
Grading, utilities installation					145,744	
Foundations installation					217,519	
Structural steel installation					49,731	
G&A, R&D, Sales & Marketing, Profit Allowance						5,544,303
Total Plant Cost						26,835,954
Spare Parts Allowance						246,914
Startup						150,000
Land						20,000
Total Capital Requirement						27,252,868

As indicated in the trade-study discussion, Section 3.4.1, a hybrid power system with a lower installed cost and lower efficiency could be configured that would, in the $3 fuel case, have a lower COE than the high-efficiency power system because the system capital cost is the dominant COE parameter. With higher fuel costs, that would not be the case, and the higher-cost, higher-efficiency power systems would become more attractive.

Table 3.7 — Power System Cost of Electricity Estimate

COE Calculation Basis		Cost Summary	
No. round-the-clock power system operators	1		
No. plants on system	5	**Fixed O&M, $/kW-year**	
Operator labor cost, $/man-hour	75	Plant operation & control	6.9
Housekeeping maintenance, man-hours/week/system	20	Housekeeping maintenance	1.4
Housekeeping labor cost, $/man-hour	25	Administration (30% of operation & maintenance labor)	2.5
System rating, MW net ac	19.0	**Total Fixed O&M, $/kW-year**	10.7
Gas turbine rating, MW ac	4.1		
SOFC module rating, MW dc	16.571	**Variable O&M, mills/kWh**	
Gas turbine maintenance cost, $/GT kWh	0.01	**SOFC replacement**	2.1
SOFC replacement cost, $/SOFC generator module	468,920	**Gas turbine maintenance**	2.1
SOFC replacement interval, years	10	**Desulfurizer adsorbent/catalyst replacement**	0.1
Power plant capacity factor	0.92	**Total Variable O&M, mills/kWh**	4.3
Desulfurizer adsorbent & catalyst, $/year	8,919		
Interest rate (SOFC replacement cost calculation), %	6.0	**Total O&M COE, mills/kWh**	5.6
Power system efficiency (net AC/LHV), %	67.3	**Capital COE, mills/kWh**	26.6
Capital charge rate, %/year	15	**Fuel COE, mills/kWh**	16.9
Power system capital cost, $/kW	1,431	**Total COE, mills/kWh**	49.1
Fuel Cost, $/MMBtu	3.0		
		COE, Relative to Conventional Technology	1.032

Table 3.8 — Conventional-Technology Power System Cost of Electricity Estimate

Information Source: Gas Turbine World 1997 Handbook, p. 24			
System Classification: Gas Turbine/Steam Turbine Combined Cycle			
Gas Turbine: General Electric LM 1600			
Steam Turbine Cycle: Two-pressure, 4.8 MWe			
Net System Power Output: 17.9 MWe			
System Efficiency: 47.9% (net AC/LHV)			
Turnkey Price: $14.9M ($830/kWe)			
Basis		**COE Summary**	
No. round-the-clock power system operators	1	**Fixed O&M, $/kW-year**	
No. plants on system	5	Plant operation & control	7.3
Operator labor cost, $/man-hour	75	Housekeeping maintenance	1.5
Housekeeping maintenance, man-hours/week/system	20	Administration (30% of operation & maintenance labor)	2.6
Housekeeping labor cost, $/man-hour	25	Total	11.4
Power system maintenance, $/kWh	0.007		
Power system capacity factor	0.92	**Variable O&M, mills/kWh**	7.0
Power system capacity, net AC kWe	17900		
Power system efficiency (net AC/LHV), %	47.9	**Total O&M COE, mills/kWh**	8.4
Capital charge rate, %/year	15		
Power system capital cost, $/kW	830	**Capital COE, mills/kWh**	15.4
Fuel cost, $/MMBtu (HHV)	3.00		
		Fuel COE, mills/kWh	23.7
		Total	47.6

3.4 Conceptual Design Trade-Off Studies

3.4.1 SOFC Generator Sizing and Pressure Ratio Selection

The PSOFC/GT hybrid-cycle power system in this analysis uses the intercooled recuperated Rolls Royce Allison reheat gas turbine. Earlier analyses to size the SOFC generator for this 20 MWe system, and also to select a compressor pressure ratio, assumed the staged-cell, crossflow stack configuration, and they applied the preliminary estimate of the staged-cell voltage effect that was used in the proposal effort. That estimate took the form of an adder on the conventional cocurrent-flow cell V-I characteristic, with the adder increasing as the cell current decreased. As a result, that model tended to favor design for low-pressure ratios. Low ratios are needed to support system operation at the low current densities that are necessary for high-efficiency operation, and with the crossflow voltage adder model, the cell efficiency gain that occurred as the current was reduced more than compensated for the loss in turbine power that occurred due to the pressure ratio reduction. Thus, from the efficiency standpoint, the staged-cell voltage model tended to drive the system design point to the very lowest pressure ratios. Without the crossflow adder, the increase in cell voltage as the cell current is reduced is not strong enough to compensate for the drop in turbine power, and after some minimum cell current is reached, there is no incentive to go to lower currents and pressure ratios. The crossflow analysis indicates that the performance gains by employing the staged-cell would actually be less than those predicted originally, and it was therefore concluded that the cocurrent-flow stack configuration should be retained. As a result, the generator sizing analysis and the calculations to select a design pressure ratio needed to be re-visited.

The earlier generator sizing analyses also assumed that the power turbine and generator were mounted on a shaft separate from the gasifier shaft, and that the gasifier produced no net power. This constrained the analysis in that the expansion across the gasifier turbine was therefore set to work-balance the turbine and compressor, and the power turbine was then required to accept the remaining expansion. To better control the hybrid system, it is now believed that the turbine should be a single-shaft machine. This means that the expansion across the gasifier turbine could be an independent variable, and that it could be selected for optimum system efficiency performance.

Considering both system performance and the cost of electricity (COE), an analysis has been done to final-size the SOFC generator for the 20 MWe high-efficiency power sys-

tem, and also to evaluate the effect of pressure ratio. The SOFC generator cell stacks were of the conventional cocurrent flow configuration, and the compressor and expander wheels in the reheat gas turbine were all assumed to be installed on a single shaft. Results of the analysis are summarized in this note

3.4.1.1 Analysis Basis

- Cycle configuration – Figure 3.43.
- SOFC generator configuration – the generator is composed of pressurized generator modules. Each module is a horizontal pressure vessel housing twenty 576-cell substacks, or the equivalent of ten EDB/ELSAM 100 kW cell stacks. In the reheat power system, there are high pressure (HP) and low pressure (LP) generator sections. The number of modules in each section is to be determined by this analysis. For cost-estimating purposes, it has been assumed that the same module design is applied to both sections.
- Cell V-I characteristic – the mature-product characteristic.
- SOFC stoichs model – the stoichs profile determined by thermal-hydraulic analysis for the 1020°C peak cell temperature and 870°C combustion zone exhaust temperature (air feed tube heat transfer enhancers out) was used. The HP generator modules generally operate at higher cell currents than do the LP modules, and the air flow in the cycle is therefore set by the air flow requirement of the HP modules.
- Gas turbine – the turbine is intercooled and recuperated, with all rotating components mounted on a single shaft. The compressor pressure ratio is to be determined by this analysis. The turbine has two compressor stages, separated by the intercooler. The intercooler air exit temperature is 23°C (73°F), 8°C (14°F) above the ambient air temperature. The pressure ratio across each stage is the square root of the compressor pressure ratio, with an allowance for a 6% intercooler pressure drop.
- The gas turbine combustors and the air heaters are not fired during normal steady-state power operations.
- SOFC fuel consumption – 90%
- SOFC cell stack fuel bypass leakage – 1%
- Power lead cooling air flow – 0
- Power lead and stack internals power loss – assumed 1% of cell power. For comparison, at 500 generator amps, the EDB/ELSAM 100 kW terminal voltage is 0.5% less than the sum of the bundle voltages, based on 2/5/98 data sheet analysis. Therefore, the 1% loss assumption is reasonable, given the uncertainty in the power takeoff design.
- SOFC power conditioning system overall efficiency – 94%, mature-product value.

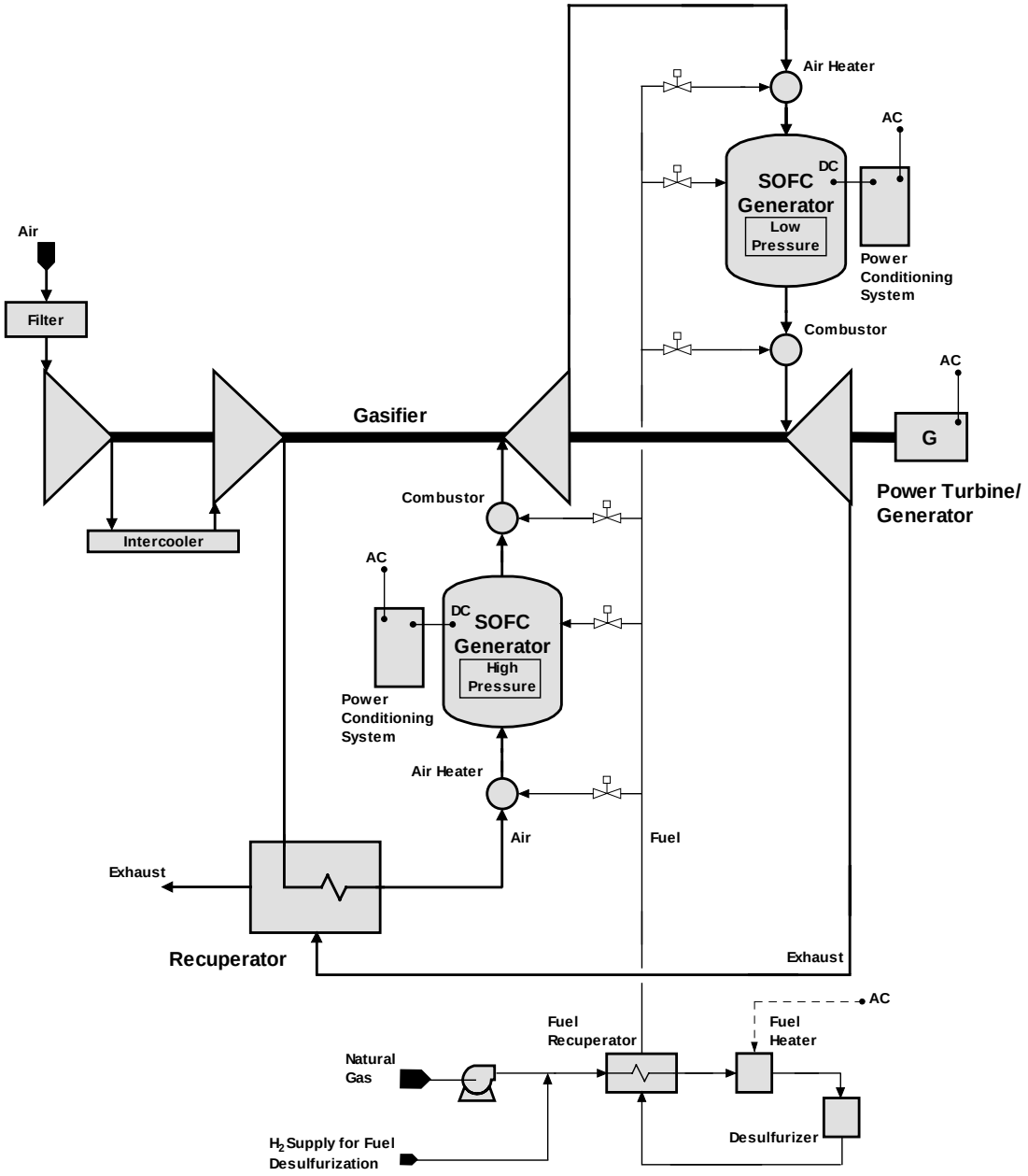

Figure 3.43 — High-efficiency power system cycle.

3.4.1.2 Discussion

System Efficiency - Effects of Pressure Ratio, Gasifier Expansion Ratio, and the Number of SOFC Modules. Results of calculations to evaluate the sensitivity of system performance to variations in compressor pressure ratio (PRAT) and gasifier turbine expansion ratio (turbine outlet pressure/inlet pressure) are shown in Figure 3.44. For these particular calculations, the power system included four HP SOFC generator modules, and four LP modules. Given a PRAT value, a curve of system efficiency can be drawn vs. power output, with each point on the curve applying to a different value of the turbine expansion ratio. In Figure 3.44, three such points, applying to expansion ratios of 0.4, 0.5, and 0.6, are identified on the PRAT= 6 curve. As the expansion ratio is increased, there is less pressure drop across the gasifier turbine, and the inlet temperature at the LP SOFC modules increases, meaning those modules will have to operate at lower cell current to maintain the required combustion zone exhaust temperature. With less expansion across the gasifier turbine, there must be more across the power turbine. This will cause lower gas temperatures at the HP SOFC module inlets, and the cell currents in those modules will therefore have to increase. Thus, with an increasing gasifier turbine expansion ratio, the tendency is for more power to be produced in the HP modules, and less in the LP modules, and there will be an optimum expansion ratio value at which the system efficiency is maximized. For PRAT = 6, that ratio is 0.50. As PRAT increases, the optimum expansion ratio decreases, because that will tend to result in less expansion across the power turbine, and higher inlet temperatures at the HP SOFC module inlets, which supports HP SOFC operation at lower, higher-efficiency cell currents.

There is also an optimum PRAT value that results in maximum system efficiency. That value weighs the positive efficiency effect of increasing pressure on cell voltage against the negative effect that is caused by the tendency to balance at higher cell currents as PRAT increases.

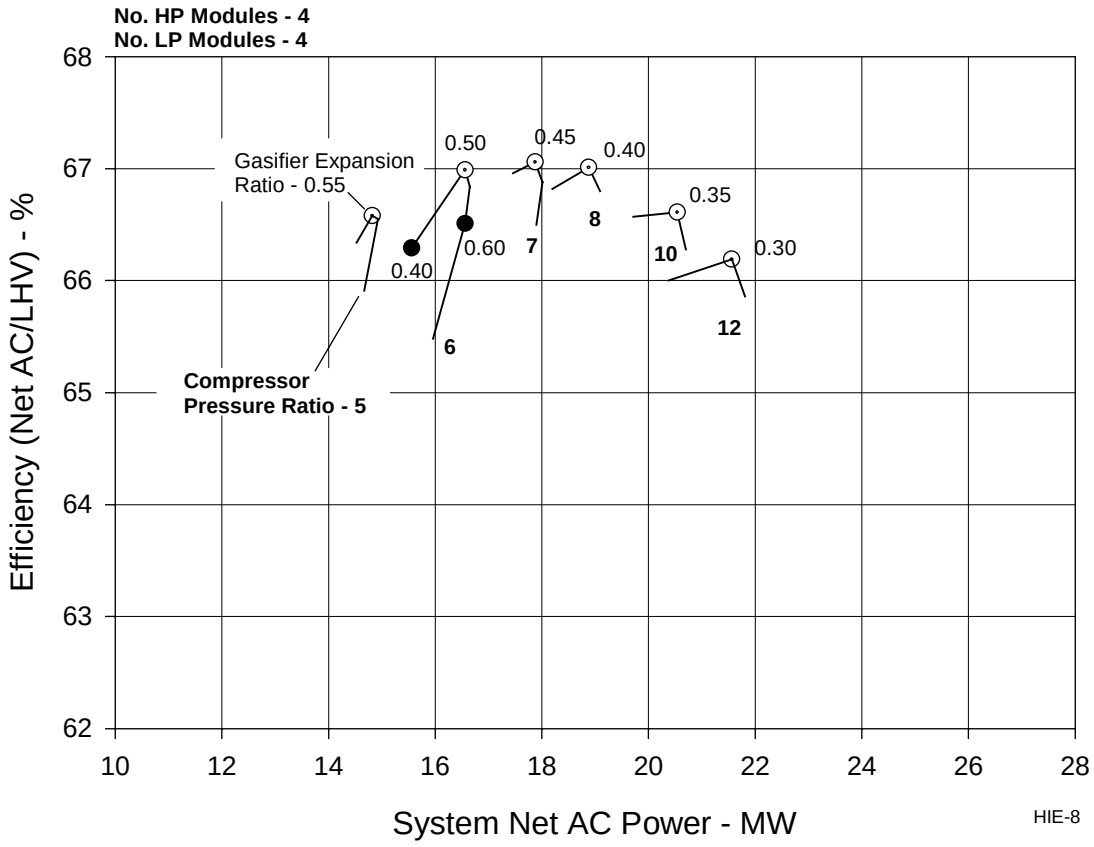

Figure 3.44 — Effect of pressure ratio and gasifier expansion ratio for 4/4 module configuration.

Figure 3.45 shows the same curves for the case in which the power system is equipped with an additional LP SOFC module, and higher system efficiencies result. Adding LP SOFC surface area will generally have a positive effect on efficiency because the LP cells will now be able to operate at lower, higher-efficiency currents, the gas temperature at the HP SOFC inlet will tend to increase, meaning the HP SOFC modules can be operated at higher-efficiency cell currents as well. Similarly, adding an HP SOFC module will generally result in lower system efficiencies - compare Figure 3.44 and Figure 3.46.

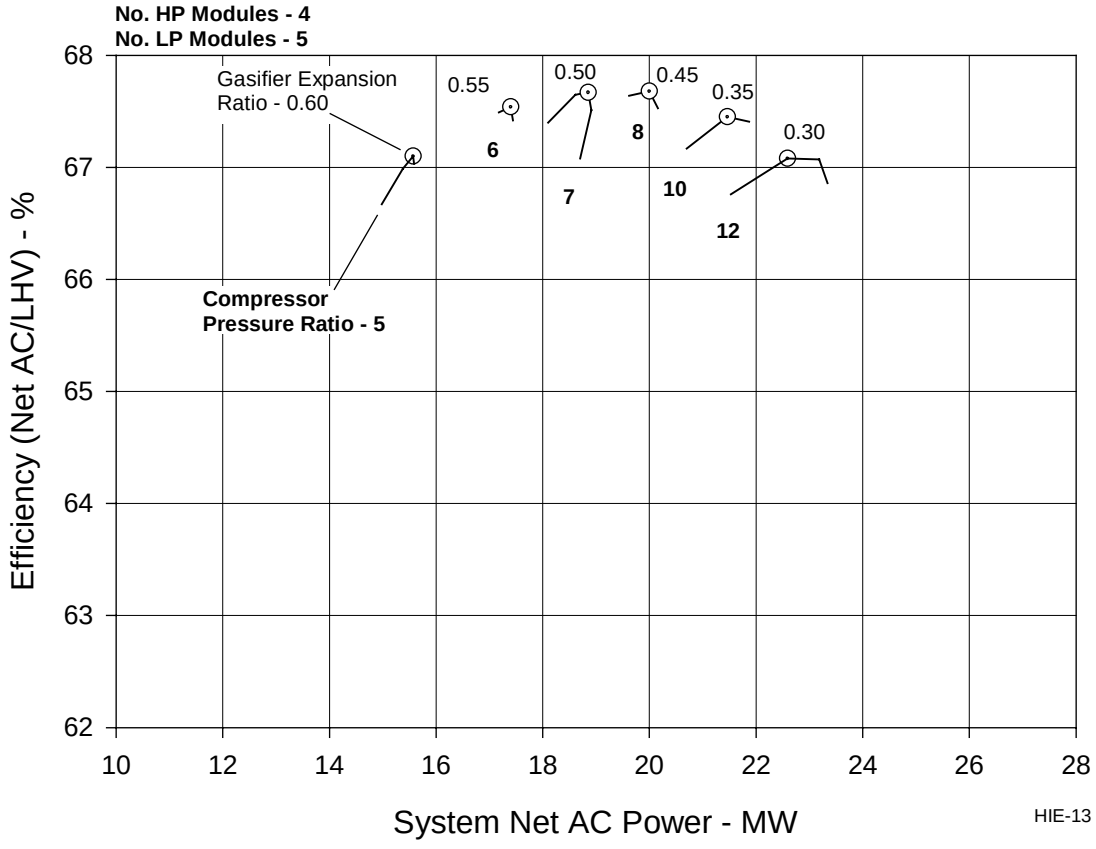

Figure 3.45 — Effect of pressure ratio and gasifier expansion ratio for 4/5 module configuration.

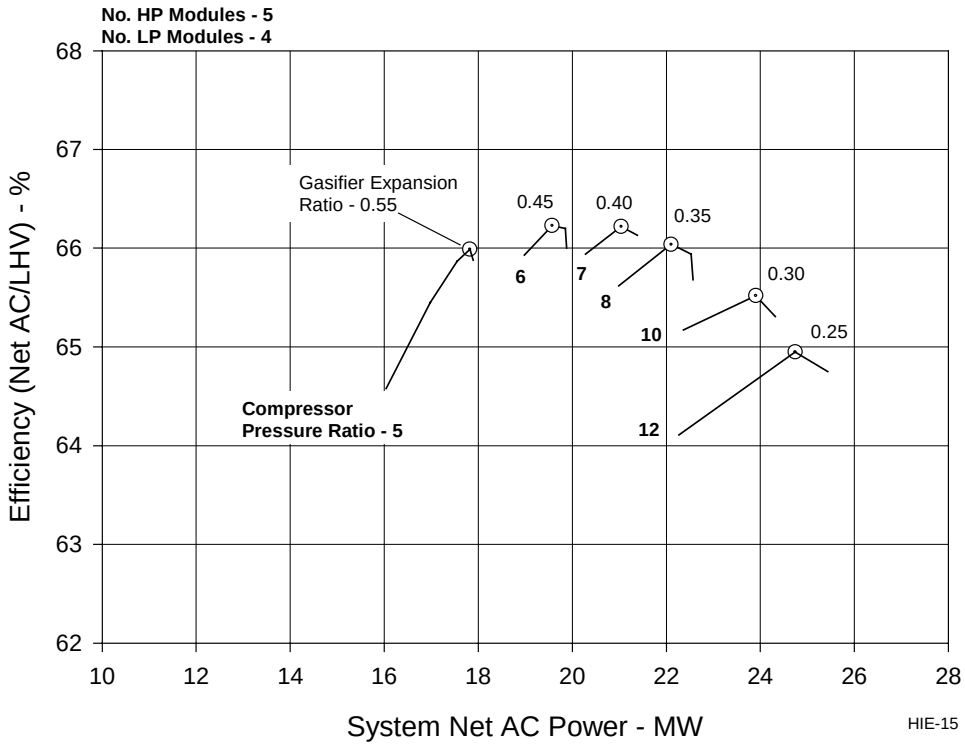

Figure 3.46 — Effect of pressure ratio and gasifier expansion ratio for 5/4 module configuration.

Performance curves for four HP modules and three LP modules are presented in Figure 3.47. The efficiencies are similar to the values reported in the Figure 3.46 for five HP and four LP modules, but the predicted power outputs are generally lower due to the overall smaller SOFC system.

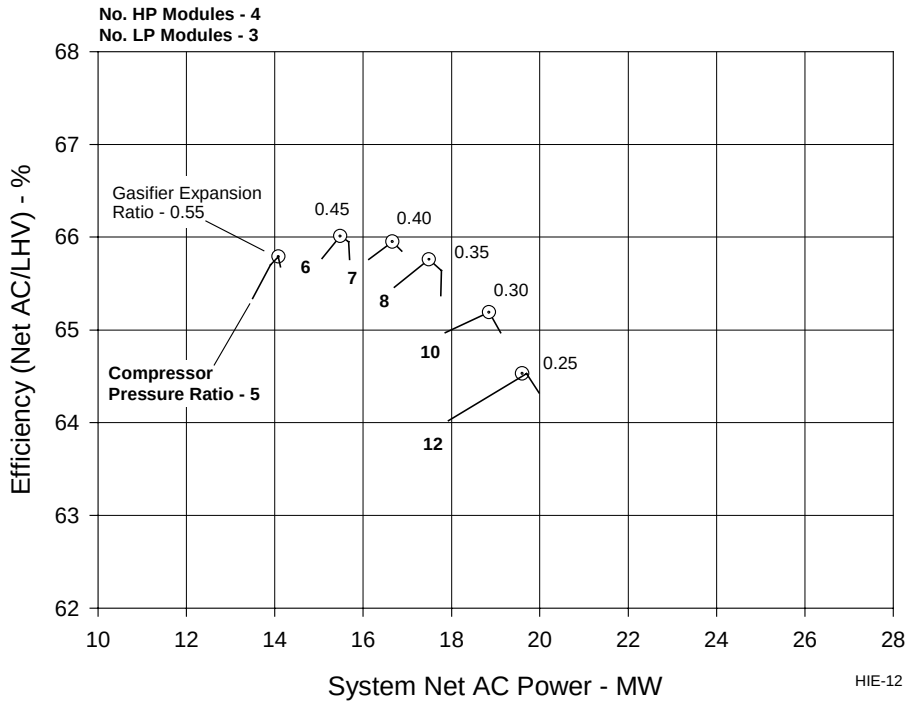

Figure 3.47 — Effect of pressure ratio and gasifier expansion ratio for 4/3 module configuration.

The peak efficiency points from Figure 3.44 to Figure 3.47 for the four combinations (4/4, 4/5, 5/4, and 4/3) of HP and LP SOFC modules are graphed in Figure 3.48. The highest efficiencies occur for the 4/5 configuration. For that configuration, 20 MWe are generated with a compressor pressure ratio in the 7:1 to 8:1 range. The possibility of further unbalancing the module distribution further in favor of the LP modules (e.g., 4/6 or 3/5) to achieve higher efficiencies has not been analyzed. Large flow imbalances between the HP and LP modules can result, and their effects on module temperatures and cell voltages would need to be considered.

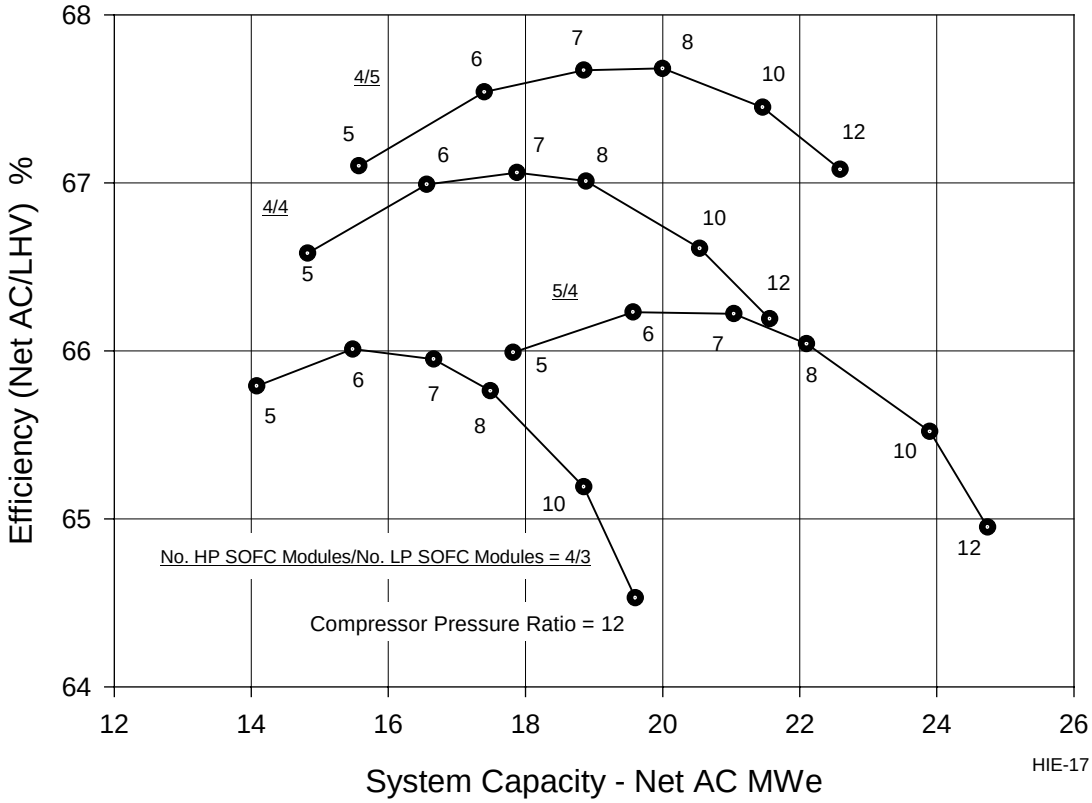

Figure 3.48 — Peak-performance estimates vs. module configuration and pressure ratio.

3.4.1.3 Cost of Electricity

Corresponding to the peak-efficiency curves of Figure 3.48, and based upon this study's reference fuel cost of $3/MMBtu, relative cost-of-electricity (COE) curves for the power system are plotted in

Figure 3.49. The figure shows that with this fuel cost, the minimum COE value, at near 20 MWe, occurs with a 4/3 SOFC module combination and a high compressor pressure ratio (lowest SOFC capital cost, and maximum power from the relatively low cost gas turbine), and Figure 6 shows that the minimum COE point coincides with system operation at the minimum efficiency value. This simply confirms that with low-cost fuel, the system capital cost can be the major COE driver, and the lowest COE and the highest fuel efficiency may not occur at the same system design point.

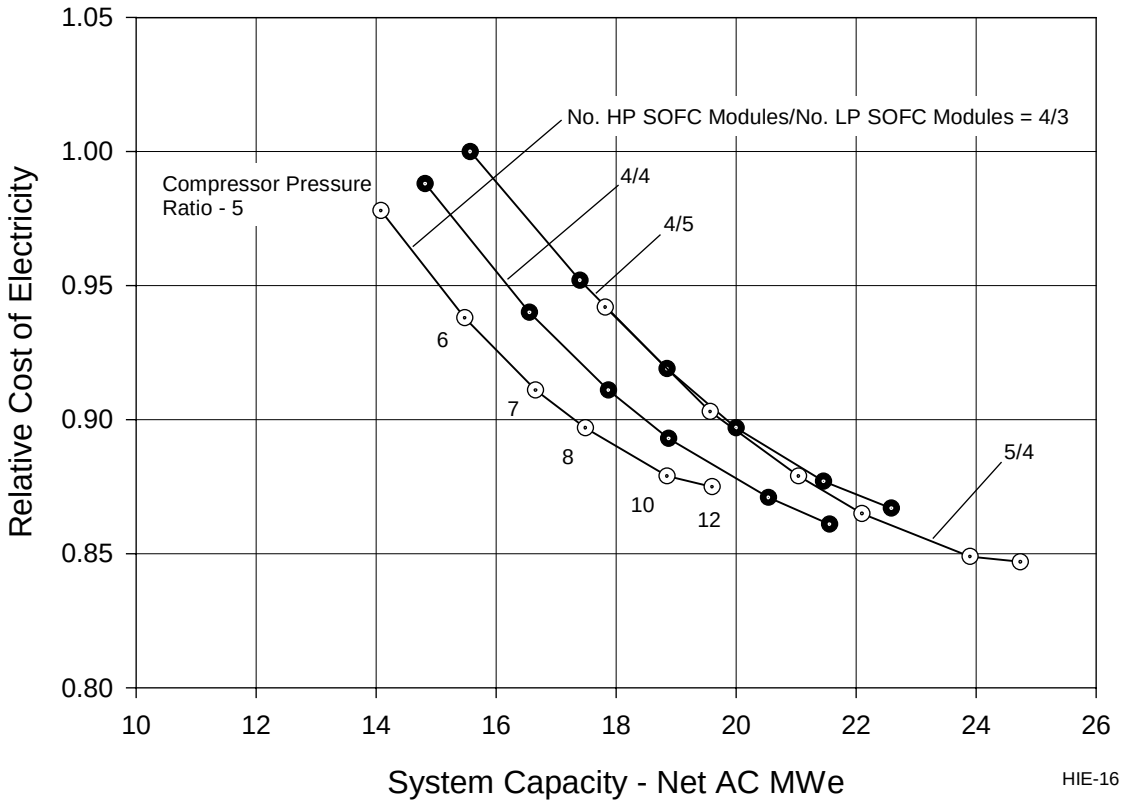

Figure 3.49 — Relative COE estimates vs. module configuration and pressure ratio (Fuel cost = $3.00/MMBtu).

Table 3.9 provides a COE estimate for the conventional competing technology, which for this study, is assumed to be a 20 MWe-class gas turbine combined cycle power system. Using base assumptions similar to those used in calculating the COE for the SOFC/GT hybrid power system; the estimated COE for the competing-technology system is 47.6 mills/kWh. For the high-efficiency system study, the target COE for the PSOFC/GT system is to be 10% to 20% below the competing-technology value. With the current system cost calculations, the 10% goal will possibly be reached at a relative COE in the 0.85 to 0.87 range (see

Figure 3.49).

Table 3.9 — Conventional Technology Power System COE Estimate

Information Source: Gas Turbine World 1997 Handbook, p. 24			
System Classification: Gas Turbine/Steam Turbine Combined Cycle			
Gas Turbine: General Electric LM 1600			
Steam Turbine Cycle: Two-pressure, 4.8 MWe			
Net System Power Output: 17.9 MWe			
System Efficiency: 47.9% (net AC/LHV)			
Turnkey Price: $14.9M ($830/kWe)			
Basis		**COE Summary**	
No. round-the-clock power system operators	1	**Fixed O&M, $/kW-year**	
No. plants on system	5	Plant operation & control	7.3
Operator labor cost, $/man-hour	75	Housekeeping maintenance	1.5
Housekeeping maintenance, man-hours/week/system	20	Administration (30% of operation & maintenance labor)	2.6
Housekeeping labor cost, $/man-hour	25	Total	11.4
Power system maintenance, $/kWh	0.007		
Power system capacity factor	0.92	**Variable O&M, mills/kWh**	7.0
Power system capacity, net AC kWe	17900		
Power system efficiency (net AC/LHV), %	47.9	**Total O&M COE, mills/kWh**	8.4
Capital charge rate, %/year	15		
Power system capital cost, $/kW	830	**Capital COE, mills/kWh**	15.4
Fuel cost, $/MMBtu (HHV)	3.00		
Fuel higher heating value, Btu/lb	21873	**Fuel COE, mills/kWh**	23.7
Fuel lower heating value, Btu/lb	19711	Total	47.6

3.4.1.4 Reference Power System Specifications

If we place the emphasis on system efficiency, the reference power system should have the following characteristics:

No. HP SOFC modules – 4 (Icell = 290A, Vcell = 0.681V)

No. LP SOFC modules – 5 (Icell = 181A, Vcell = 0.726V)

Gas turbine pressure ratio – 7

Gasifier turbine expansion ratio – 0.50

Compressor air intake rate – 18 Kg/s

Gas turbine AC power capacity – 4 MWe

System capacity – 19.0 MWe net AC

System efficiency – 67.6%

The gas turbine specs are fairly close to those already developed by RR Allison, except for the pressure ratio that is 7:1 vs. 6:1 in RR Allison design.

3.4.2 Effect of Compressor Intercooling on Power System Efficiency and Cost of Electricity

Intercooling the compressor increases the gas turbine power output, and in a recuperated cycle, it increases the power system efficiency as well. Both effects are seen in the efficiency and power curves of Figure 3.50. The curves apply to a high-efficiency PSOFC/GT hybrid-cycle power system with fixed SOFC generator design (four HP SOFC generator modules, five LP SOFC modules), but the gas turbine design varies from point to point with the changing compressor pressure ratio. The curves indicate that with intercooling, the peak-efficiency operating point occurs at a higher pressure ratio, and that intercooling adds approximately one-half of one percentage point to the peak power system efficiency, and two to three megawatts to the peak-efficiency power output. The analysis considered both the heat-rejection parasitic-power requirement that intercooling imposes on the power system, as well as the direct effect of intercooling on compressor and system power output.

The predicted effect of intercooling on COE is indicated in Figure 3.51. The estimates consider the capital cost of the intercooling equipment, and also the increased maintenance requirements that intercooling imposes on the power system. Figure 3.51 indicates that with the project reference fuel cost ($3/MMBtu), and for a desired system net AC power output, intercooling will add to the system COE – even though it increases both power and efficiency. For the reference power system design, and consistent with the project high-efficiency focus, the intercooling feature was adopted because of its positive effect on system efficiency.

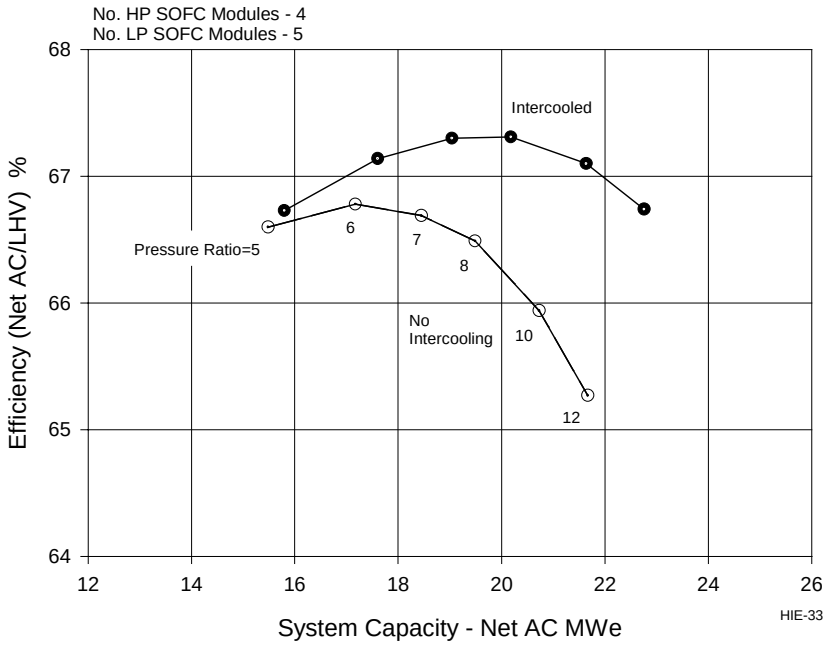

Figure 3.50 — Effect of compressor intercooling on hybrid system efficiency and power output.

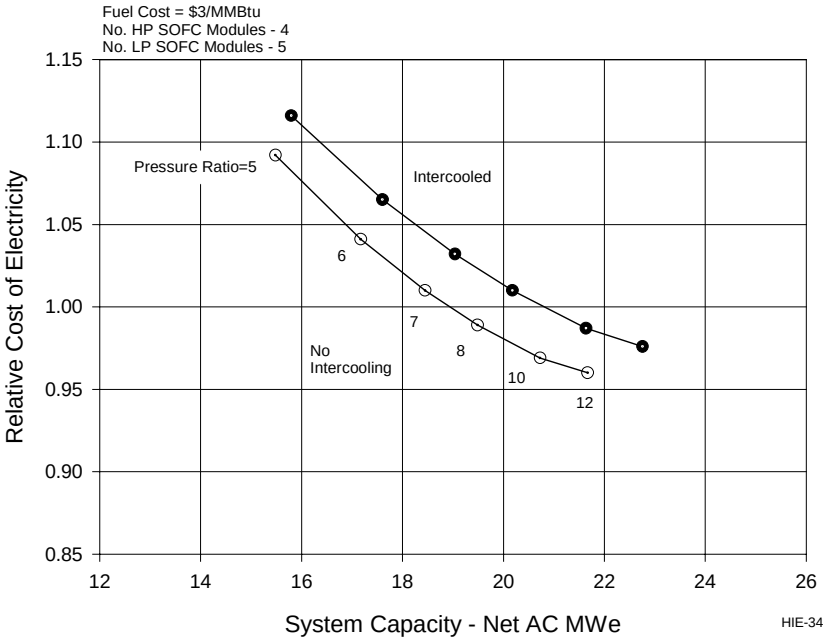

Figure 3.51 — Effect of compressor intercooling on power system cost of electricity.

3.4.3 Power System Arrangement Studies

The power plant arrangement studies investigated the differences resulting from use of SOFC vessels that had process air inlet and exhaust nozzles on opposite ends versus the nozzles on the same end. Since the process air piping will be large, heavy, and expensive, arrangements were examined to minimize the quantity of process air piping.

The arrangement that minimizes the process air piping for SOFC vessels with nozzles on opposite ends is the reference arrangement that is discussed in Section 3.1.4. Although the amount of piping is greater, it has been selected for ease of installation and continuing inspection and maintenance activities. It occupies a slightly larger amount of real estate (0.6 acres vs. 0.5 acres) than the plant arrangements that support SOFC vessels with inlet and exhaust nozzles on the same end.

Two alternative plant arrangements that use SOFC vessels with process air connections on the same end were also considered. The alternative 1 system is depicted in Figure 3.52 and Figure 3.53 and alternative 2 is shown in Figure 3.54 and Figure 3.55.

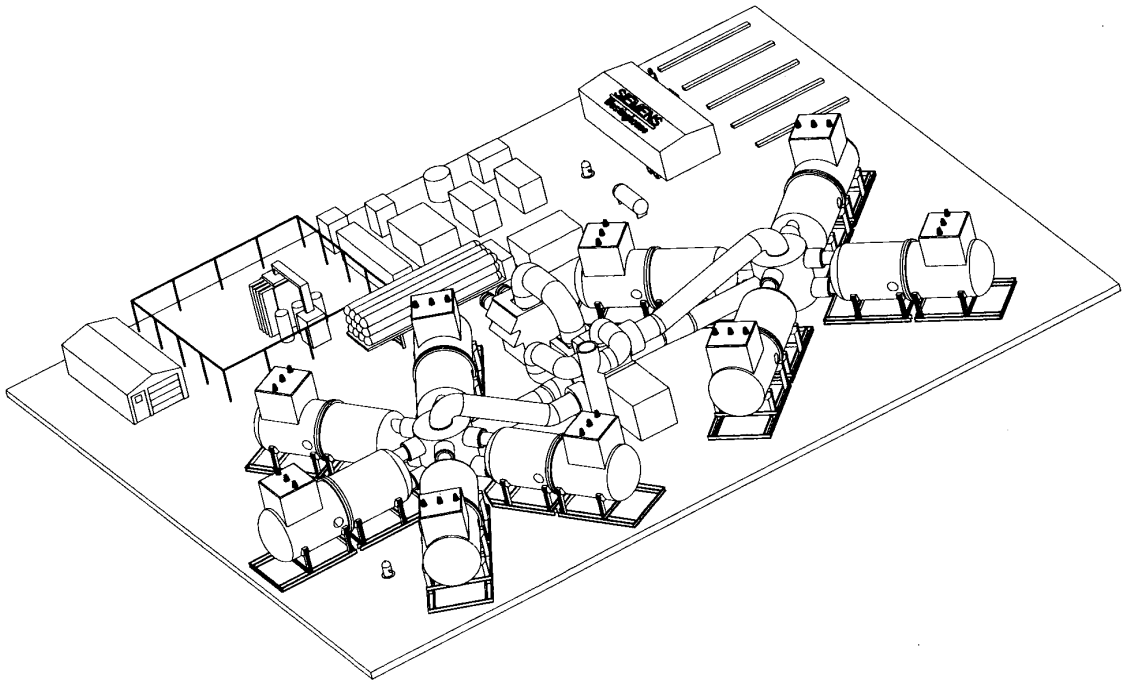

Figure 3.52 — Alternative 1 System Arrangement — Isometric View.

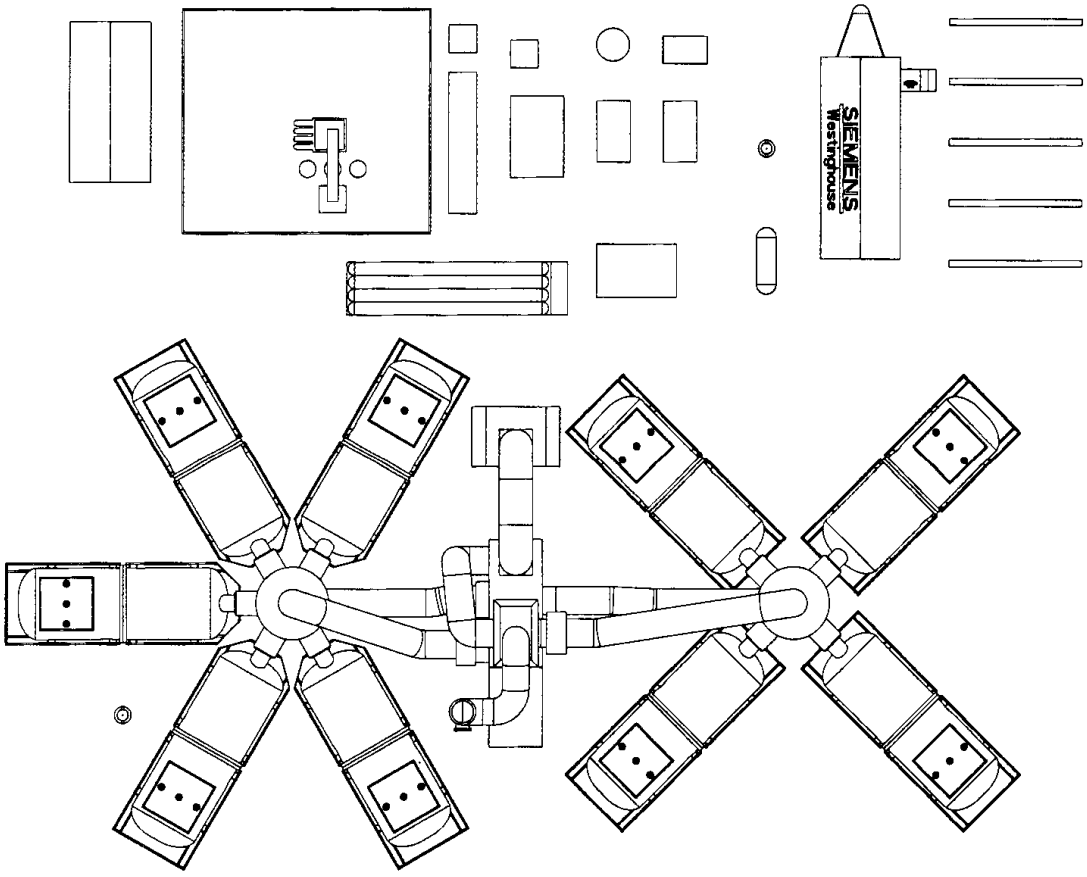

Figure 3.53 — Alternative 1 System Arrangement — Plan View.

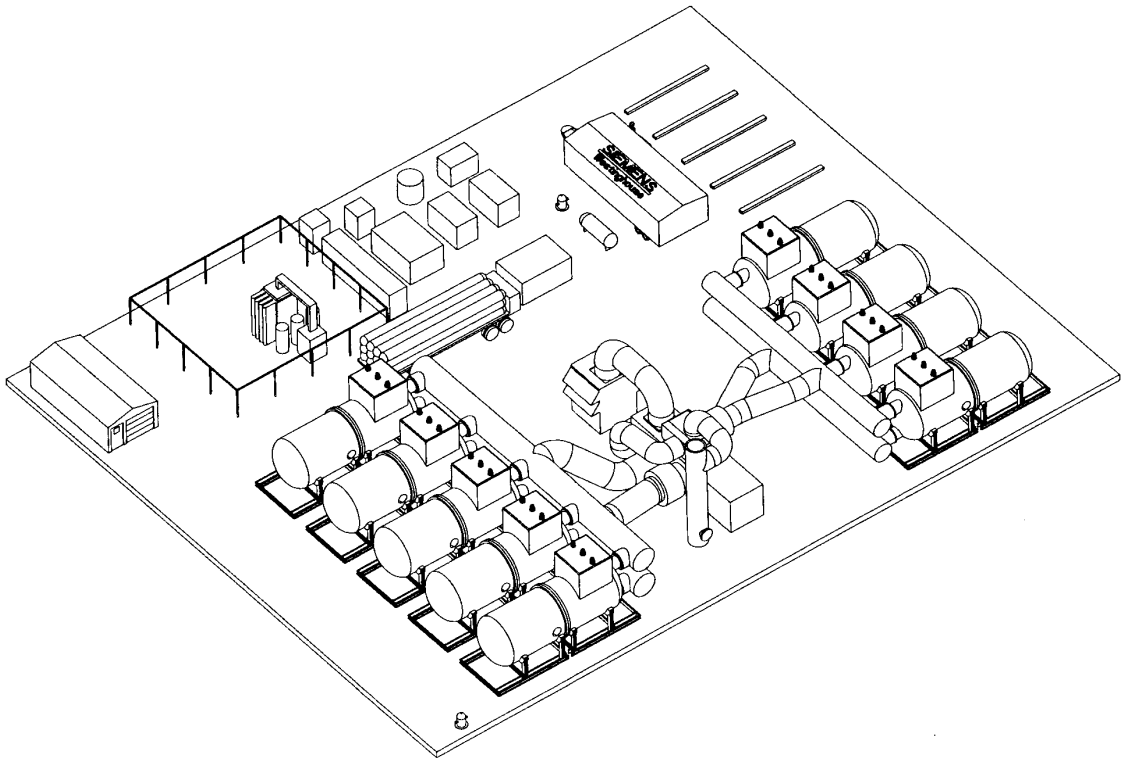

Figure 3.54 — Alternative 2 System Arrangement — Isometric View.

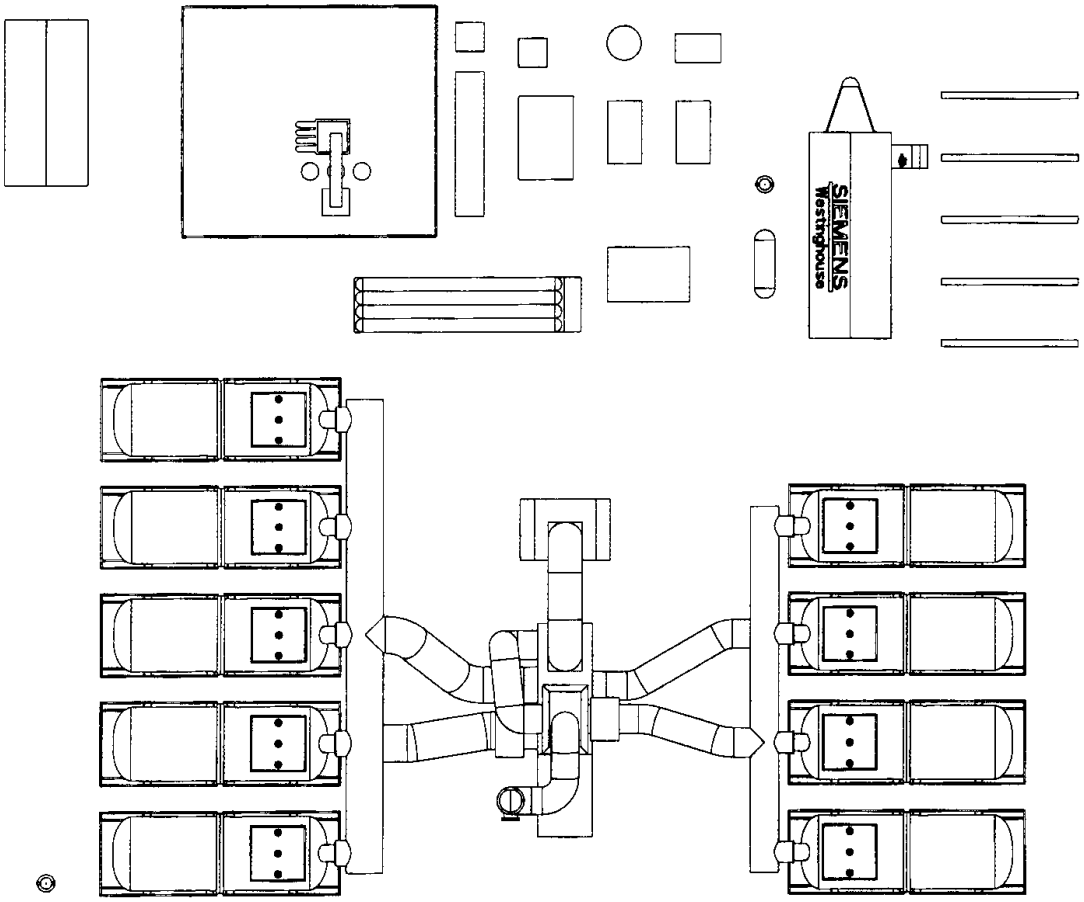

Figure 3.55 — Alternative 2 System Arrangement — Plan View.

3.4.3.1 Alternative 1 System Arrangement

This arrangement is shown on a site 51 m (167 ft) by 41 m (134 ft), or 0.5 acres. The vessels are set like the spokes of a wheel on radii from a central air distribution plenum. This plant uses a vessel design where the process air inlet and outlet nozzles are on the same end of the vessel. The vessel and SOFC stack design are relatively more difficult due to the need to ensure uniform air distribution within the stack.

Its advantage is the minimization of the quantity of large bore, internally and externally insulated piping. The cost savings for elimination of the process air piping is partially offset by the cost of the air distribution plenum vessels. This arrangement was investigated for its potential to yield lowest cost. It was hoped that the reduction in land area and process piping length would override the disadvantages. This was not the result. The advantage that was hoped to be gained by the alternative 1 configuration in its use of less land area did not materialize.

The primary disadvantages of the arrangement are inefficient routing of high voltage lines, difficult initial installation, and poor access to the SOFC vessels for maintenance.

3.4.3.2 Alternative 2 System Arrangement

This system would be installed on a site 51 m (167 ft) by 41 m (134 ft), or 0.5 acres. The plan dimensions are the same as those for the alternative 1 system. The vessels are set in rows receiving and returning process air to air distribution headers at one end of the vessels. The vessel and SOFC stack designs are relatively more difficult due to the need to ensure uniform air distribution within the stack.

The alternative 2 site has vehicle access roadways on both ends of the vessels. Routing of high voltage electric power lines from the SOFC vessels to the switchyard is efficient.

The primary disadvantages of the arrangement are difficult initial installation and poor access to the SOFC vessel halves that have the process air nozzles.

3.4.4 Desulfurization System Cost Study

This study compared an ambient temperature activated carbon desulfurization system with a heated catalytic hydrolization and adsorption system. The results of the study shows the heated system to be advantageous as discussed below.

The demonstration SOFC plants have used activated carbon beds contained within carbon steel pressure vessels to desulfurize natural gas. The significant advantage of the activated carbon is that the process works at room temperature. The main disadvantage is that the adsorption process does not produce a strong chemical bonding on the carbon and consequently the amount of sulfur adsorbed per unit amount of carbon is relatively low. As a result, the activated carbon vessels are large and the adsorbent must be replaced frequently.

A study was performed to assess the cost of using alternate sulfur adsorbents. The use of zinc oxide was found to be very attractive. The volumetric consumption of zinc oxide is about two orders of magnitude less than the consumption of activated carbon for the same duty. In order for zinc oxide to be effective, however, the natural gas temperature must be above 277°C (530°F). The optimum desulfurization temperature is at about 400°C (750°F). Operation at elevated pressures also produces a substantial improvement in sulfur removal.

If using activated carbon as an adsorbent, a 20 MW_e plant is projected to consume 173 m^3 (6100 ft^3) of activated carbon per year. The material replacement cost is $578,000 at $2.50 per pound. Additionally, the disposal cost is $145,000 at $175 per 55-gallon drum. The annual cost for activated carbon is $723,000.

This is compared to the annual consumption of only 0.85 m^3 (30 ft^3) of zinc oxide which operates at 12.4 barg (180 psig) and 400°C (750°F). The material replacement cost is $8100 at $270 per cubic foot. The disposal cost is estimated as $715 per year for four 55-gallon drums. The desulfurization process does not consume the cobalt molybdenum catalyst. It will slowly become poisoned over a long period of time. It will probably require replacement after some time greater than ten years. Assuming the catalyst is replaced after ten years, the annual replacement cost is $920 for two 0.57 m^3 (20 ft^3) Co-Mo catalyst beds. The spent cobalt-molybdenum can be sold to a reclaiming company for about $0.50 per pound. This gain is offset by the shipping cost with the result being no net gain or loss to dispose of the Co-Mo. The annual cost for desulfurization

adsorbent and catalyst cost is $9735. Combined with the cost of consuming about 180 kW for electrolysis of water to produce hydrogen, the total annual desulfurization cost is about $90,000. This is considerably less than the cost to use activated carbon.

The first cost of the large vessels for activated carbon would be higher than the combined cost for the much smaller vessels for heated zinc oxide, the H_2 generator, the natural gas recuperator and electric gas heater, even with the added complexity of supporting separate adsorbent and catalyst beds. The study concluded that the preferred fuel desulfurization technique employs the cobalt molybdenum catalyst and zinc oxide adsorbent.

3.4.5 Cover Gas System Cost Study

This study compared three alternatives for providing a protective mixture of nitrogen cover gas to the SOFC stacks. The alternatives were buying bottled nitrogen gas, buying liquefied nitrogen and generating nitrogen on site and storing it in pressurized bottles. The most cost-effective alternative is to generate nitrogen on site and store it for use as discussed below.

The demonstration SOFC plants have relied upon supplies of NHMIX cover gas stored in pressurized bottles. As the numbers of cells increased, the quantities of NHMIX increased proportionally. It became a source of concern that the large number of SOFCs in a 20 MW_e plant would require a large allocation of real estate for storing NHMIX in addition to the continuing cost of replenishing the cover gas.

Limited testing of SOFCs has shown that under some conditions it is not necessary to provide a reducing atmosphere on the fuel side of the SOFCs. It is expected that by the time that a 20 MWe plant is supplied, the process conditions and possibly even the SOFC may modify chemistry such that NHMIX is not needed. This study has proceeded upon this assumption.

In the current commodity gas market, 28.3 m^3 (1000 ft^3) of bottled nitrogen costs $12.03.

The required quantity of nitrogen which must be stored at the plant are based on the following assumptions:

- The initial stack temperature is 566°C (1050°F). The stack-cooling rate after shutdown is -3°C/minute. Cover gas is needed until the stack temperature is reduced to 260°C (500°F). Thus, the minimum supply of cover gas must be sufficient for 183 minutes.
- The amount of cover gas needed for starting up the plant is the same, as that needed for cooling the plant after shut down.
- An additional 33% is added to the gas quantities for uncertainty and conservatism.
- 242.5 cc/minute of nitrogen is needed for each SOFC. To support the 73,728 SOFCs in the plant, this results in 17.9 m^3/min (632 scfm) of nitrogen.

Each plant start up or shut down consumes 4376 m^3 (154,525 scf) of nitrogen. The gas consumption cost is $1859 for nitrogen for a single shut down. For one plant start and stop per year, the direct annual gas usage costs are $3718. In addition to the cost of the gas, the demurrage for a large nitrogen tube trailer is $950/month. The delivery fee for a trailer is built into the demurrage. Total costs for use of purchased bottled nitrogen gas is $15,108 per year.

The costs for using purchased bottled gas are considered constant because the compressed gas industry is mature and gas is supplied as a commodity. Over a twenty year plant life, the cover gas costs based upon using bottled gases sum to $302,000.

The amount of nitrogen merits consideration for buying and storing in the liquid form. The dewar for storing 4376 m^3 (11234 pounds or 154,525 scf) of liquid nitrogen must be at least 70.8 m^3 (250 ft^3). Liquid nitrogen costs $3.40 per 28.3 m^3 (1000 scf). The delivery to fill the dewar will include an excess of 5% (225 lbm) to allow for vaporization. This cost is $552 for 4594 m^3 (162251 scf) of liquid nitrogen plus a $125 delivery fee. Every month the dewar must be topped off with an additional 5% to maintain the minimum required inventory. This is an additional $28 for the nitrogen plus a $125 delivery fee. The dewar and instrumentation rental is a monthly cost of $750. Total costs for two fills of purchased liquid nitrogen, monthly replenishment and equipment rental is $11,388 per year. Over a twenty year plant life, the cover gas costs based upon using bottled hydrogen and liquid nitrogen sum to $228,000.

As a basis of comparison, the installation of nitrogen generating equipment was assessed and resulted in the preferred (lowest cost) option. A prepackaged nitrogen generator system with accumulator, compressor, vent, pressure relief and pressure control is available for about $20,500. The high-pressure gas storage bottles cost about $60,000. The unit has been sized to fill the high-pressure storage accumulator in seven days. While operating, the unit will consume electrical power and compressed air. Once the accumulator is filled, the unit will normally be idle. It will start upon low-pressure demand signal from the accumulator and operate until the accumulator is re-filled. The functional specifications for the unit are shown in Table 3.10.

Table 3.10 — Nitrogen Generator/Compressor Characteristics

Nitrogen production rate	28.3 m^3/hr (1000 scf/hr)
Nitrogen pressure before compression	6.9 barg (100 psig)
Nitrogen pressure after compression	165 barg (2400 psig)
Nitrogen purity	>98%
Process used	Selective Membrane
Package size	1.52 m x 1.83 m x 1.93 m (60" x 72" x 76")
Nitrogen separator storage tank	1.9 m^3 (500 gallons), ASME tank
Nitrogen compressor accumulator	twelve – 2.19 m^3 (77.5 ft^3)ASME/CGA bottles
Electrical power requirements	110 vac/60 Hz/1 phase for separator 440 vac/60 Hz/3 phase, 5 kW for compressor
Compressed air supply required	1.9 m^3/min (66 scfm) @ 175 psig

The equipment costs for the nitrogen generating and storage system sum to about $80,500. The initial expenditure of this amount is justified compared to the continuing annual cost of purchasing bottled or liquid nitrogen.

Table 3.11 summarizes the costs for the various options investigated for supply of a nitrogen system.

Table 3.11 — Costs for Options Investigated for Supply of Nitrogen System

	Bottled Nitrogen	Liquid Nitrogen	Nitrogen Generating System
	$3,718 Annual Gas Cost (Delivery Included)	$2,388 Annual Gas Cost & Delivery Fees	$20,500 Initial N_2 Equipment Cost (one time cost)
	$11,400 Annual Bottle Trailer Demurrage	$9000 Storage Dewar & Instrumentation Annual Rental	$60,000 Bottle Trailer (one time cost)
Annual Cost	$15,108	$11,388	$4025 pro-rated
20 Year Cost	$302,000.	$228,000	$80,500

3.4.6 Hydrogen Gas Generation Cost Study

The use of a hydrogen generating system has already been justified due to the value of adding hydrogen to the natural gas to support catalyst assisted desulfurization using heated zinc oxide.

There are several suppliers of commercially available hydrogen generating equipment both in the USA and Canada. A prepackaged hydrogen generator/compressor system with accumulator and pressure control is currently available for $245,000, but can be purchased in quantity (>100 unit per year) for $61,250 to $122,500 (Supplier's estimates). The functional specifications for the unit are shown in Table 3.12.

Table 3.12 — Hydrogen Generator Characteristics

Hydrogen production rate	0.57 m3/min (20 scfm)
Hydrogen pressure	12.4 barg (180 psig)
Process used	electrolysis
Package size	1.82 m x 5.49 m x 3.05 m high (6' x 18' x 10') high
Package weight	7484 kg (16,500 pounds)
Hydrogen accumulator size	119 sm^3 (4200 scf) @ 12.4 barg (180 psig) or 8.98 m^3 (317 ft^3)
Power	180 kW
Water consumption	35 liters/hr (9.24 gph)

3.4.7 Process Piping Cost Study

The first task in the process piping cost study was to determine the required flow area. When the airflow was assumed to be about 61 m/sec (200 fps or ~10% of sonic speed) an internal protective liner was necessary to prevent erosion of the insulation.

At air temperatures in the range of 815°C to 870°C (1500 to 1600°F) metallic liners are unsuitable except for short lengths due to their high thermal expansion. Ceramic liners were found which have excellent erosion resistance but are unsuitable for other reasons. The ceramic liner materials are necessarily dense with high thermal conductivity and are fabricated by casting. The casting process requires a thickness of one inch. This dense ceramic adds 5 cm (two inches) to the piping inner diameter, provides no thermal insulation benefit, adds weight and is a very costly process.

When the inner flow area was selected to keep the gas speed to less than 30 m/sec (100 fps), conventional vacuum-formed alumina-silica insulation can be used. This does require that the piping be larger, but the complexity of fabricating insulated piping results in lower total cost.

The estimated costs of internally and externally insulated piping for the 20 MW_e plant are shown in Table 3.13.

Table 3.13 — High Temperature Piping[1] Costs

Application	Open Flow Area ID, inches	Pipe Size (0.375" wall)	Cost per linear foot[2]
High Pressure Header (88 psia)	22	38	$1104
High Pressure Branch (88 psia)	14	30	$838
Low Pressure Header (37 psia)	41	58	$1813
Low Pressure Branch (37 psia)	28	44	$1301

Notes:
1. 3" exterior insulation
2. Cost for piping and insulation only, no fittings, flanges or bolting materials

Several plant layouts were considered to minimize the amount of process piping. Figure 3.9, Figure 3.52, and Figure 3.54 show some preliminary layouts of a gas turbine/compressor skid with four high-pressure SOFC vessels and five low-pressure SOFC vessels. Figure 3.9 shows an arrangement that uses SOFC vessels that have nozzles on both ends. This arrangement results in the largest footage of insulated piping. It has an advantage of providing the most pneumatically balanced flow resistances. The other figures show plant arrangements that use a vessel with the air inlet and outlet connections on the same head. Figure 3.52 is a layout with a star shaped arrangement of vessels that minimizes the plan area of the plant. This minimal plan area arrangement has the disadvantages of requiring expensive air distribution vessels and

limiting access to the vessel halves that are closest to the air distributor vessels. These disadvantages are also shared by the butterfly plant arrangement (Figure 3.54 and Figure 3.55.

4. CONCLUSIONS

Study conclusions can be summarized as follows:

- A PSOFC/GT system concept of near 20 MW capacity has been devised that is conservatively capable of 67% efficiency, a value ten points greater than that achievable with the best available large-plant conventional power generation technology, and twenty points above the efficiency achieved by a conventional 20 MW-class gas turbine combined cycle power system.
- The specific power system concept developed during this study, integrating HP and LP SOFC generators with an intercooled, SOFC-reheated gas turbine, achieves an estimated power output of 19 MWe at an efficiency of 67.3% (net AC/LHV). Improvements in the performance of major system components, particularly in the SOFC PCS, for which there was no study design task, and employment of an ambient-temperature passive sorbent technology for fuel desulfurization would cause the system efficiency estimate to approach very closely the 70% efficiency target; adding a steam turbine system will result in efficiency >70%.
- The staged-cell SOFC stack design does not offer the large SOFC efficiency gain (over the standard cocurrent axial flow stack design) that was projected originally. Cell cooling in the fuel-entry cell rows reduces the average cell voltage, while there is little increase in average fuel utilization at the last cell row at meaningful current densities because of the hazard of anode oxidation.
- For the reference fuel cost of $3.00/MMBtu, the estimated COE for the HEFPP system is 3% higher than the COE estimate for a conventional 20 MW-class gas turbine/steam turbine power system. Leveraged by its significantly higher efficiency, the HEFPP system would have a COE advantage in a higher fuel cost environment. For example, with $6 fuel, the HEFPP COE would be 7% less than the conventional-system COE.

Recommendations:

- Desulfurization technologies not requiring a source of hydrogen, and capable of operation at ambient-temperature levels, should be developed. For the reference power system, this would increase the system efficiency by approximately 0.5 of a percentage point.
- For high efficiency SOFC/GT power systems, the SOFC power conditioning efficiency affects strongly the overall system efficiency. For example, a gain in PCS efficiency of one percentage translates to a system efficiency gain of nearly 0.6 of one percentage point. Power conditioning topologies with greater than 95% efficiency should be developed.
- Small, efficient, highly-reliable, recuperated gas turbines with turbine inlet temperatures commensurate with SOFC exhaust gas exit temperatures (870°C) are needed for deployment in hybrid cycle SOFC/gas turbine power systems. Effort

should be focused on the specification of such gas turbines (circa 4 MWe capacities for use in 20 MWe hybrid cycle power systems) and their development should be undertaken.

- A PSOFC/GT power system of 70% efficiency potential should be developed and demonstrated at the smallest capacity class practical for proof-of-concept.
- SOFC development should be pursued to improve fuel cell power density and efficiency. As with the SOFC power conditioning system, improvements in cell efficiency are effective in increasing the efficiency of high-efficiency SOFC/GT power systems.
- In the conventional SOFC generator design, reformed fuel enters the cell stack at the bottom and flows upwards in the system of communicating, parallel-flow channels defined by the cell exterior surfaces. The gas density increases as oxidation products are produced, and this could foster parallel channel instabilities, particularly at elevated operating pressures where buoyancy effects are more significant. Development work should be undertaken to confirm the operational feasibility of the conventional SOFC generator configuration at elevated pressures beyond three atmospheres.

APPENDIX

The Effect of Staging on Efficiency of Isothermal SOFC Stacks

The purpose of this section is to describe the effect of staging of the fuel stream on the efficiency of fuel cells. Staging of the fuel flow path is described as having the fuel pass a number of separate or segmented electrical circuits on its way through the fuel cell array. The current density is not uniform within any cell or stage that has a large difference in fuel concentration between the inlet and outlet locations. The terminal voltage across a stage is uniform, but the internal Nernst potential varies due to the change in reactant concentrations. With staging, one can either divide the cell structure into many regions or the fuel supply for many cells can pass sequentially through or past the cells. With staging the current density distribution becomes more uniform because the Nernst potential varies by a smaller amount within each stage. More uniform current density lowers the Joule losses and polarization losses. The voltage gain in the fuel rich stages is greater than the loss in the fuel poor stages.

It will be shown that the improvement in efficiency is small at economically viable operating current density conditions, namely at current densities near the maximum power point. The maximum power point occurs at the current density that maximizes the power output per unit area of the cell.

ISOTHERMAL ANALYSIS

The analysis is simplified by assuming that leakage of O_2 is negligible, that the cells are isothermal, and that the cathode gas is supplied at high stoich conditions. These conditions are favorable to the benefits of staging. For example, non-isothermal conditions within a stage create restraints on the flow and geometrical arrangements necessary to achieve uniform fuel consumption within the stages.

Consider that the fuel is being consumed by an electrochemical conversion as it flows along a path through a number of stages. The properties used in the analysis are applicable to solid oxide fuel cells but the generalized analysis is independent of the specific cell geometry. If the total in-stack fuel consumption along the path is F_c, the consumption in each of the n stages will be F_c/n and the consumption at the end of stage i is z_i = (i/n) Fc. The local fuel consumption within a stage is denoted by z. The change in consumption, dz, that occurs in elemental area, dA, is related to the local current density, j, by

$$dz = F_c\,(j\,dA/I_o) = (F_c/j_{av})\,j\,dA/A_o = (F_c/j_{av})\,j\,dx$$

or

$$dx/dz = j_{av}/(j\,F_c) \qquad (A.1)$$

where dA/A has been replaced by dx.

If one also assumes that the electrical potential produced by CO is equal to that produced by H_2, the fuel mole fraction (the sum of H_2 and CO mole fractions) is uniquely determined by the fuel consumption and the inlet composition. Thus with uniform cathode concentration or cathode composition also a function of consumption, the Nernst potential can be stated to be a function of the fuel consumption, $E_n = E_n(z)$.

The local current density at a location where the fuel consumption is z is given by

$$j = (E_n(z) - v_i)/R_c \qquad (A.2)$$

Substituting this into equation (1) gives

$$dx/dz = (j_{av}\,R_c/F_c)/(E_n(z) - v_i) \qquad (A.3)$$

After integration over the stage, the equation defining the cell voltage in each stage becomes

$$\int_{z_{i-1}}^{z_i} \frac{R_c\,dz}{\left(E_n(z) - v_i\right)} = \frac{F_c\,\Delta x}{j_{av}} \qquad (A.4)$$

For n equal area stages, $\Delta x = 1/n$ for each stage. The solution for the v_i of each stage is found by iteration using numerical integration of equation (4). If the resulting value of Δx is too small/large for an assumed v_i, the value of v_i in the next iteration must be increased/decreased subject to the limit that $0 < v_i \le E_n(z_i)$. The solutions presented here were obtained by numerical integration of equation (4). The cell resistance, R_c, was calculated as the sum of the internal resistance, the diffusion polarization resistance's for each electrode, and the activation polarization resistance. The polarization resistance's were obtained by dividing the anode or cathode polarization by the local current density. After one obtains the v_i, it is easy to plot the current density versus the non-dimension area using the values from the final iteration. The value of dimensionless area, x, corresponding to a given value of z in stage i is given by

$$x = (i-1)\Delta x + \frac{j_{av}}{F_c}\int_{z_{i-1}}^{z} \frac{R_c\,dz}{(E_n(z) - v_i)} \qquad \text{(A.5)}$$

The current density at this x location is given by equation (2).

RELATIONS FOR MOLE FRACTIONS, DIFFUSION POLARIZATION, AND NERNST POTENTIAL

The mole fraction of fuel in the anode gas stream at fuel consumption z is

$$y_F(z) = y_{Fo}(1-z)$$

The mole fraction of oxygen in the cathode gas stream at fuel consumption z is

$$y_O(z) = \frac{(1 - z/s)}{(1/y_{OO} - z/s)}$$

where y_{OO} is the mole fraction of oxygen at inlet to the stack. The partial pressure of oxygen in the anode gas stream is found using an effective equilibrium constant for the methane derived fuel mixture,

$$p_{OA}(z) = \left\{\frac{(1 - y_F(z) - y_N)K}{y_F(z)}\right\}^2$$

The Nernst potential based on the concentration in the gas streams is

$$E_n(z) = \frac{RT}{4F}\ln\left(\frac{p y_O(z)}{p_{OA}(z)}\right)$$

The anode diffusion polarization is

$$\eta_A = \frac{RT}{4F}\ln\left(\frac{p_{OA}(z)}{p_{OAE}(z)}\right)$$

where

$$p_{OAE}(z) = K^2\left(\frac{1 - y_N - y_{FAE}(z)}{y_{FAE}(z)}\right)^2$$

$$y_{FAE}(z) = y_F(z) - j(z)/S_3$$

$$p_{OA}(z) = K^2\left(\frac{(1-y_N-y_F(z)}{y_F(z)}\right)^2$$

The cathode diffusion polarization is

$$\eta_C = -\frac{RT}{4F}\ln(1-j(z)/S_1 y_O(z))$$

ISOTHERMAL ANALYSIS RESULTS

The example is based on representative properties of a solid oxide fuel cell at 1000°C. The fuel selected was the DOE fuel: 96% methane, 2% nitrogen and 2% CO_2. The inlet fuel composition to the first stage is based on internal reformation with a recirculation ratio that gives an oxygen to carbon ratio, OCR, equal to 2.1. Results are obtained at two system fuel consumption levels, 85% and 95%. The corresponding in-stack fuel consumption values, F_c, are 0.6839 and 0.8946. The combined fuel mole fraction of the inlet fuel is y_{Fo} = 0.6326 for both fuel consumption levels.

The reference current density was selected to be the value that gives the maximum power density for a single stage cell configuration. A plot of terminal voltage and power density as a function of current density is shown in Figure A.1 for Fcs = 0.85. The values of current density at the maximum power point are j_{maxP} = 0.522 and 0.498 A/cm^2, for the 0.85 and 0.95 fuel consumption values, respectively.

Figure A.2 compares the current density and voltage distributions for single stage and four stage configurations at maximum power density for 85% system fuel consumption. For the four stage configuration, the total area is divided into four equal parts. The upper two curves, the Nernst potentials, are almost indistinguishable. The middle set of curves show the uniform voltage of the single stage and the four individual voltages of the four stage configuration. The bottom set of curves compare the current density distributions. Note that the maximum to minimum change in current density is reduced for the four-stage case. Since the average stage voltage is higher than the single stage voltage at the same current density and fuel consumption, the ratio of voltage in the same as the ratio of average power densities of the staged versus single stage cells. The average power density for this current density is increased by 0.58% above the value for a single stage cell for the limiting case of 16 stages.

Figures A.3 and A.4 show the same comparison at reduced current densities, $j_{maxP}/5$ and $j_{maxP}/20$, respectively. The staged power density only increases significantly at the lower current densities. Note that current density scales were changed in these figures to separate the two sets of curves.

Figures A.5, A.6, and A.7 provide similar comparison for 95% system fuel consumption. Table A.1 compares improvements in power density at 16 stages to that at a single stage. This table illustrates that the power density can be increased by significant amounts at a specified current density only for power densities that are well below the maximum power point. Thus the benefit of increased efficiency due to staging is only available at low power densities. Since staging is only beneficial at low power per cell, many more cells are required to compensate for the low power operation. Figure A.8 shows the relative number of cells required for a fixed plant output as a function of the current density.

The analysis was also applied to a generic planar cell configuration with a significantly lower total effective resistance. The total resistance including concentration polarization losses was held constant at 0.20 ohm-cm^2. The maximum power density for this single stage planar cell occurs at a current density of 2.10 A/cm^2 for FC = 85% and at 2.05 A/cm^2 for FC = 95%.

The increase in power output for Siemens Westinghouse cylindrical cells is compared to that of planar cells in Figure A.9. The curves show the increase in power output as a result of staging. The increase is shown as a percentage of the power output of the corresponding single stage cell. The current density has been made dimensionless on the respective current density at the maximum power point for the single stage cell condition. It is seen that the use of normalized current density results in an excellent correlation of the improvement in efficiency due to staging. The slight difference in the curves for the two geometries is due to the change in diffusion polarization resistance with current density in the cylindrical cell model. Otherwise the gains appear to be a function of normalized current and utilization.

Although the curve shows significant increase in output for FC = 0.95, the partial pressure of O_2 at the anode/electrolyte interface exceeds the limit which is two orders of magnitude less than the equilibrium partial pressure of O_2 for the Ni/NiO/O_2 reaction. Oxidation of the anode is considered likely under these conditions. The diffusion con-

ductance of Siemens Westinghouse Power Corporation cells was used to evaluate the partial pressure of fuel at the electrolyte interface. For recirculated fuel, the fuel utilization limit is FU = 91% when the partial pressure of O_2 is maintained below the limit given above.

The effect of once through fuel flow on the increase in output due to staging was also considered. With the same fuel supply, external reformation at oxygen to carbon ratio of 2.1 gives a fuel inlet mole fraction of 0.780. The in-stack fuel utilization value equals the system fuel utilization. Results for the planar cell with constant resistance are shown in Figure A.10 for 85% and 95% system fuel utilization. As expected, the gain due to staging increases significantly if one can push the operation to higher fuel utilization for once through fuel flow (external fuel reformation). Limiting the partial pressure of O_2 to two orders of magnitude below the equilibrium value restricts fuel utilization to FU = 89%.

SUMMARY OF ISOTHERMAL ANALYSIS

The results demonstrate that the effect of fuel staging on fuel cell power output is very small for current densities near the maximum power point. This is shown to be valid also for other geometries that have considerably lower resistance than the cylindrical cell. With fuel recirculation, the output at the maximum power point increases by 0.58 and 1.15% at 85 and 95% fuel utilization, respectively. The improvement due to fuel staging increases as current density is reduced or as fuel utilization is increased. Oxidation of the fuel electrode is likely with recirculated fuel for utilization above 91%.

The improvement due to staging is greater for systems with once through fuel flow as compared to those with recirculated fuel. However, oxidation of the anode is likely for once through flow when fuel utilization exceeds 89%. Although fuel staging could increase output at low current densities by more than 10% at 95% utilization, the low power density would result in a large increase in system cost.

Nomenclature for Appendix A

A_o	Total cell area, [cm^2]
E_n	Nernst potential, [V]
F_c	In-stack fuel consumption, [-]
F_{cs}	Overall system fuel consumption, [-]
I_o	Total cell current generated by n stages = j_{av} A_o.
i	Stage index, [-]
j	Local current density, [A/cm^2]
j_{av}	Average current density for the stage, [A/cm^2]
j_{maxP}	Current density that gives maximum average power density for a single stage Cell, [A/cm^2]
K	Effective equilibrium constant for the methane derived fuel mixture, [-]
n	Number of stages,[-]
p	Pressure of the fuel cell gases, [Atm]
Pd	Average power density, [W/cm^2]
$p_{OA}(z)$	Local partial pressure of oxygen in the anode gas stream, [Atm]
$p_{OAE}(z)$	Local partial pressure of oxygen at the anode electrolyte, [Atm]
R_c	Cell resistance index, [ohm-cm^2]
S_1	Diffusion conductance of the air electrode at one Atm, [A/cm^2-Atm]
S_3	Diffusion conductance of the fuel electrode at one Atm, [Atm/cm^2-Atm]
v_i	Terminal voltage of stage i, [V]
x	Non-dimensional cell area, = A/Ao, [-]
Δx	Non-dimensional area per stage, [-]
$y_F(z)$	Mole fraction of fuel in the anode gas at fuel consumption z, [-]
$y_{FAE}(z)$	Mole fraction of fuel at the anode electrolyte at fuel consumption z, [-]
y_{Fo}	Fuel mole fraction in anode gas at inlet to the stack, [-]
y_N	Mole fraction of nitrogen in the fuel at inlet to the stack, [-]
$y_O(z)$	Mole fraction of oxygen in the cathode gas stream at fuel consumption z, [-]
y_{OO}	Mole fraction of oxygen in the cathode gas at inlet to the stack, [-]
z	Local in-stack fuel consumption, [-]
z_i	In-stack fuel consumption at exit of stage i, [-]
η_A	Anode diffusion polarization, [V]
η_C	Cathode diffusion polarization, [V]

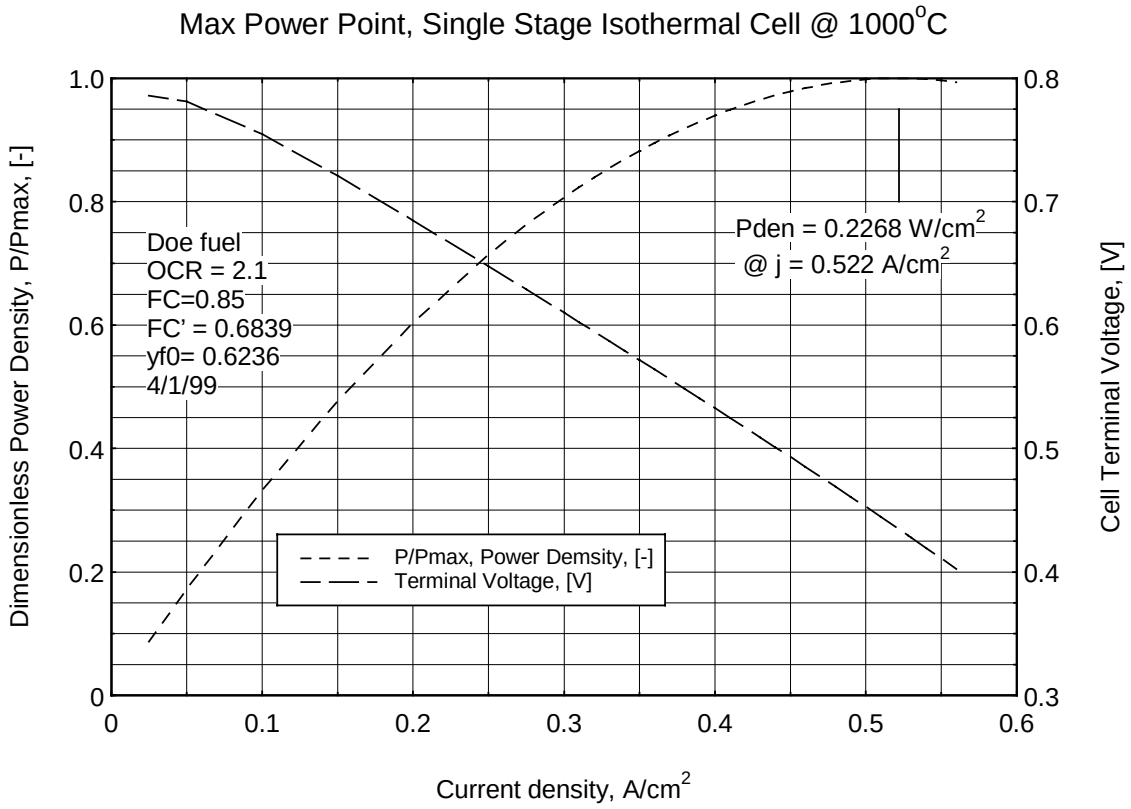

Figure A.1 — Power Density and Terminal Voltage for a Single Stage Cell.

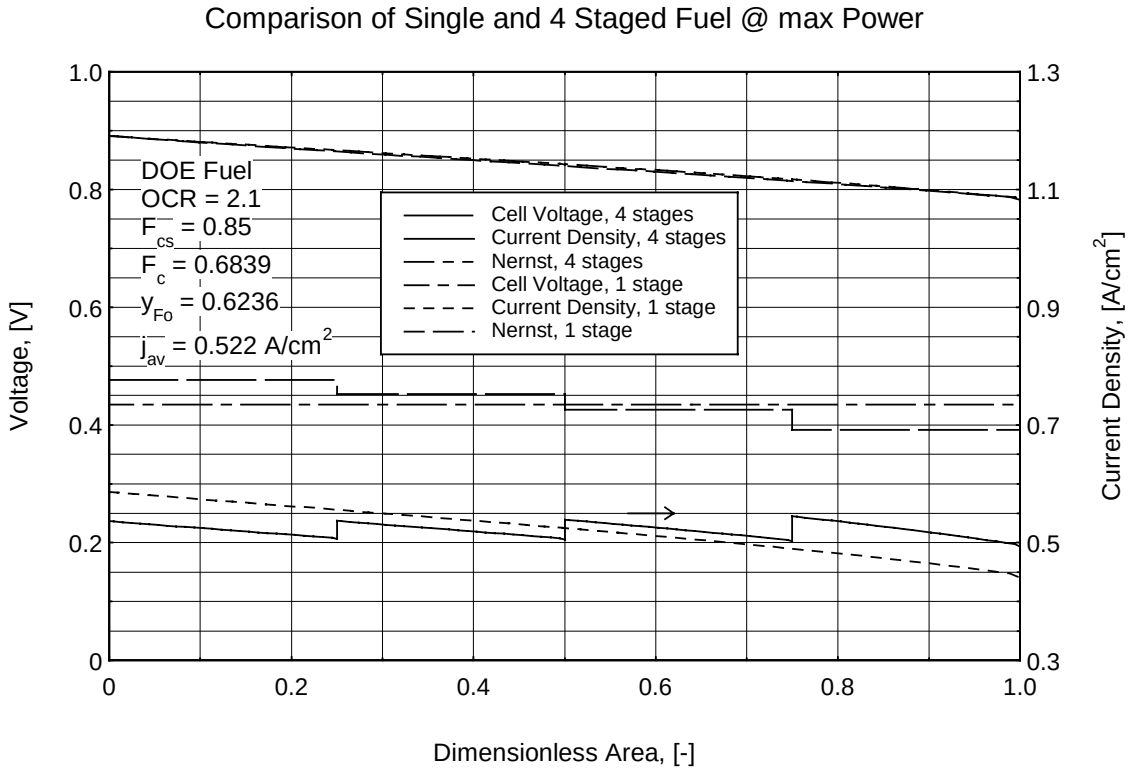

Figure A.2 — Emf and Current Density Distributions in a 4 Staged Fuel Cell.

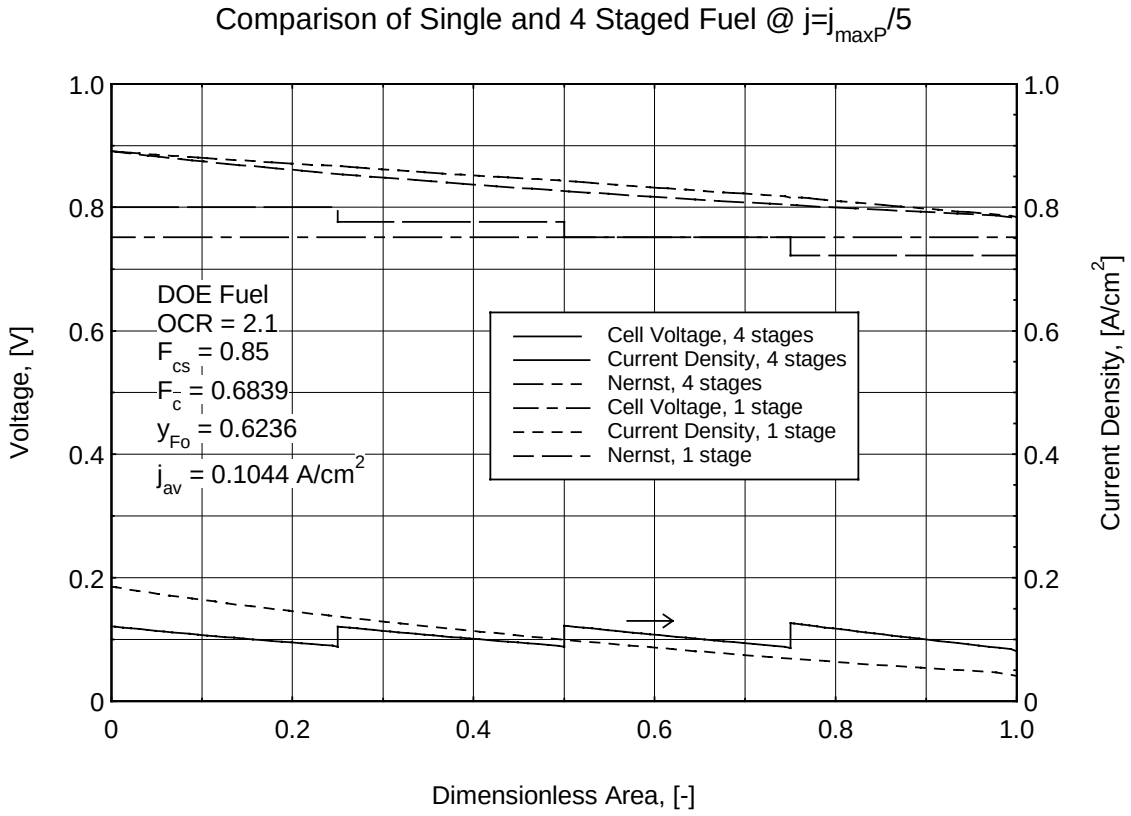

Figure A.3 — Emf and Current Density for Single and 4 Staged Cell.

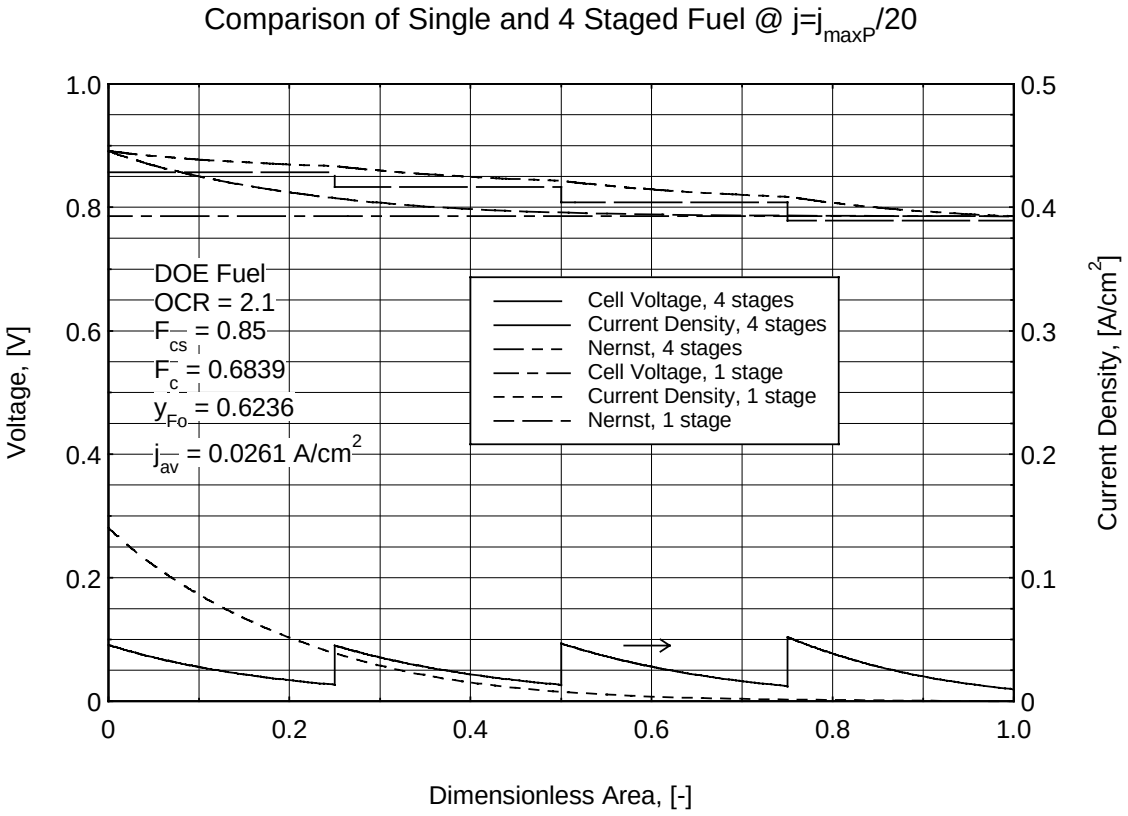

Figure A.4 — Emf and Current Density for Single and 4 Staged Cell.

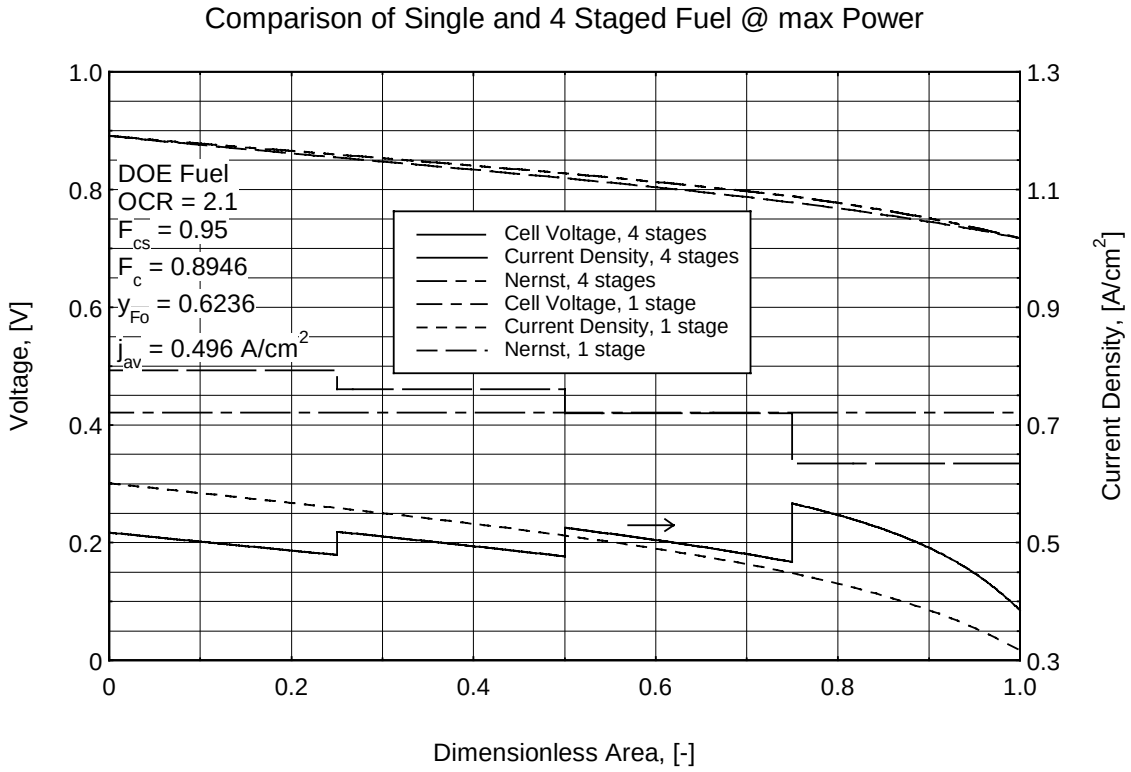

Figure A.5 — Emf and Current Density for Single and 4 Staged Cell.

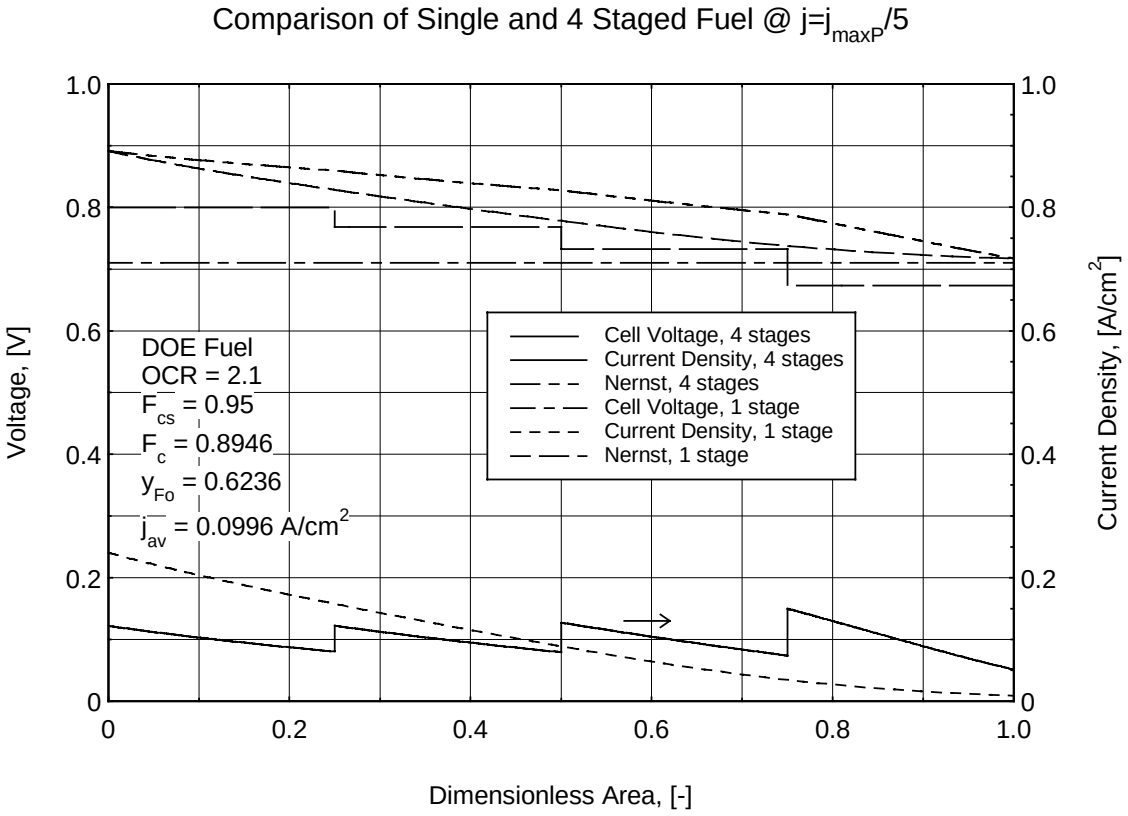

Figure A.6 — Emf and Current Density for Single and 4 Staged Cell.

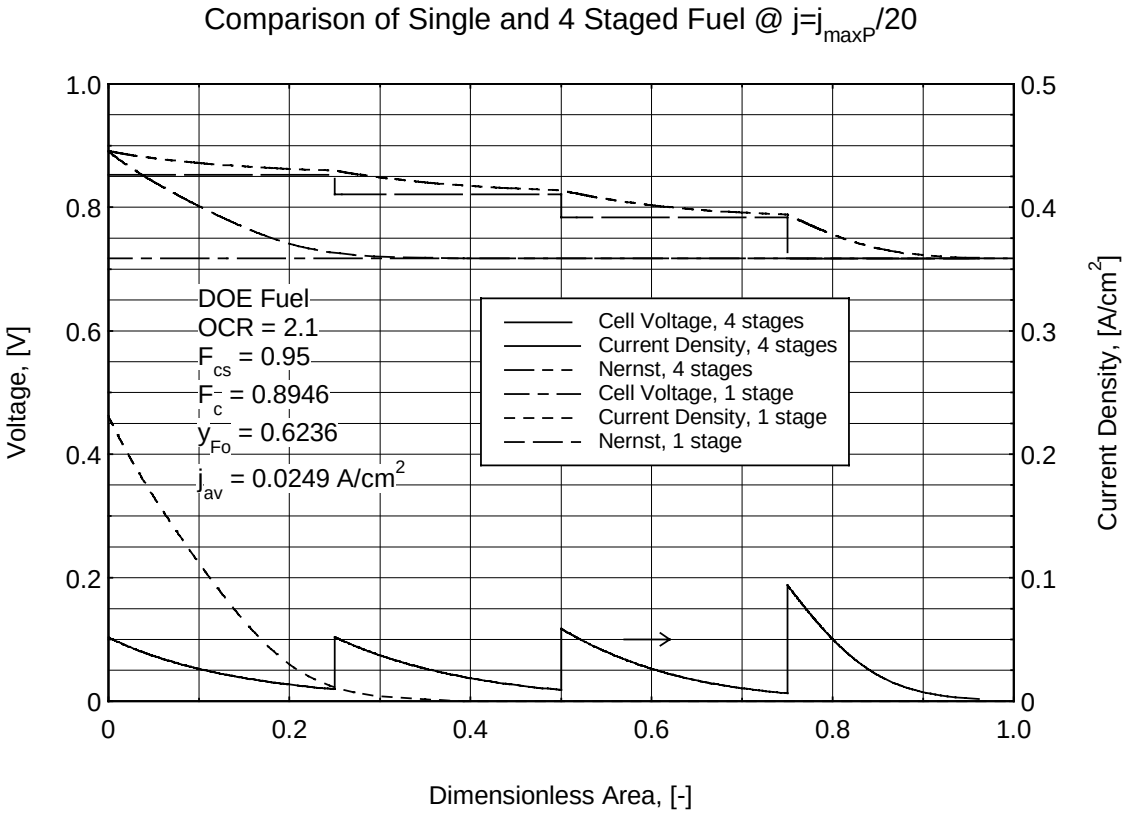

Figure A.7 — Emf and Current Density for Single and 4 Staged Cell.

Table A.1
Effect of Staging on Average Voltage or Power Density

j_{av}, [A/cm^2]	F_{cs}, [-]	P_d for 1 stage, [W/cm^2]	$\Delta P_d/P_d$ for 16 stages, [%]
0.5220	0.85	0.2268	0.58
0.1044	0.85	0.0785	1.53
0.0261	0.85	0.0205	4.58
0.4980	0.95	0.2099	1.15
0.0996	0.95	0.0707	5.06
0.0249	0.95	0.01786	11.87

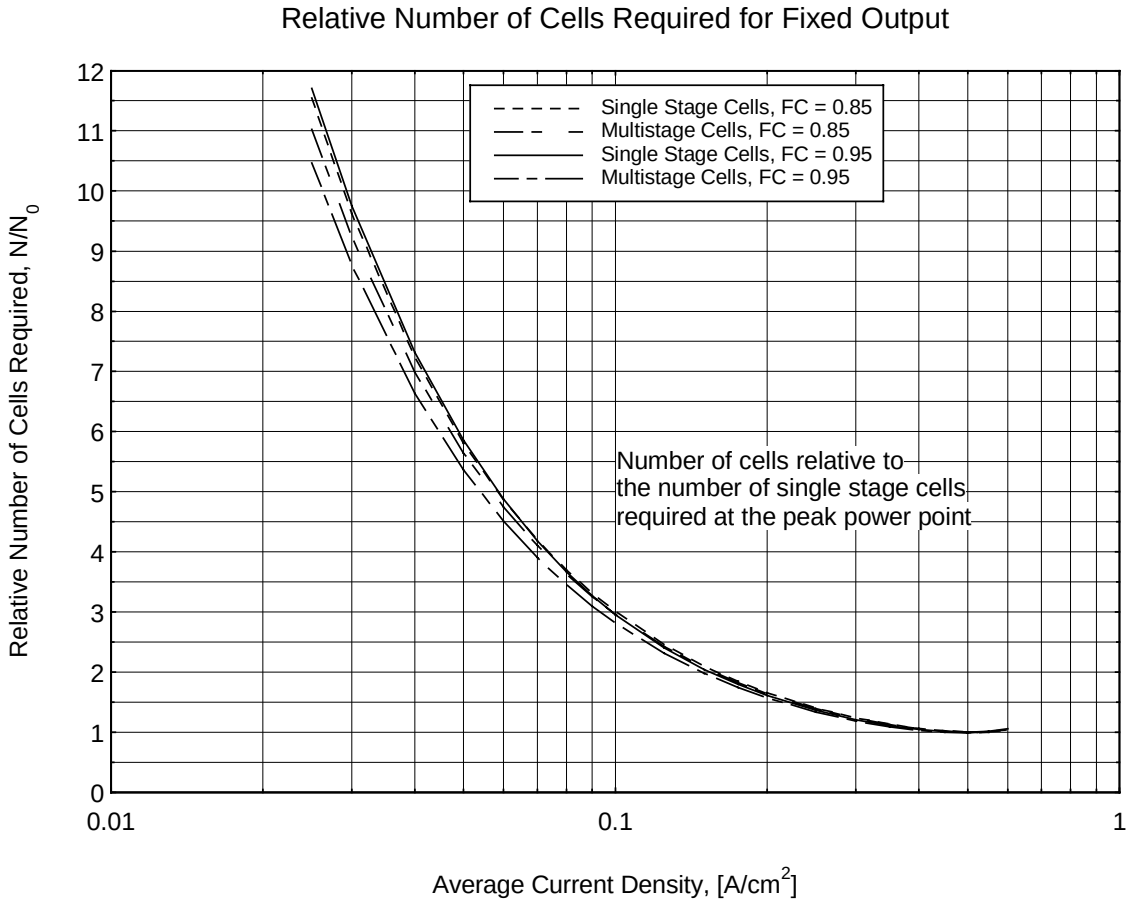

Figure A.8 — Relative Number of Cells Required for Fixed Power Output as a Function of Current Density.

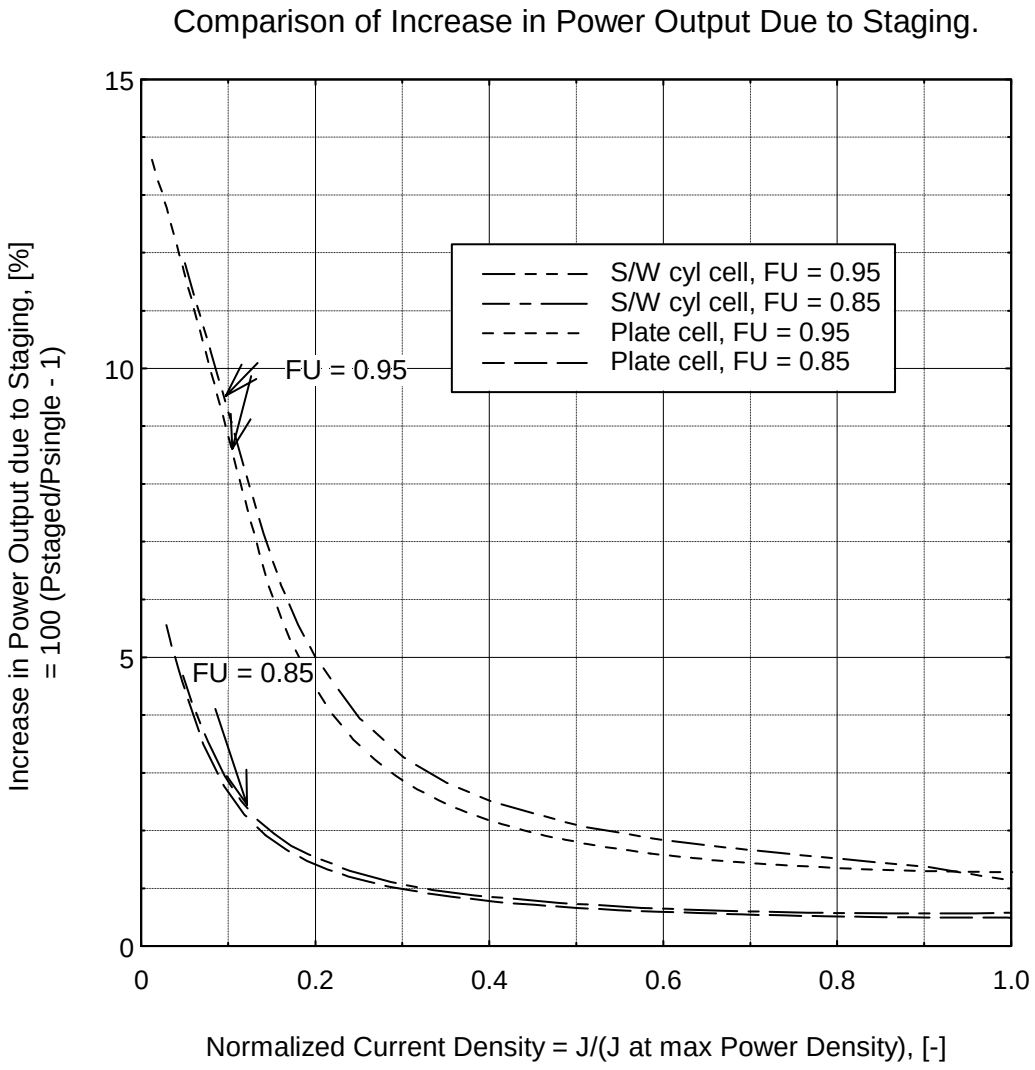

Figure A.9 — Increase in the Power Output Due to Staging for Planar and Cylindrical Cells vs. Dimensionless Current Density.

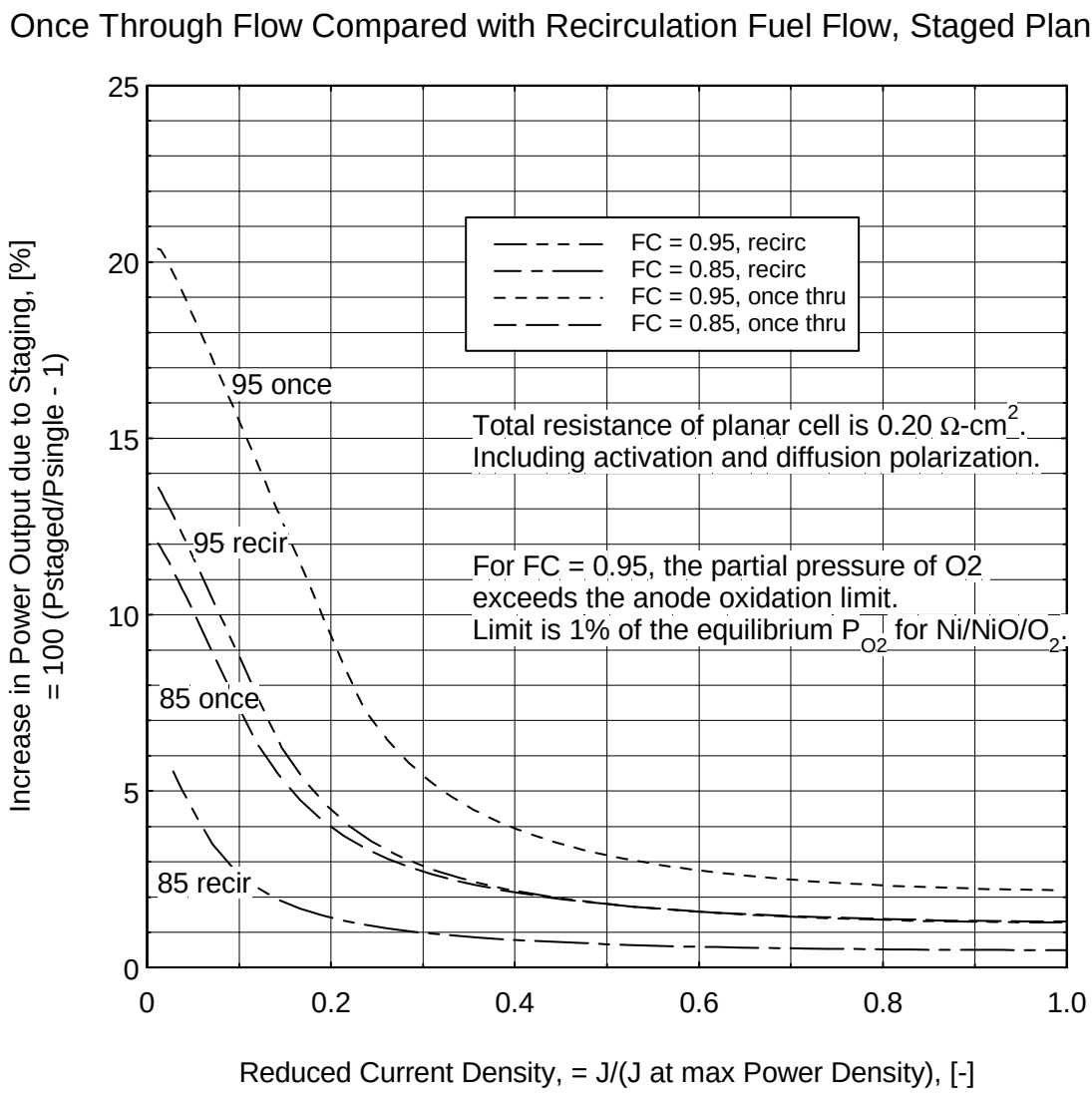

Figure A.10 — Comparison of Effect of Once Through and Recirculation Fuel Flow on the Benefits of Cell Staging.